Volume 2

Chapter 4

Diverse Jurassic Magmatic Arcs of the Colombian Andes: Constraints from Petrography, Geochronology, and Geochemistry

https://doi.org/10.32685/pub.esp.36.2019.04
Published online 12 May 2020

Gabriel RODRÍGUEZ–GARCÍA[1]*, Ana María CORREA–MARTÍNEZ[2], Gilberto ZAPATA–GARCÍA[3], María Isabel ARANGO–MEJÍA[4], Gloria OBANDO–ERAZO[5], Juan Pablo ZAPATA–VILLADA[6], and José Gilberto BERMÚDEZ[7]

Abstract New field, petrographic, whole–rock geochemical, and U–Pb zircon geochronological data obtained from Jurassic plutonic rocks of the Santander Massif, plutonic and volcanic rocks in the Upper Magdalena Valley, and plutonic rocks in the northern block of the Ibagué Batholith provide evidence that the Jurassic igneous activity that is recorded in several blocks of the Colombian Andes began in the Late Triassic and ended in the Early Cretaceous. This magmatism developed in at least three different magmatic arcs, during clearly defined time periods, over basements with different characteristics. The first stationary continental margin arc was active between the Late Triassic (ca. 214 Ma) and the Early Jurassic (ca. 184 Ma). It is located in the Santander Massif and is primarily represented by monzogranitic, peraluminous plutons generated by multiple magmatic pulses that involved varying degrees of crustal melting. This study proposes, for the first time, that most of the arc was emplaced into primarily Ordovician basement and that a small part was emplaced into early Neoproterozoic basement. The second arc, which is located in the Upper Magdalena Valley, developed between the Early Jurassic (ca. 197 Ma) and the Middle Jurassic (ca. 167 Ma) during at least three magmatic pulses related to arc migration, which is evidenced by compositional and temporal variations in which the plutons evolved from metaluminous monzodiorites to peraluminous granites, and the volcanic rocks evolved from andesites to rhyolites. This second arc was emplaced into Neoproterozoic metamorphic basement, Paleozoic sedimentary rocks, Permian igneous rocks, and Triassic sedimentary rocks. The third continental margin arc, which is located in the northern block of the Ibagué Batholith, formed from the Late Jurassic (ca. 158 Ma) to the Early Cretaceous (ca. 138 Ma). It is characterized by at least two pulses that are represented by a western syntectonic pluton and an eastern post–tectonic pluton, both of which have calc–alkaline metaluminous tonalitic compositions, that are separated by a band of metamorphic basement rocks of Late Jurassic age, not Neoproterozoic or Permian – Triassic as was previously thought.

Keywords: *continental arc magmatism, U–Pb zircon geochronology, metamorphic basement, peraluminous magmatism, metaluminous magmatism.*

1 grodriguez@sgc.gov.co
Servicio Geológico Colombiano
Dirección de Geociencias Básicas
Grupo de Estudios Geológicos Especiales
Calle 75 n.° 79A–51
Medellín, Colombia

2 amcorrea@sgc.gov.co
Servicio Geológico Colombiano
Dirección de Geociencias Básicas
Grupo de Estudios Geológicos Especiales
Calle 75 n.° 79A–51
Medellín, Colombia

3 gilbertozapatag@yahoo.com
Servicio Geológico Colombiano
Calle 24A n.° 50A–31 Ap. 901
Edificio Santa Clara
Bello, Colombia

4 isabelara84@hotmail.com
Carrera 14 n.° 22–18
Cartago, Valle del Cauca, Colombia

5 gbando@sgc.gov.co
Servicio Geológico Colombiano
Dirección de Geociencias Básicas
Grupo de Estudios Geológicos Especiales
Calle 75 n.° 79A–51
Medellín, Colombia

6 jpzapata@sgc.gov.co
Servicio Geológico Colombiano
Dirección de Geociencias Básicas
Grupo de Estudios Geológicos Especiales
Calle 75 n.° 79A–51
Medellín, Colombia

7 jbermudez@sgc.gov.co
Servicio Geológico Colombiano
Dirección de Geociencias Básicas
Grupo de Estudios Geológicos Especiales
Calle 75 n.° 79A–51
Medellín, Colombia

* Corresponding author

Supplementary Information:

S: https://www.sgc.gov.co/LibroGeologiaColombia/tgc/sgcpubesp36201904s.pdf

Citation: Rodríguez–García, G., Correa–Martínez, A.M., Zapata–García, G., Arango–Mejía, M.I., Obando–Erazo, G., Zapata–Villada, J.P. & Bermúdez, J.G. 2020. Diverse Jurassic magmatic arcs of the Colombian Andes: Constraints from petrography, geochronology, and geochemistry. In: Gómez, J. & Pinilla–Pachon, A.O. (editors), The Geology of Colombia, Volume 2 Mesozoic. Servicio Geológico Colombiano, Publicaciones Geológicas Especiales 36, p. 117–170. Bogotá. https://doi.org/10.32685/pub.esp.36.2019.04

Resumen Nuevos datos de campo, petrografía, litogeoquímica y geocronología U–Pb en circón de plutones jurásicos del Macizo de Santander, plutones y volcanitas del Valle Superior del Magdalena y plutones del bloque norte del Batolito de Ibagué demuestran que la actividad ígnea jurásica registrada en varios bloques de los Andes colombianos comenzó en el Triásico Tardío y finalizó en el Cretácico Temprano. Este magmatismo se desarrolló en por lo menos tres arcos magmáticos diferentes, durante intervalos de tiempo claramente definidos y sobre basamentos con distintas características. El primer arco de margen continental estacionario estuvo activo entre el Triásico Tardío (ca. 214 Ma) y el Jurásico Temprano (ca. 184 Ma). El registro de este arco se encuentra en el Macizo de Santander y está representado por plutones principalmente monzograníticos, peraluminosos, generados por múltiples pulsos magmáticos que involucraron diversos grados de fusión cortical. En este estudio se propone, por primera vez, que la mayor parte del arco se emplazó en basamento principalmente ordovícico y otra menor en basamento neoproterozoico temprano. El segundo arco se localiza en el Valle Superior del Magdalena y se desarrolló entre el Jurásico Temprano (ca. 197 Ma) y el Jurásico Medio (ca. 167 Ma) durante al menos tres pulsos magmáticos relacionados con la migración del arco. Esto se evidencia por las variaciones composicionales y temporales en las cuales los plutones evolucionaron de monzodioritas metaluminosas a granitos peraluminosos y las rocas volcánicas, de andesitas a riolitas. El segundo arco se emplazó en basamento metamórfico neoproterozoico, sedimentario paleozoico, ígneo pérmico y sedimentario triásico. El tercer arco de margen continental se encuentra localizado en el bloque norte del Batolito de Ibagué y se formó durante el Jurásico Tardío (ca. 158 Ma) al Cretácico Temprano (ca. 138 Ma). Se caracteriza por al menos dos pulsos representados en un plutón sintectónico occidental y un plutón postectónico oriental, ambos compuestos por tonalitas metaluminosas calcoalcalinas separadas por una franja de rocas metamórficas del basamento de edad jurásica temprana y no del Neoproterozoico ni del Pérmico–Triásico como se consideraba anteriormente.

Palabras clave: *magmatismo de arco continental, geocronología U–Pb en circón, basamento metamórfico, magmatismo peraluminoso, magmatismo metaluminoso.*

1. Introduction

The Upper Triassic – Jurassic igneous rocks of the Colombian Andes are plutonic and volcanic rocks with ages between ca. 214 Ma to ca. 145 Ma that are distributed in tectonic blocks located on the eastern margin of the Central Cordillera, Magdalena River Valley, Eastern Cordillera, Sierra Nevada de Santa Marta, and Upper Guajira (Figure 1a). These units have been studied by several authors (Álvarez, 1983; Aspden et al., 1987; Bustamante et al., 2010; Gendall et al., 2000; Goldsmith et al., 1971; Leal–Mejía, 2011; Mantilla–Figueroa et al., 2013; Noble et al., 1997; Rodríguez et al., 2018a; van der Lelij, 2013; van der Lelij et al., 2016; Villagómez et al., 2011; Ward et al., 1973).

Previous tectonic models of the Jurassic magmatism in the northern Andes have been based on two hypotheses: 1) the development of an intracontinental rift related to the breakup of Pangaea (Cediel et al., 2003; Cochrane et al., 2014; Mojica et al., 1996; Pindell & Dewey, 1982; Ross & Scotese, 1988) and 2) the establishment of continental arc magmatism (Bustamante et al., 2010, 2016; Leal–Mejía, 2011; McCourt et al., 1984; Meschede & Frisch, 1998; Rodríguez et al., 2015a; Spikings et al., 2015; Toussaint, 1995; van der Lelij et al., 2016; Villagómez et al., 2015; Zapata et al., 2016a). The latter is the consensus model; however, different authors have presented several variations. Spikings et al. (2015) suggest that an arc formed by a single subduction zone located west of the South American margin was active between 209 and 114 Ma, whereas Bustamante et al. (2016) proposed that a stationary continental margin arc was active for at least 40 Ma due to oblique convergence between the Farallón Plate and the northwestern margin of South America. Bayona et al. (2010) and Villagómez et al. (2015) proposed that a continental arc, encompassing the blocks of Jurassic rocks in the Upper Magdalena, Central Cordillera, serranía de San Lucas, and Sierra Nevada de Santa Marta, moved from a southern

Figure 1. (a) Occurrences of Jurassic igneous rocks in the Colombian Andes. Retrieved and modified from Gómez et al. (2015a). Data source: U–Pb ages from several authors compiled by Gómez et al. (2015b). **(b)** Proposed distribution of metamorphic basement in the regions related to Jurassic magmatism and volcanism.

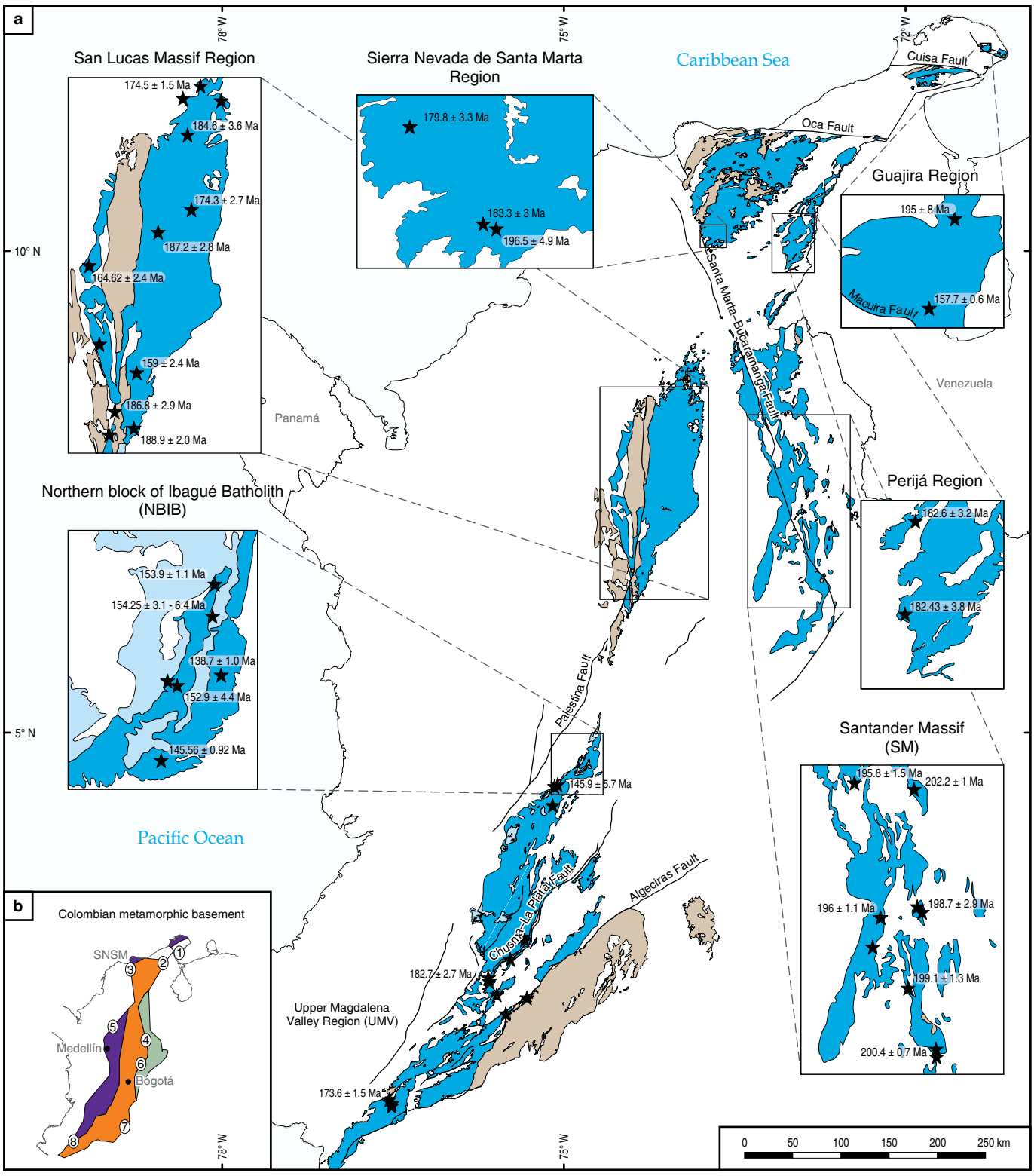
a
78° W
75° W
72° W
10° N
5° N
San Lucas Massif Region
174.5 ± 1.5 Ma
184.6 ± 3.6 Ma
174.3 ± 2.7 Ma
187.2 ± 2.8 Ma
164.62 ± 2.4 Ma
159 ± 2.4 Ma
186.8 ± 2.9 Ma
188.9 ± 2.0 Ma
Sierra Nevada de Santa Marta Region
179.8 ± 3.3 Ma
183.3 ± 3 Ma
196.5 ± 4.9 Ma
Caribbean Sea
Cuisa Fault
Oca Fault
Guajira Region
195 ± 8 Ma
157.7 ± 0.6 Ma
Macuira Fault
Santa Marta–Bucaramanga Fault
Venezuela
Panamá
Northern block of Ibagué Batholith (NBIB)
153.9 ± 1.1 Ma
154.25 ± 3.1 - 6.4 Ma
138.7 ± 1.0 Ma
152.9 ± 4.4 Ma
145.56 ± 0.92 Ma
Perijá Region
182.6 ± 3.2 Ma
182.43 ± 3.8 Ma
Palestina Fault
145.9 ± 5.7 Ma
Pacific Ocean
Santander Massif (SM)
195.8 ± 1.5 Ma
202.2 ± 1 Ma
196 ± 1.1 Ma
198.7 ± 2.9 Ma
199.1 ± 1.3 Ma
200.4 ± 0.7 Ma
Algeciras Fault
Chusma–La Plata Fault
182.7 ± 2.7 Ma
Upper Magdalena Valley Region (UMV)
173.6 ± 1.5 Ma
b
Colombian metamorphic basement
SNSM
Medellín
Bogotá
0 50 100 150 200 250 km
Jurassic units (plutons and volcanic units)
Jurassic basement
Precambrian basement
Triassic – Jurassic Central Cordillera basement
Paleozoic metamorphic basement
Neoproterozoic basement
U–Pb
1 Cuisa Fault
2 Oca Fault
3 Santa Marta Fault
4 Bucaramanga Fault
5 Espíritu Santo Fault
6 Altamira Fault
7 Algeciras Fault
8 Suaza Fault

location northward (Bayona et al., 2006, 2010), which masked the original tectonic relationships between the units (Bayona et al., 2010; Villagómez et al., 2015; Zapata et al., 2016a; Zuluaga et al., 2017).

We present new petrographic, whole–rock geochemical, and LA–ICP–MS U–Pb zircon geochronological data and compile published data from three Colombian blocks: the Santander Massif (SM), Upper Magdalena Valley (UMV), and northern block of the Ibagué Batholith (NBIB), to understand the Jurassic geological evolution of the northern Andes as well as the distribution of blocks and metamorphic terranes associated with the Jurassic plutonism and volcanism in Colombia. The compositional and geochronological differences between the metamorphic basement units and Jurassic rocks of the three blocks are discussed. A redefinition of the northern section of the Ibagué Batholith is also proposed based on geological data that indicate that it is not homogeneous.

2. Geologic Framework

The geologic configuration of Colombia is the result of the interactions between the Caribbean, South American, North American, and Pacific Plates, which throughout geologic history have formed the Andean province on the northwestern margin of South America (Mantilla–Figueroa et al., 2013; van der Lelij et al., 2016; Zuluaga et al., 2017). This province is composed of accreted and diverse continental and oceanic terranes that amalgamated during multiple subduction and orogenic events from Proterozoic to Cenozoic times (Cediel et al., 2003; Etayo–Serna et al., 1983; Kennan & Pindell, 2009; Restrepo & Toussaint, 1988, 1989). Their boundaries remain unclear; however, the province is separated from the crystalline basement of the Amazonian Craton by the Borde Llanero Fault (Forero–Suárez, 1990).

This Andean province includes the SM, the UMV, and the NBIB, which are the focus of this study (Figure 1a).

2.1. Santander Massif (SM)

The SM is located in the Colombian Eastern Cordillera and is part of a triangular regional block that is delimited by the Santa Marta–Bucaramanga Fault on the west, the Oca Fault on the north, and the Boconó Fault on the east (Cediel et al., 2003; Mantilla–Figueroa et al., 2013; van der Lelij et al., 2016).

The metamorphic basement of the SM includes the Bucaramanga Gneiss, the Silgará Formation, and granitic orthogneisses (Ward et al., 1973). The Bucaramanga Gneiss consists of sillimanite–cordierite gneisses with garnet, amphibolic gneisses, quartz feldspar granofels, and amphibolites with migmatitic structures (Ward et al., 1973), and it is traditionally considered to have a Proterozoic age and to be related to the Grenville Orogeny (Cordani et al., 2005; García & Ríos, 1999; Goldsmith et al., 1971; Ordóñez–Carmona et al., 2006; Restrepo–Pace et al., 1997; Ward et al., 1973). However, recent studies report metamorphic ages of approximately 477 Ma (van der Lelij, 2013; van der Lelij et al., 2016) that are associated with the Caparonensis Orogeny, which is also known as the Famatinian Orogeny (van der Lelij, 2013; van der Lelij et al., 2016; Zuluaga et al., 2017). Overlying the Bucaramanga Gneiss, the Silgará Formation (Ward et al., 1973), which is also called the Silgará Schists by Mantilla–Figueroa et al. (2016), consists of Paleozoic schists, phyllites, metamudstones, metasandstones, and marbles (Clavijo et al., 2008; Mantilla–Figueroa et al., 2012; Ordóñez–Carmona et al., 2006; Ríos et al., 2003; van der Lelij et al., 2016; Zuluaga et al., 2017). These rocks are possibly related to the main Famatinian orogenic event (Mantilla–Figueroa et al., 2016; Restrepo–Pace, 1995; Restrepo–Pace & Cediel, 2010). Deformed Ordovician granitoids ("Orthogneiss Unit" of Ward et al., 1973) intrude the Bucaramanga Gneiss and the Silgará Formation. These three units record a common Ordovician metamorphic event (Mantilla–Figueroa et al., 2012, 2013; Restrepo–Pace et al., 1997) that affected the entire SM basement (van der Lelij et al., 2016; Zuluaga et al., 2017).

Paleozoic magmatism is represented by orthogneisses and plutonic and volcanic rocks that originated during magmatic events before and after the Famatinian Orogeny, most of which developed in a continental arc environment. The igneous plutons are Ordovician, Silurian, Lower Devonian, and Carboniferous (Leal–Mejía, 2011; Mantilla–Figueroa et al., 2012; Restrepo–Pace, 1995; Rodríguez et al., 2017a; Ulloa & Rodríguez, 1982; van der Lelij, 2013; van der Lelij et al., 2016). Mesozoic magmatism occurred mainly during the Late Triassic to Late Jurassic and is represented by batholiths and subordinate stocks in the core and along the western edge of the SM (Figure 2). These include the Mogotes Batholith (Correa–Martínez et al., 2016; Ward et al., 1973), Pescadero Granite (Ward et al., 1973; Zapata et al., 2016b), Santa Bárbara Monzogranite (Rodríguez et al., 2017b; Ward et al., 1973, 1977a); La Corcova Monzogranite (Goldsmith et al., 1971; Rodríguez et al., 2017c; Ward et al., 1973), Páramo Rico Pluton (Dörr et al., 1995; Royero & Clavijo, 2001; Ward et al., 1973), San Martín Tonalite (Arias–Tauta & Vargas–Higuera, 1978; Rodríguez et al., 2017d), Rionegro Monzogranite (Arango et al., 2016; Arias–Tauta & Vargas–Higuera, 1978; Daconte & Salinas, 1980a; Ward et al., 1973), and three porphyritic bodies: the Alto de Los Cacaos Rhyolite, San Joaquín Rhyolite, and El Uvo Rhyolite (Correa–Martínez et al., 2018; Rodríguez et al.,

Figure 2. Distribution and U–Pb zircon ages of Late Triassic – Early Jurassic plutons in the Santander Massif. Modified from Ward et al. (1973, 1977a, 1977b, 1977c, 1977d, 1977e, 1977f); Daconte & Salinas (1980b, 1980c); Vargas & Arias (1981a, 1981b); Vargas et al. (1984); Clavijo (1994); Royero & Clavijo (2001); and Arias & Morales (2003).

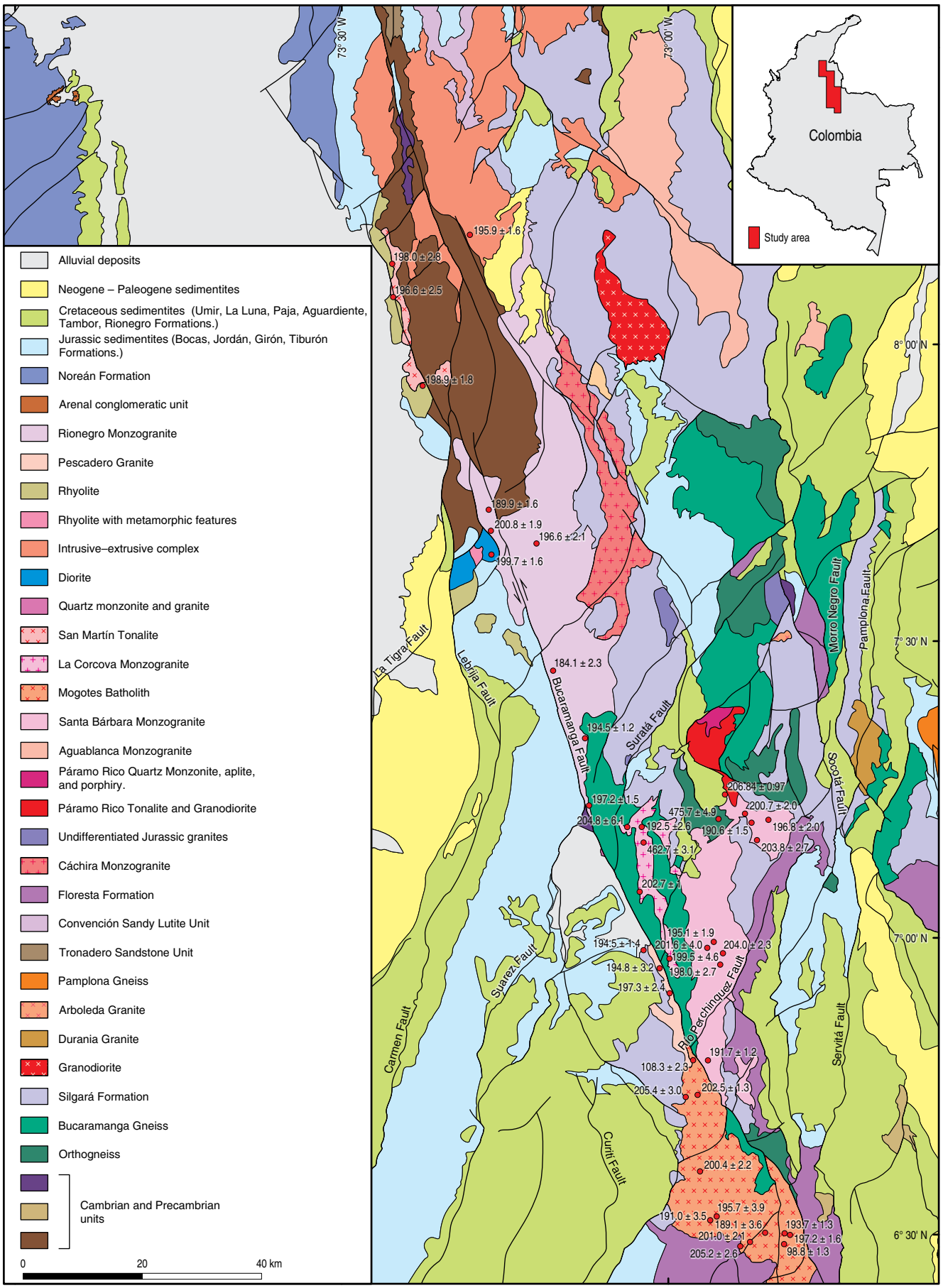
Colombia
Study area
Alluvial deposits
Neogene – Paleogene sedimentites
Cretaceous sedimentites (Umir, La Luna, Paja, Aguardiente, Tambor, Rionegro Formations.)
Jurassic sedimentites (Bocas, Jordán, Girón, Tiburón Formations.)
Noreán Formation
Arenal conglomeratic unit
Rionegro Monzogranite
Pescadero Granite
Rhyolite
Rhyolite with metamorphic features
Intrusive–extrusive complex
Diorite
Quartz monzonite and granite
San Martín Tonalite
La Corcova Monzogranite
Mogotes Batholith
Santa Bárbara Monzogranite
Aguablanca Monzogranite
Páramo Rico Quartz Monzonite, aplite, and porphiry.
Páramo Rico Tonalite and Granodiorite
Undifferentiated Jurassic granites
Cáchira Monzogranite
Floresta Formation
Convención Sandy Lutite Unit
Tronadero Sandstone Unit
Pamplona Gneiss
Arboleda Granite
Durania Granite
Granodiorite
Silgará Formation
Bucaramanga Gneiss
Orthogneiss
Cambrian and Precambrian units
0
20
40 km
73° 30' W
73° 00' W
8° 00' N
7° 30' N
7° 00' N
6° 30' N
La Tigra Fault
Lebrija Fault
Bucaramanga Fault
Suratá Fault
Morro Negro Fault
Pamplona Fault
Soapta Fault
Suarez Fault
Carmen Fault
Río Perchinquez Fault
Servitá Fault
Curití Fault
195.9 ± 1.6
198.0 ± 2.8
196.6 ± 2.5
198.9 ± 1.8
189.9 ± 1.6
200.8 ± 1.9
196.6 ± 2.1
199.7 ± 1.6
184.1 ± 2.3
194.5 ± 1.2
197.2 ± 1.5
204.8 ± 6.1
206.84 ± 0.97
200.7 ± 2.0
475.7 ± 4.9
192.5 ± 2.6
190.6 ± 1.5
196.8 ± 2.0
203.8 ± 2.7
462.7 ± 3.1
202.7 ± 1
195.1 ± 1.9
194.5 ± 1.4
201.6 ± 4.0
204.0 ± 2.3
199.5 ± 4.6
194.8 ± 3.2
198.0 ± 2.7
197.3 ± 2.4
191.7 ± 1.2
108.3 ± 2.3
205.4 ± 3.0
202.5 ± 1.3
200.4 ± 2.2
195.7 ± 3.9
191.0 ± 3.5
189.1 ± 3.6
193.7 ± 1.3
201.0 ± 2.1
197.2 ± 1.6
205.2 ± 2.6
98.8 ± 1.3

2018b; Zapata et al., 2018). Few small microtonalite dikes of Albian – Cenomanian age also intrude the Triassic – Jurassic granitoids (Correa–Martínez et al., 2016).

Cretaceous marine sedimentary successions discordantly overlie the Paleozoic and/or Jurassic rocks (Mojica & Villarroel, 1984; Ward et al., 1973). Porphyritic bodies with Miocene gold mineralization exist locally (Leal–Mejía, 2011; Mantilla–Figueroa et al., 2013).

2.2. Upper Magdalena Valley (UMV)

The UMV is located between the Colombian Central and Eastern Cordilleras in the southern sections of the Magdalena River Valley.

The metamorphic basement of the UMV includes migmatites, granofels, granulites, anatectic granites, and gneisses of granulite to high amphibolite facies that form the Garzón Group, the Guapotón and Mancagua Gneisses, Las Minas Migmatites, and El Recreo Granite of Neoproterozoic age (Ibañez–Mejia et al., 2011; Jiménez–Mejía et al., 2006; Kroonenberg & Diederix, 1982; Rodríguez, 1995a, 1995b; Rodríguez et al., 2003; Velandia et al., 2001a, 2001b). Paleozoic sedimentary rocks, such as the Mudstones and Granadillo Limestones, La Jagua Paleozoic, El Hígado Formation, and La Batalla Limestones and Sandstones, discordantly overlie the Precambrian crystalline basement (Mojica et al., 1988; Velandia et al., 2000, 2001b; Villarroel & Mojica, 1988; Stibane & Forero, 1969). The Permian units are represented by La Plata Granite continental margin arc granitoids that intrude the basement rocks (Leal–Mejía, 2011; Rodríguez, 1995a; Rodríguez et al., 1998, 2017a; Velandia et al., 2001b).

The Neoproterozoic basement, Paleozoic sedimentary formations, Permian arc granitoids, and Triassic limestones are intruded by Jurassic plutons and covered by Jurassic volcanic rocks (Rodríguez et al., 2018a) and continental and marine sedimentary successions of late Mesozoic and Cenozoic age. These rocks are faulted and uplifted in blocks bounded by strike–slip and thrust faults, such as the Algeciras Fault (Velandia et al., 2005), the Betania–El Agrado Fault, and La Plata–Chusma Fault, which expose the Jurassic rocks and basement to varying degrees. None of these faults correspond to the boundary of the Neoproterozoic metamorphic basement, which appears to be fragmented. Similar blocks with Jurassic rocks border the western margin of the South American Plate, such as the serranía de San Lucas, Sierra Nevada de Santa Marta, and Upper Guajira, where the Neoproterozoic basement crops out near fragments of Permian granitoids and Jurassic arc rocks (Rodríguez et al., 2018a).

The assemblage described above is separated by the Avirama Fault from the Tahamí Terrane (Restrepo & Tousssaint, 1989) or the Cajamarca Complex (Maya & González, 1995). These metamorphic terranes consist of schists, quartzites, gneisses, granofels, and amphibolites (Feininger et al., 1972; González, 1980; Hall et al., 1972; Maya & González, 1995; Restrepo & Toussaint, 1988; Rodríguez et al., 2005) that are separated into blocks that have yielded Triassic (Martens et al., 2014; Restrepo et al., 2009; Vinasco et al., 2006), Jurassic (Blanco–Quintero et al., 2014), and Cretaceous ages (Restrepo et al., 2012; Rodríguez et al., 2016a).

2.3. Northern Block of the Ibagué Batholith (NBIB)

The Ibagué Batholith is exposed along the eastern slope of the Central Cordillera from Armero, in the Tolima Department, to La Plata, in the Huila Department (Nelson, 1957, 1962). It is considered to be the largest Jurassic pluton in Colombia, and it covers approximately 11 000 km^2 (Bustamante et al., 2016; Gómez et al., 2015a; Nelson, 1957, 1962; Núñez, 2001, 2002; Rodríguez & Núñez, 1999; Velandia et al., 2001b). A summary of the geochronological data from other studies is presented in Table 1.

Based on whole–rock geochemical data, Álvarez (1983) noted the absence of a genetic relationship between the Ibagué Batholith and several intrusives that outcrop to the south (e.g., the Páez River Pluton, the San Agustín and Gallego granitoids, and the Suaza Pluton). He suggested that these plutons likely corresponded to previous magmatic pulses. More recent U–Pb zircon geochronology and whole–rock geochemistry studies have enabled researchers to divide and separate large blocks, such as the Páez Quartz Monzodiorite (Álvarez, 1983; Rodríguez et al., 2018a; Zapata et al., 2015) and La Plata Granite (Rodríguez, 1995b, 2018a; Velandia et al., 2001b), and show that the so–called Ibagué Batholith is composed of different plutons that were generated in a continental arc environment in the Permian and Jurassic. These plutons were emplaced into different metamorphic basement rocks in different geotectonic positions (Rodríguez et al., 2018a). The results from the "Jurassic Magmatism of Colombia" project also show that the northern part of the Ibagué Batholith, north of the Ibagué Fault, is not a homogeneous unit, and the geological division of this block, called the northern block of the Ibagué Batholith (NBIB), is presented in this study.

The metamorphic basement of the NBIB consists of gneisses, amphibolites, quartzites, sericitic quartz–schist, greenschist, and graphitic schists known as the Tierradentro Gneisses and Amphibolites, which are likely Precambrian (Barrero & Vesga, 1976; Núñez, 2001). Bustamante et al. (2017) found Permian and Triassic crystallization ages in the orthogneisses and amphibolites of the Tierradentro protolithic unit, respectively, and interpreted that the granodioritic magma of the Ibagué Batholith intruded into Permian – Triassic basement. Farther south, Zapata et al. (2016a) concluded that this metamorphic basement, which is represented by La Cocha–Río Téllez Migmatitic Com-

Table 1. K/Ar, Ar–Ar, and LA–ICP–MS U–Pb zircon ages in the NBIB from other authors.

Sample	Latitude N	Longitude W	Classification	Unit	Age (Ma)	Method	Source
GCC6	4° 47' 44.27''	75° 2' 5.75''		Anzoátegui Metatonalite	158.17 +1.17/–0.35	U–Pb	Bustamante et al. (2016)
Cl11	4° 38' 47.63''	75° 2' 15.17''		Anzoátegui Metatonalite	152.61 +1.82/–0.74	U–Pb	Bustamante et al. (2016)
IGM–69974	4° 39' 35.99''	74° 57' 0.06''	Quartz diorite	Ibagué Tonalite	142 ± 9	K/Ar–Hbl	Vesga & Barrero (1978)
Cl 9B	4° 44' 40.13''	74° 57' 35.90''		Ibagué Tonalite	142.07 +1.08/–0.86	U–Pb	Bustamante et al. (2016)
Cl2	4° 39' 36.47''	74° 57' 54.76''		Ibagué Tonalite	143.52 +1.38/–0.64	U–Pb	Bustamante et al. (2016)
Cl15	4° 51' 53.58''	74° 56' 19.71''		Ibagué Tonalite	145.71 +0.72/–1.42	U–Pb	Bustamante et al. (2016)
	4° 39' 36.02''	75° 0' 0.05''		Tierradentro Gneisses and Amphibolites	146 ± 3	K–Ar–RT	McCourt et al. (1984)
DV04	4° 47' 0.19''	74° 58' 31.44''	Diorite	Tierradentro Gneisses and Amphibolites	159.2 ± 5.2	Ar–Ar–Hbl	Villagómez et al. (2011)

plex, may correspond to a Jurassic terrane that is correlated with the Jurassic metamorphic assemblage southwest of the NBIB that was studied by Blanco–Quintero et al. (2014).

3. Materials and Methods

To analyze the Jurassic magmatism in the SM, UMV, and NBIB, regional mapping studies and published articles were compiled. Field and sampling campaigns and petrography, geochemistry, and geochronology analyses were performed. Finally, the results were analyzed and interpreted separately for each block.

3.1. Petrography

The petrographic analyses included descriptions of thin sections from new samples and the reanalysis of samples from previous projects of the Servicio Geológico Colombiano (SGC). The plutonic igneous rocks were classified according to Streckeisen (1974), and the volcanic rocks were classified according to Streckeisen (1979) based on the recommendations for the classification and nomenclature of igneous rocks provided by Le Maitre et al. (2002). The mineral abbreviations in the rock descriptions are based on Siivola & Schmid (2007).

3.2. Whole–Rock Geochemical Analyses

Whole–rock analyses were performed in the laboratory of the SGC in Bogotá. Major oxides were determined using the X–ray fluorescence (XRF) method, including trace elements such as V, Mo, Nb, Ta, W, Zr, and Hf, in an Axios–Mineral PANalytical XRF spectrometer. Major oxides were quantified in melted samples with lithium metaborate and tetraborate, and minor elements were quantified in pressed samples. MRC–GSP–2 was used as a reference, and it produced a difference of <5% between the certified and measured values. Major oxides were recalculated on an anhydrous basis before interpretation. Trace elements were measured by inductively coupled plasma mass spectrometry (ICP–MS) in a PerkinElmer NEXION ICP mass spectrometer. The rock samples were dissolved by multi–acid digestion with strong inorganic acids (HF, HNO_3, $HClO_4$, and HCl). The process was conducted in an open system using different temperature ramps and heating times. The AGV–2 (andesite) USGS references were used with most of the trace elements and produced a difference of <10% between the certified and measured values. The elements Eu, Gd, and Tb produced higher values than the certified reference.

The rock samples for the geochemical analyses were selected based on: 1) no evidence of high–grade mineral alteration under microscopic inspection and 2) Loss on ignition (LOI) values lower than 2%.

3.3. U–Pb Zircon Geochronology

The U–Pb zircon dating was performed at the Isotopic Studies Laboratory (LEI) at the Centro de Geociencias of the Universidad Autónoma de México (UNAM) and the Laser Ablation Laboratory of the SGC.

The concentration of zircon crystals was obtained by panning and using a Frantz isodynamic magnetic separator. Zircon grains from each sample were selected under an Olympus binocular microscope and subsequently embedded in epoxy resin (Struers EpoFix).

Cathodoluminescence (CL) images of the zircons were acquired using an ELM–3R Luminoscope (Marshall, 1988) at LEI, UNAM. The U–Pb zircon isotopic analyses were performed using the laser ablation method (LA–ICP–MS) with a Resolution M50 "Resonetics" consisting of an LPX 220 193 nm wavelength excimer laser coupled to a Thermo Scientific X–Series quadrupole plasma mass spectrometer (ICP–MS). The diameter of the laser beam was 23 μm. The analyses included measurements of the concentrations of Th, Si, P, Ti, Y, Zr, Nb, Hf, and rare earth elements (REE) in the zircon crystals, which

were used as petrogenetic tracers. The methodological details are available in Solari et al. (2010). A glass standard (NIST 610) and two natural zircon standards, including one primary (91500; Wiedenbeck et al., 1995) and one secondary (Plešovice; Slama et al., 2008), were intercalated in the analytical sequences for quality control.

Prior to the isotopic analyses at the Laser Ablation Laboratory, SGC, cathodoluminescence images of the zircons were acquired. Some samples were photographed at the Lithological Characterization Laboratory (LCL) of the Universidad Nacional de Colombia, Red Nacional de Laboratorios de Geociencias, using a CITL CL8200 MK–5 Optical Cathodoluminescence System adapted to a Leica DM 2500 P versatile modular polarization microscope at 220 μA and a 15 kV current. Cathodoluminescence, secondary, and backscattered images of other samples were acquired using a JEOL scanning electron microscope, model JSM IT–300LV, operating at high and low vacuum conditions. It was equipped with a tungsten filament that works at accelerating voltages of electrons from 300 V to 30 kV and was equipped with four detectors: secondary (SE) and backscattered (BED) electron and Energy–Dispersive X–ray Spectroscopy (EDS, OXFORD 51–XMX 1181) and cathodoluminescence (CL; Gatan miniCL EGA 0028). Isotopic analyses were performed at the Laser Ablation Laboratory, SGC, using the LA–ICP–MS method in an Element 2 ICP–MS coupled to a Photon Machines laser ablation system with a 193 nm Excite laser. The ablation points were 30 micrometers in diameter. The Plešovice, 91500, and M. Dromedary crystals were used as reference standards. The Iolite IGOR-Pro software was used for data reduction. Integration times of 0 s to 38 s were used for the baseline, whereas integration times of 32.5 s to 8 s were used for the samples and reference standards. The final results correspond to mean data assessed after discriminating at 2 standard deviations. The data were processed using the routines of the Isoplot V3.5 software, and the correction of common lead was calculated according to the evolution model of Stacey & Kramers (1975). The geochronological data were plotted using Isoplot (Ludwig, 2012).

4. Results

4.1. Santander Massif

This study presents the results from the following plutons: the Mogotes Batholith, Pescadero Granite, Santa Bárbara Monzogranite, La Corcova Monzogranite, Páramo Rico Pluton, San Martín Tonalite, Rionegro Monzogranite, and three porphyritic bodies, including the Alto de Los Cacaos Rhyolite, San Joaquín Rhyolite, and El Uvo Rhyolite (Figure 2).

Most of the plutons intrude metasedimentary rocks of the Bucaramanga Gneiss and the Silgará Formation and metaigneous felsic rocks of the granitic orthogneiss. Additionally, the Rionegro Monzogranite intrudes the Cáchira Monzogranite in the east and a unit of amphibolites and migmatites that have been traditionally included as a part of the Bucaramanga Gneiss in the west. The San Martín Tonalite is in faulted contact with the Rionegro Monzogranite along the Bucaramanga Fault and is apparently in both intrusive and faulted contact with the overlying amphibolites and migmatites.

4.1.1. Petrography

The Late Triassic – Early Jurassic plutons of the SM consist of monzogranites, granodiorites, syenogranites, and tonalites (Figures 3, 4b, 4d) with no notable changes in their interior. Subvolcanic rocks of rhyolitic and dacitic compositions are also present (Figures 3, 4c). All of these rocks are white mottled with pink and black, gray mottled with black, and pink mottled with white spots. They are equigranular to inequigranular, fine to medium–grained, and some are bimodal. Graphic, perthitic, and symplectitic textures are locally developed. The rocks contain pink and white potassium feldspar, plagioclase, and quartz, and the most common mafic mineral is biotite, although rocks with hornblende and marginal rocks with clinopyroxene occur locally. The accessory minerals include apatite, magnetite, ilmenite, pyrite, titanite, allanite, and very rare garnet and muscovite. Chlorite, sericite, epidote, and clay aggregates are common alteration minerals. Enclaves of microdiorites, andesites, and dacites are present and may contain xenoliths of the Bucaramanga Gneiss, orthogneisses, and the Silgará Formation (Figure 4e, 4f).

The plutons are intersected by dikes and veins of syenogranites and aplitic saccharoidal and granophyric monzogranites, which have been described as alaskites (Mantilla–Figueroa et al., 2013). Dikes of micro quartz diorites, microdiorites, andesites, quartz latites, and rhyolites are also present.

4.1.2. Geochemistry

The Triassic – Jurassic granitoids of the SM have SiO_2 contents ranging from 65% to 79% in most rocks, K_2O ranging from 3% to 5.4%, and TiO_2 <1%. TiO_2, Al_2O_3, MgO, CaO, P_2O_5, and FeO decrease and K_2O increases with increasing SiO_2 concentration. The chemical classification of the rocks is highly consistent with the petrographic classification, with a predominance of granitic rocks and subordinate granodiorites, quartz monzonites, and quartz monzodiorites. The Mogotes Batholith and the Rionegro Monzogranite have the greatest lithological variations, as shown in the TAS diagram of Middlemost (1985) (Figure 5a; see Table 1, Supplementary Information).

The rocks that plot in the field of the high–K calc–alkaline series (Figure 5b, 5c) are mostly peraluminous (Figure 5d) and felsic with A/CNK ratios ranging from 1 to 1.4 and A/NK ratios ranging from 1 to 2. This indicates a contribution of crustal material to the parental magma as well as high magmatic

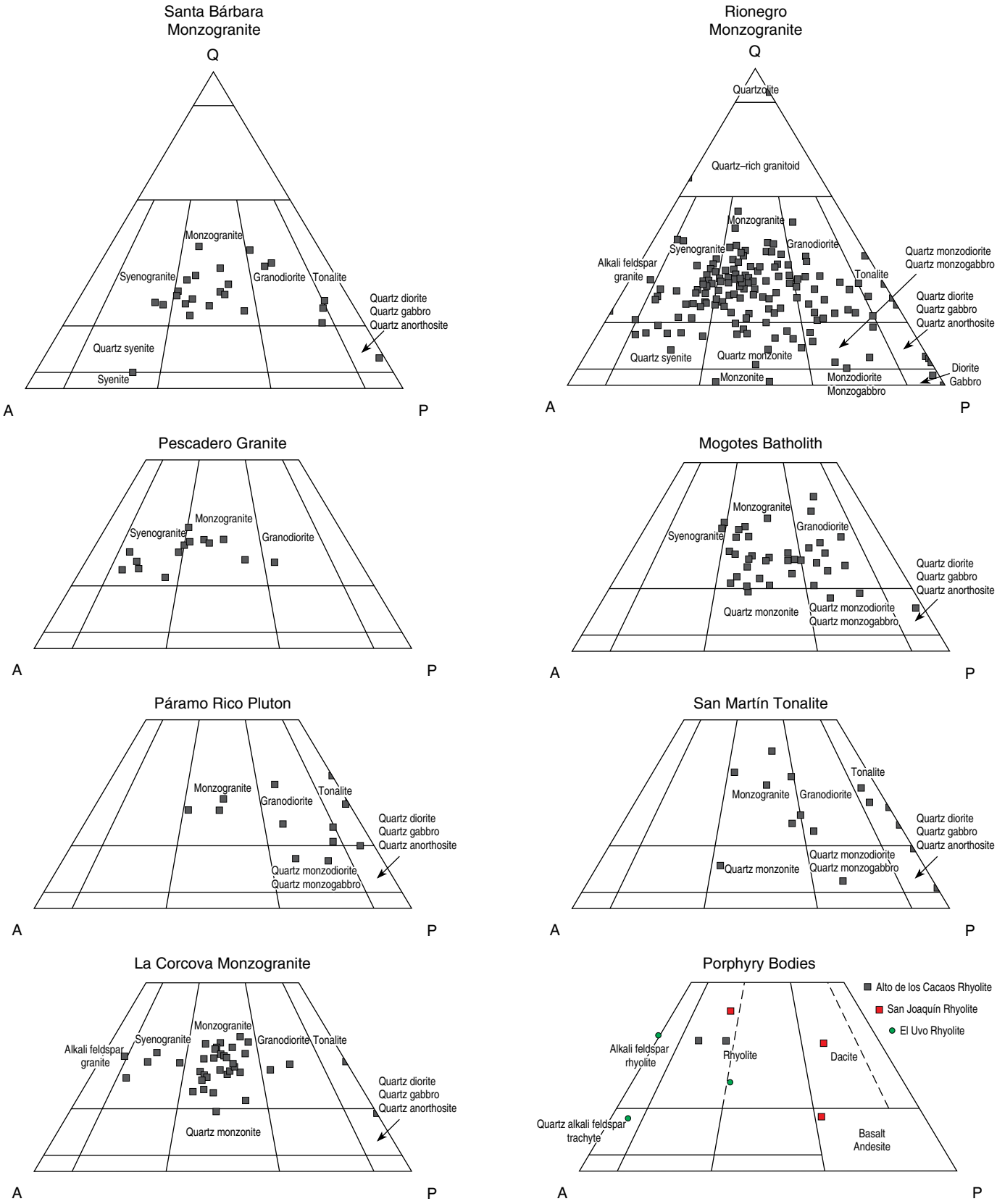

Figure 3. Modal compositions of Triassic – Jurassic granitoids from the Santander Massif in Quartz, Alkali feldspar, Plagioclase, Feldspathoid (QAPF) diagrams of Streckeisen (1974, 1979). Data sources: Arango et al. (2016); Correa–Martínez et al. (2018); Rodríguez et al. (2017c, 2017d, 2018c); Zapata et al. (2016b, 2017b).

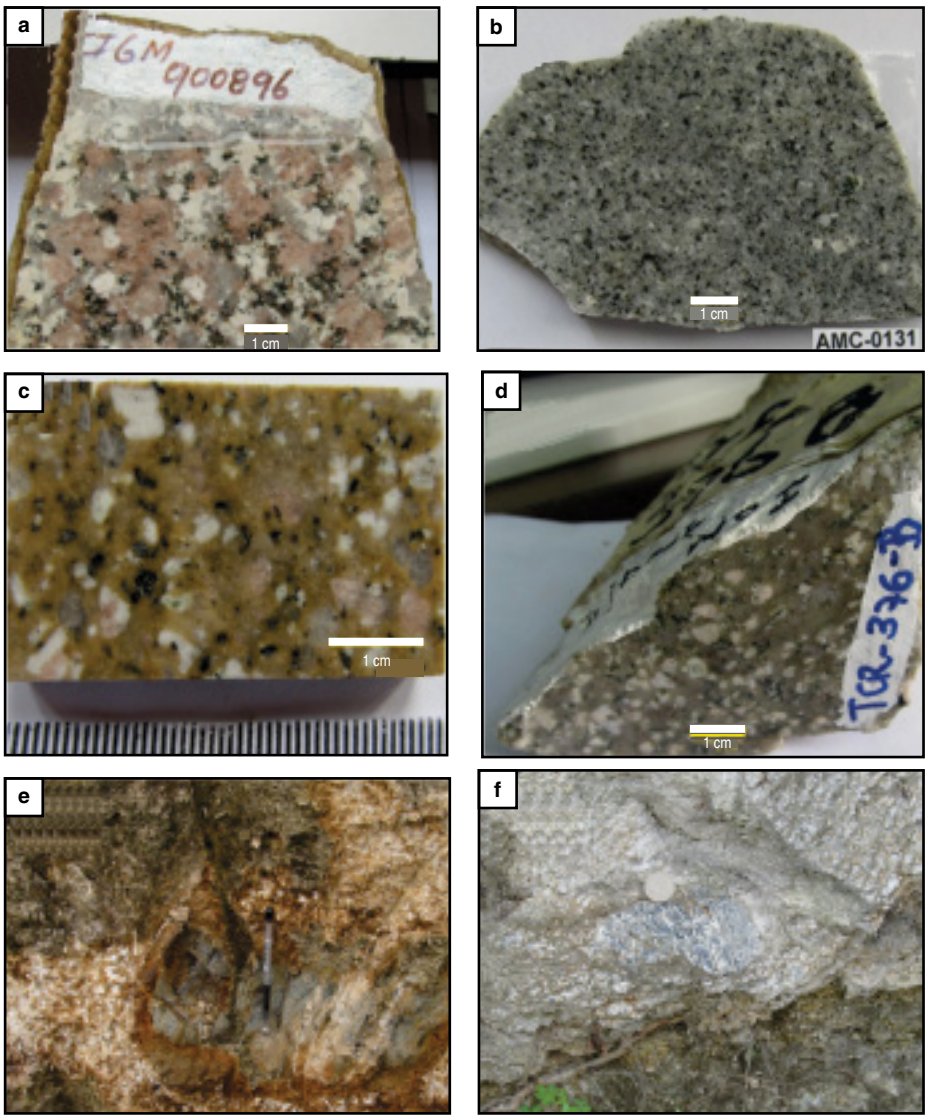

Figure 4. Macroscopic view of igneous rocks in the SM: **(a)** Santa Bárbara Monzogranite, **(b)** La Corcova Monzogranite, **(c)** San Joaquín Rhyolite, **(d)** Mogotes Batholith, **(e)** schist xenolith in La Corcova Monzogranite, **(f)** gneiss xenolith in La Corcova Monzogranite.

differentiation. Most are I–type plutons (Figure 5e), although some rocks in the same pluton plot in the fields of both I–type and S–type granites (Figure 5e). This phenomenon may be due to the variable extent of crustal melting in the different pulses that generated the plutons.

The granitoids of the SM have markedly negative Nb, Ti, and P anomalies as well as positive anomalies and high values of Cs, Ba, Th, Sr, K, Pb, and Rb, which are typical of continental margin magmatic arc environments (Figure 5f; Pearce, 1996, 2008), and gradual depletion from large ion lithophile elements (LILE) to high field strength elements (HFSE) (Figure 6).

The rare earth element (REE) patterns differ between rocks of similar compositions within each pluton (Figure 7), suggesting multiple magmatic pulses during their formation. The patterns resemble those of rocks generated in subduction environments above the subducted plate, with enrichment in light rare earth elements (LREE), depletion in heavy rare earth elements (HREE), and negative Eu anomalies (Eu/Eu* < 1) in most samples (Table 2). In rocks with higher SiO_2 contents, Eu/Eu* ratios <1 are more prominent.

The $(La/Yb)_n$ ratios are greater than 2 in all samples and vary markedly in the same intrusive body from one REE pattern to another compared to chondrites. The sums of the rare earth element contents (∑ REE = sum of the rare earth element values before normalization) range from 63.97 to 586.13. The rocks of the Rionegro Monzogranite have the lowest values, and those of the Mogotes Batholith have the highest values (Table 2).

4.1.3. Geochronology

Forty–one samples of the rocks and saprolites of the main granitoids in the SM and a few small dikes and minor intrusives of

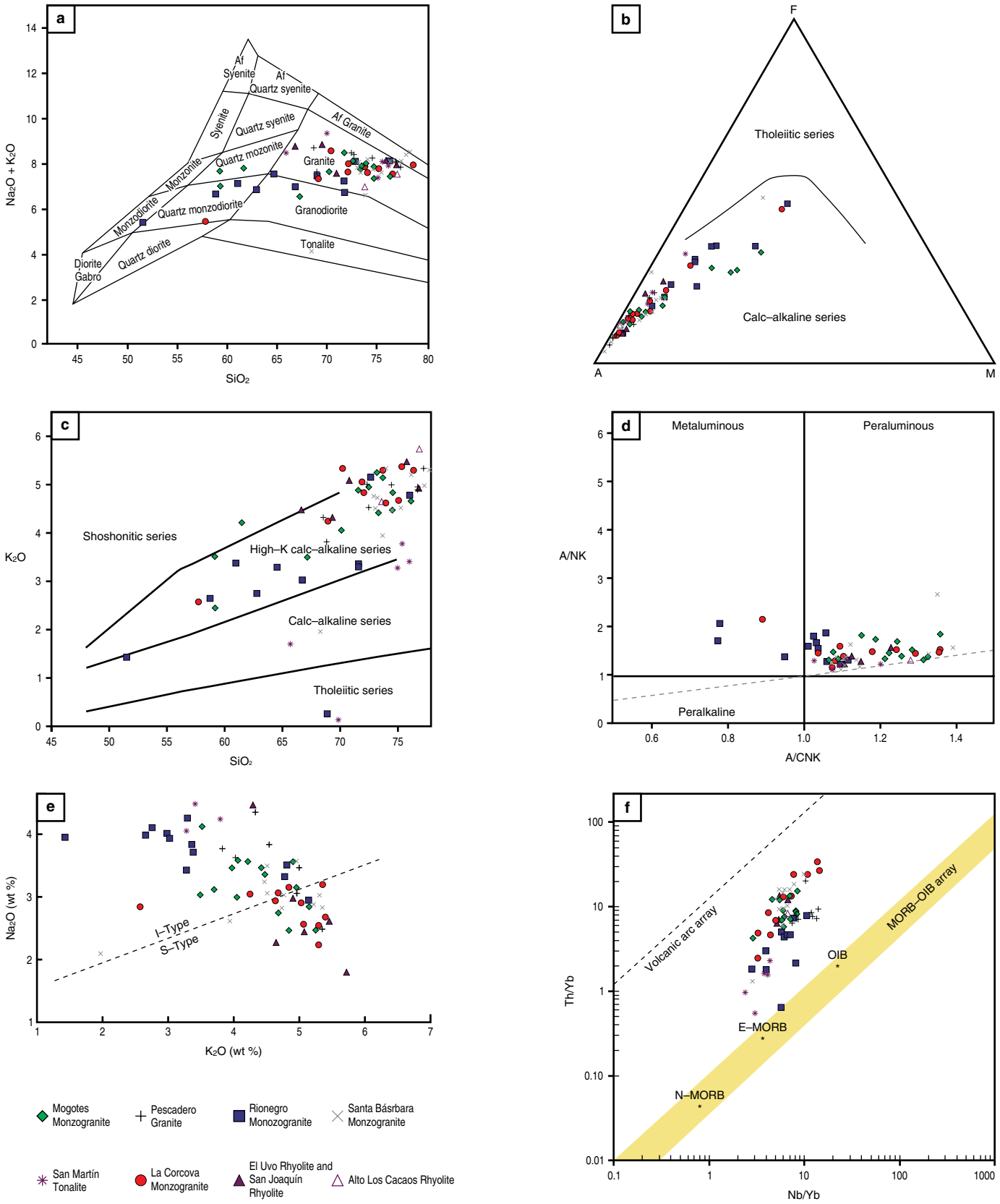

Figure 5. Classification and discrimination diagrams for Triassic – Jurassic granitoids in the SM: **(a)** TAS diagram of Middlemost (1985), **(b)** AFM diagram (Irvine & Baragar, 1971), **(c)** alkalinity index diagram of Peccerillo & Taylor (1976), **(d)** alumina saturation index diagram of Shand (1943); **(e)** K_2O vs. Na_2O diagram of Chappell & White (1974) discriminating between I–type and S–type granites, **(f)** Nb/Yb vs. Th/Yb diagram of Pearce (2008).

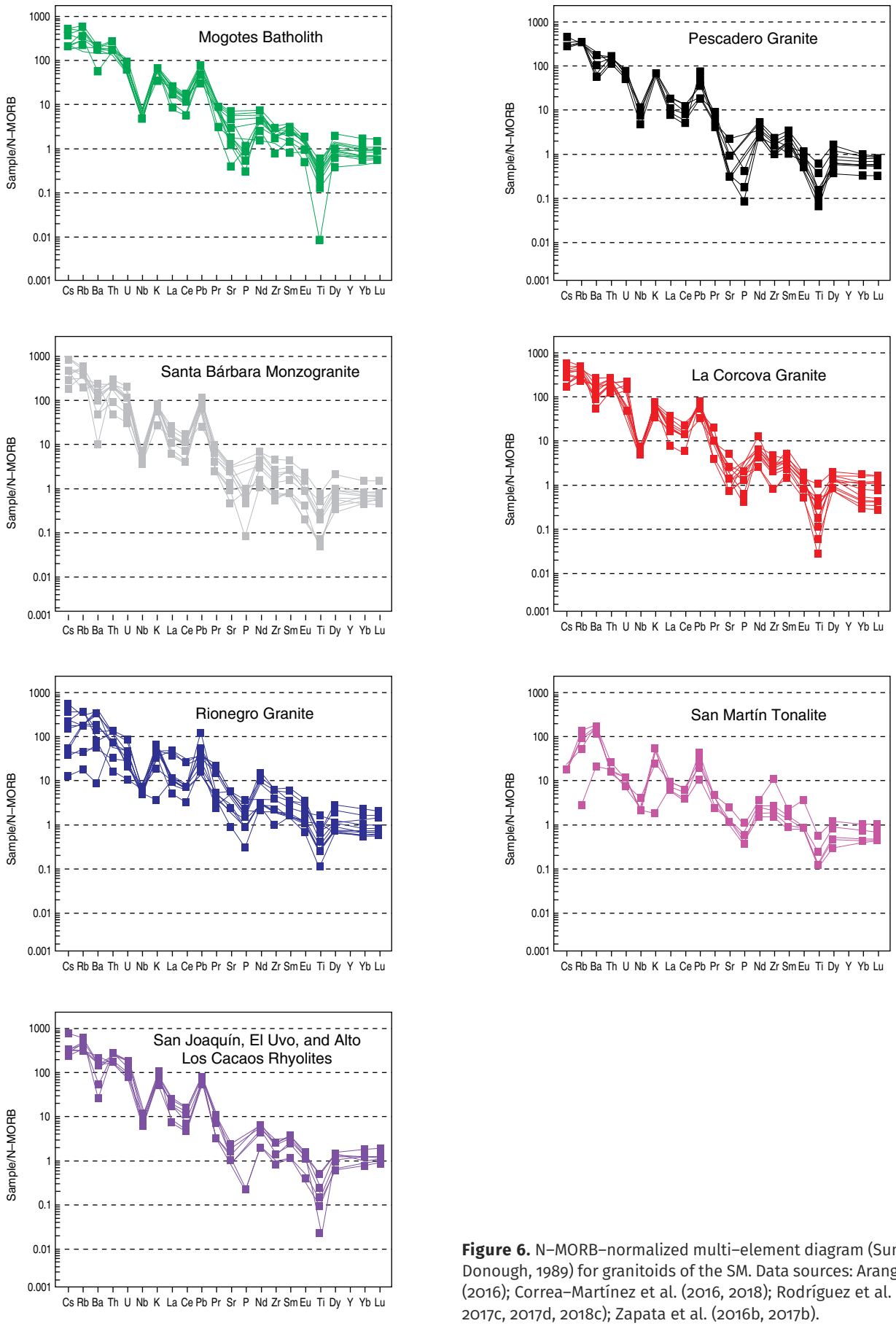

Figure 6. N–MORB–normalized multi–element diagram (Sun & McDonough, 1989) for granitoids of the SM. Data sources: Arango et al. (2016); Correa–Martínez et al. (2016, 2018); Rodríguez et al. (2017b, 2017c, 2017d, 2018c); Zapata et al. (2016b, 2017b).

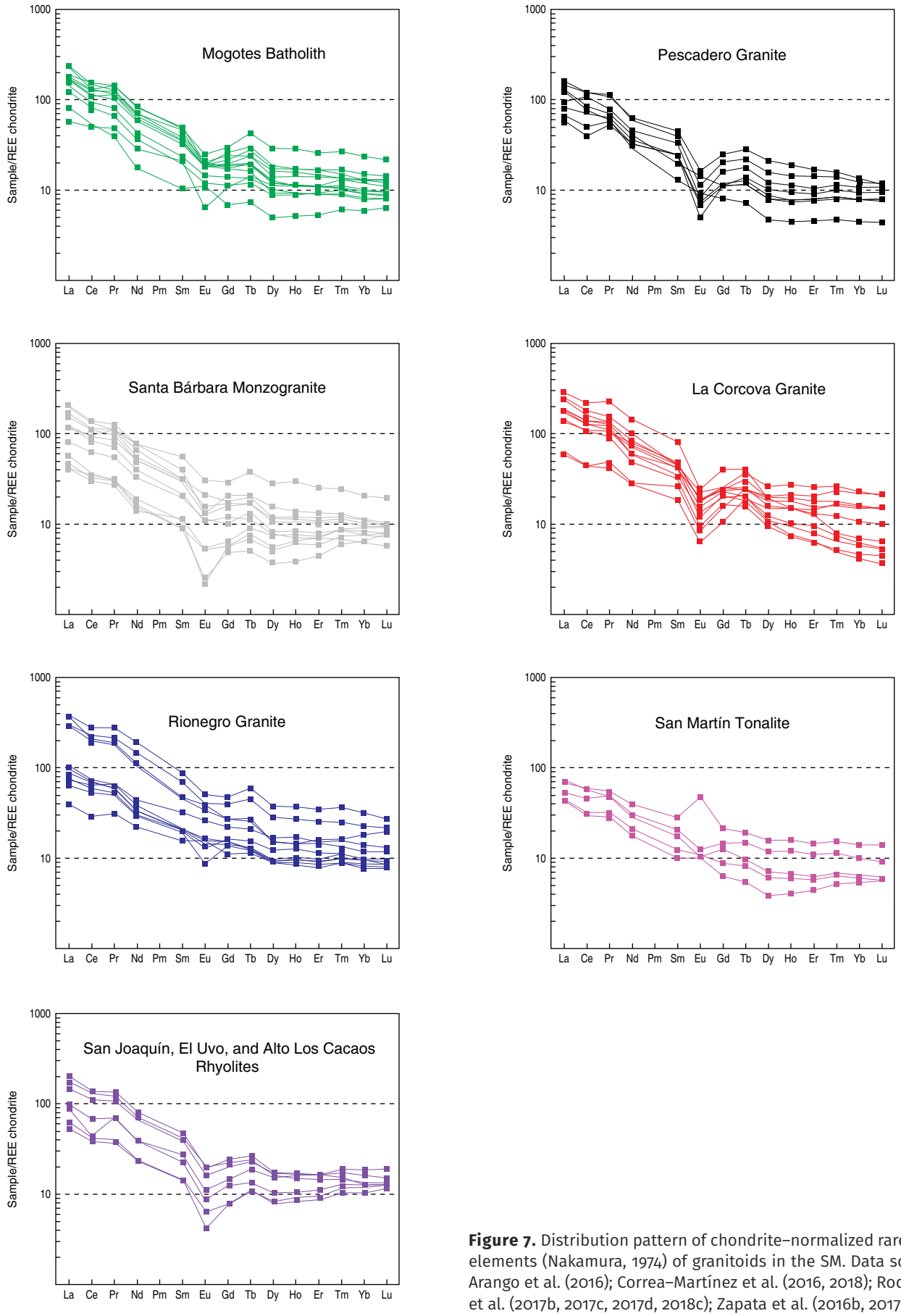

Figure 7. Distribution pattern of chondrite–normalized rare earth elements (Nakamura, 1974) of granitoids in the SM. Data sources: Arango et al. (2016); Correa–Martínez et al. (2016, 2018); Rodríguez et al. (2017b, 2017c, 2017d, 2018c); Zapata et al. (2016b, 2017b).

Table 2. Chondrite–normalized rare earth element diagram (Nakamura, 1974) for SM granitoids.

Sample	Unit	Eu/Eu*	$(La/Yb)_n$	$(La/Sm)_n$	$(Ce/Yb)_n$	$(Ce/Sm)_n$	$(Eu/Yb)_n$	∑REE
900910	Santa Bárbara Monzogranite	0.76	5.55	2.06	4.6	1.71	1.48	226.12
900941	Santa Bárbara Monzogranite	0.91	20.56	6.31	13.77	4.22	2.25	254.88
900857	Santa Bárbara Monzogranite	0.47	18.25	5.17	12.14	3.44	1.2	277.55
900920	Santa Bárbara Monzogranite	0.68	16.68	5.28	11.36	3.59	1.58	222.02
900882	Santa Bárbara Monzogranite	0.62	12.06	4.02	9.09	3.03	1.3	182.25
900870	Santa Bárbara Monzogranite	0.67	19.32	5.57	13.51	3.89	1.73	159.87
900896	Santa Bárbara Monzogranite	0.59	13.57	5.2	9.93	3.8	1.15	211.01
900933	Santa Bárbara Monzogranite	0.8	10.77	4.06	8.45	3.18	1.52	123.24
900908	Santa Bárbara Monzogranite	0.73	7.91	6.45	4.97	4.06	0.71	73.01
900911	Santa Bárbara Monzogranite	0.63	5.09	3.7	3.64	2.65	0.65	63.97
900881	Santa Bárbara Monzogranite	0.37	7.06	5.19	4.95	3.63	0.37	65.17
900935	Santa Bárbara Monzogranite	0.29	4.48	3.79	3.75	3.18	0.24	69.75
900862	La Corcova Monzogranite	0.4	45.44	4.5	33.62	3.33	2.86	264.4
900861	La Corcova Monzogranite	0.5	40.78	5.8	29.62	4.21	2.55	350.7
900863	La Corcova Monzogranite	0.42	30.69	4.59	22.79	3.41	2.05	201.05
900929	La Corcova Monzogranite	0.52	30.73	5.09	22.21	3.68	2.35	241.55
900921	La Corcova Monzogranite	0.43	40.84	3.56	31.2	2.72	3.48	445.1
10DVL05	La Corcova Monzogranite	0.67	15.88	5.28	10.66	3.54	1.52	319.9
900930	La Corcova Monzogranite	0.59	15.78	3.96	12.24	3.07	1.74	250.83
900937	La Corcova Monzogranite	0.53	11.79	3.87	8.8	2.89	1.15	284.63
900931	La Corcova Monzogranite	0.45	3.77	3.13	2.88	2.39	0.4	102.71
900909	La Corcova Monzogranite	0.43	2.88	2.45	1.99	1.69	0.39	113.15
900936	La Corcova Monzogranite	0.55	5.89	2.97	4.7	2.37	0.8	241
900997	Rionegro Monzogranite	0.98	5.16	2.27	4.51	1.99	1.84	144.42
900999	Rionegro Monzogranite	1.17	5.1	2.5	3.74	1.83	2.02	71.39
900954	Rionegro Monzogranite	1.09	20.17	7.75	11.45	4.4	2.14	428.36
900949	Rionegro Monzogranite	0.78	12.1	4.34	8.65	3.1	1.59	586.13
900952	Rionegro Monzogranite	0.77	13.07	4.31	10.12	3.34	1.77	468.08
900950	Rionegro Monzogranite	0.96	24.87	6.42	16.92	4.37	2.86	388.6
900985	Rionegro Monzogranite	0.73	7.94	3.94	6.18	3.07	1.36	121.45
900973	Rionegro Monzogranite	0.87	11.11	5.01	7.87	3.55	1.63	150.28
900990	Rionegro Monzogranite	0.97	11.85	4.8	8.62	3.49	2.06	138.65
900971	Rionegro Monzogranite	0.84	8.79	4.25	6.82	3.3	1.43	134.5
900974	Rionegro Monzogranite	0.52	7.37	3.08	6.16	2.57	1.01	108.8
901002	San Martín Tonalite	1.04	7.45	3.56	5.39	2.58	1.82	71.26
901003	San Martín Tonalite	0.72	5.35	2.59	4.61	2.23	1.25	102.47
901004	San Martín Tonalite	1.26	8.2	4.35	5.53	2.93	1.87	63.85
901032	San Martín Tonalite	1.93	4.88	2.42	4.18	2.07	3.39	135.25
901033	San Martín Tonalite	0.71	11.24	4.17	8.86	3.29	1.62	111.65
900864	Pescadero Granite	0.43	8.63	2.77	6.4	2.05	0.93	108.96
900871	Pescadero Granite	0.3	10.22	3.48	8.83	3.01	0.62	132.52
900872	Pescadero Granite	0.4	12.75	4.06	9.62	3.06	0.91	233.56
900873	Pescadero Granite	0.49	10.64	3.2	8.8	2.65	1.21	236.52
900897	Pescadero Granite	0.42	6.17	2.4	4.25	1.65	0.73	98.21

Table 2. Chondrite–normalized rare earth element diagram (Nakamura, 1974) for SM granitoids *(continued)*.

Sample	Unit	Eu/Eu*	$(La/Yb)_n$	$(La/Sm)_n$	$(Ce/Yb)_n$	$(Ce/Sm)_n$	$(Eu/Yb)_n$	∑REE
900898	Pescadero Granite	0.36	8.85	2.91	10	3.29	0.76	184.71
900867	Pescadero Granite	0.89	28.59	9.83	17.47	6.01	2.04	144.13
900899	Pescadero Granite	0.94	16.54	6.56	10.79	4.28	1.79	164.94
900944	Mogotes Batholith	0.68	11.72	4.57	7.01	2.74	1.3	235.48
900887	Mogotes Batholith	0.43	4.52	2.78	3.91	2.4	0.5	104.36
900927	Mogotes Batholith	1.31	13.85	7.91	9	5.14	1.87	98.55
900965	Mogotes Batholith	0.53	18.57	5.16	11.63	3.23	1.43	298.16
900869	Mogotes Batholith	0.8	12.7	6.31	8.6	4.27	1.24	158.31
900943	Mogotes Batholith	0.66	9.74	4.87	5.48	2.74	1.04	302.12
900966	Mogotes Batholith	0.71	13.33	5.1	8.42	3.22	1.38	232.43
900874	Mogotes Batholith	0.79	17.41	6.02	11.45	3.96	1.75	183.7
900962	Mogotes Batholith	0.89	17.88	5.58	11.33	3.54	2.08	227.96
900917	Mogotes Batholith	0.79	23.14	5.76	16.61	4.13	2.35	240.22
900900	Mogotes Batholith	0.7	18.33	4.63	13.48	3.41	2	245
900903	Mogotes Batholith	0.61	15.9	3.93	12.91	3.19	1.76	295.37
900902	Mogotes Batholith	0.76	18.67	4.78	13.61	3.49	2.14	242.71
900945	El Uvo Rhyolite	0.6	5.78	4.24	3.94	2.89	0.6	91.99
900946	El Uvo Rhyolite	0.39	4.35	3.64	3.18	2.66	0.35	86.3
900890	San Joaquin Rhyolite	0.58	8.93	3.77	6.83	2.89	0.99	232.69
900891	San Joaquin Rhyolite	0.58	15.71	4.24	10.86	2.93	1.55	291.01
900892	San Joaquin Rhyolite	0.66	12.89	4.14	9.64	3.1	1.5	264.35
900876	Alto de Los Cacaos Rhyolite	0.52	7.68	4.32	5.39	3.03	0.68	144.54
900916	Alto de Los Cacaos Rhyolite	0.56	4.75	3.25	2.34	1.61	0.59	126.22

Source: Data from Arango et al. (2016); Correa–Martínez et al. (2016, 2018); Rodríguez et al. (2017b, 2017c, 2017d, 2018c); Zapata et al. (2016b, 2017b); sample 10DVL05 from van der Lelij (2013).

aplitic monzogranites (corresponding to the Mogotes Batholith, the Pescadero Granite, the Santa Bárbara Monzogranite, La Corcova Monzogranite, the Páramo Rico Pluton, the San Martín Tonalite, the Rionegro Monzogranite, and three porphyritic bodies called the Alto de Los Cacaos Rhyolite, San Joaquín Rhyolite, and El Uvo Rhyolite) were dated using U–Pb zircon LA–ICPMS (data sources: Arango et al., 2016; Correa–Martínez et al., 2016, 2018; Rodríguez et al., 2017b, 2017c, 2017d, 2018c; Zapata et al., 2016b, 2018). The zircons of the granitoids from the SM are predominantly short prisms and elongated subordinates with concentric zoning, which are typical of igneous zircons. Inherited cores are identified in multiple crystals. The ages of the different samples analyzed are shown in Figure 2 and are presented in Table 3.

4.1.4. Igneous Ages

Most of the ages obtained from the granitoids from the SM (Table 3) are between 205 to 188 Ma. The exceptions include samples MIA–648B and MIA–650B, which yielded weighted mean ages of 214.5 ± 2.7 and 184.1 ± 2.3 Ma, respectively (Arango et al., 2016), that may correspond to the initiation and the final stage of the arc, respectively. The main set of ages represents the peak magmatic activity. The geochronological results from each granitoid show different ages for rocks with similar compositions (monzogranites); however, the ages are related to nonparallel REE trends, suggesting that they correspond to plutons that resulted from multiple magmatic pulses that occurred over 17 Ma and that the arc had very little compositional variation during its activity, in which the magmatic pulses involved variable crustal melting with variable $(La/Yb)_n$ ratios.

The ages of the dikes and minor intrusive bodies have an age distribution coeval to the crystallization time of the main mass of the granitoids. These rocks are predominantly monzogranitic, suggesting that younger pulses intruded previous assemblages of crystallized monzogranites within an arc system characterized by multiple magmatic pulses.

Table 3. LA–ICP–MS U–Pb zircon ages of granitoid bodies from the SM.

Sample	Latitude N	Longitude W	Classification	Unit	Age (Ma)	Inherited ages (Ma)
AMC–0162	6° 27' 41.16''	72° 49' 52.55''	Deformed monzogranite	Mogotes Batholith	189.1 ± 3.6	224–222, n=2; 234–231, n=4; 252–248, n=2; 298–270, n=5; 386–376, n=5; 420–395, n=5; ; 445–437, n=5; 459–451, n=5 513, n=1; 360–338, n=6; 585, n=2; 680–650, n=2; 800–735, n=3; 970, n=2; 1290–115, n=4;
GZ–6831	6° 27' 39.59''	72° 48' 31.34''	Deformed quartz monzodiorite	Mogotes Batholith	193.7 ± 1.3	268.3 ± 7.6, n=1; 287.7 ± 8.8, n=1; 905 ± 25, n=1;
LMC–075	6° 28' 35.52''	72° 53' 34.39''	Monzogranite	Mogotes Batholith	195.7 ± 3.9	248.5 ± 10, n=1; 1040-1020 ± 34, n=2; 1230 ± 43, n=1
MIA–638	6° 33' 30.57''	72° 56' 16.58''	Monzogranite	Mogotes Batholith	200.4 ± 2.2	234.4 ± 7.1, n=1; 316.9 ± 6.8, n=1; 1120 ± 79, n=1; 1627 ± 77, n=1
TCR–376	6° 41' 6.91''	72° 57' 13.31''	Monzogranite	Mogotes Batholith	202.5 ± 1.3	880 ± 15, n=1
MIA–636	6° 41' 0.05''	72° 57' 59.68''	Micrographic monzogranite	Mogotes Batholith	205.4 ± 3.0	571.7 ± 6, n=1; 1316 ± 76, n=1
AMC–0144	6° 25' 27.04''	72° 50' 23.16''	Aplitic Syenogranite (dike)	Mogotes Batholith	202.1 ± 1.8	435 ± 6.7, n=1
TCR380	6° 28' 21.43''	72° 54' 17.89''	Quartz monzonite (dike)	Mogotes Batholith	191.0 ± 3.5	330–302, n=3; 267, n=1; 215, n=1; 399–391, n=2; 448–432, n=4; 923–851, n=4
AMC–136A	6° 45' 20.98''	72° 57' 21.48''	Microdiorite (dike)	Mogotes Batholith	108.3 ± 2.3	221 ± 8, n=1; 250 ± 10, n=1; 1154 ± 35, n=1; 1335 ± 40, n=1;
GZ–6829B	6° 26' 33.53''	72° 48' 33.94''	Syenogranite (dike)	Mogotes Batholith	98.8 ± 1.3	199 ± 6, n=2; 214 ± 7; 207 ± 7
TCR–389	7° 37' 59.55''	73° 16' 55.66''	Diorite	Minor Body	199.7 ± 1.6	
GZ–6823	6° 55' 14.09''	73° 0' 59.90''	Monzogranite	Pescadero Granite	194.8 ± 3.2	451 ± 18, n=10; 995 ± 20, n=2
GZ–6824	6° 53' 22.17''	72° 59' 48.41''	Monzogranite	Pescadero Granite	197.3 ± 2.4	324.18 ± 18, n=1; 432.5 ± 25, n=1; 754.1 ± 45, n=1; 959 ± 31, n=3; 1047.8 ± 64, n=1; 1873.1 ± 105
AMC–0131	7° 9' 47.68''	73° 2' 22.93''	Syenogranite	La Corcova Monzogranite	192.5 ± 2.6	338.8 ± 10, n=1; 408.5 ± 7.3,n=3
JGB–456B	6° 57' 2.43''	72° 56' 13.82''	Quartz diorite	La Corcova Monzogranite	201.6 ± 4.0	304.6 ± 15
MIA–630B	7° 2' 12.10''	73° 2' 42.78''	Quartz diorite	La Corcova Monzogranite	202.7 ± 1	
LMC–077	7° 9' 39.68''	73° 3' 40.44''	Monzogranite	La Corcova Monzogranite	204.8 ± 6.1	230, n=1; 262 ± 13, n=2; 289 ± 8, n=1; 362 ± 15, n=2; 390–415, n=2; 435–457, n=3; 463.8 ± 7.3, n=3; 490 ± 20, n=3; 618 ± 30 , n=1; 911 ± 40, n=1; 1091 ± 39, n=1; 1426 ± 38, n=1
AMC–128A	7° 8' 12.44''	73° 2' 17.93''	Meta-syenogranite Xenolith	La Corcova Monzogranite	462.7 ± 3.1	525 ± 7.8, n=1; 533.8 ± 7, n=1; 1099 ± 74, n=1
MIA–627A	6° 55' 24.42''	72° 59' 51.19''	Monzogranite-(dike)	La Corcova Monzogranite	199.5 ± 4.6	281.2 ± 5.6, n=1; 419.4 ± 7, n=1; 430.5 ± 4.7, n=1; 457.1 ± 5.0, n=11; 482.1 ± 3.1, n=3; 1498–1418, n=3
MIA–650B	7° 25' 42.08''	73° 10' 50.27''	Syenogranite	Rionegro Monzogranite	184.1 ± 2.3	928 ± 55, n=2; 1005, n=1; 1485, n=1
LMC–082	7° 42' 2.95''	73° 16' 53.05''	Diorite	Rionegro Monzogranite	189.9 ± 1.6	
GR–6743	8° 11' 22.47''	73° 19' 0.48''	Granodiorite-Monzogranite	Rionegro Monzogranite	195.9 ± 1.6	230.9 ± 7.9, n=1
GZ–6848A	7° 38' 55.80''	73° 13' 16.64''	Granodiorite	Rionegro Monzogranite	196.6 ± 2.1	451, n=1; 877.9, n=1; 93,40, n=1; 1035.2, n=1; 1143.33, n=1
MIA-648A	7° 19' 10.76''	73° 7' 40.63''	Porphyritic rhyolite (dike)	Rionegro Monzogranite	194.5 ± 1.2	1021.6, n=1
JGB-462	7° 11' 26.11''	73° 7' 26.48''	Quartz monzonite (dike)	Rionegro Monzogranite	197.2 ± 1.5	
LMC–084	7° 39' 53.04''	73° 16' 34.56''	Granodiorite with hornblende	Rionegro Monzogranite	200.8 ± 1.9	230.8 ± 5, n=2
MIA–648B	7° 19' 10.73''	73° 7' 40.61''	Granodiorite	Rionegro Monzogranite -Minor Body	214.5 ± 2.7	244.3 ± 4.0, n=6; 288–267, n=2; 320 ± 15, n=1
AMC–0137	6° 45' 18.64''	72° 55' 57.78''	Monzogranite	Santa Bárbara Monzogranite	191.7 ± 1.2	201.4–200.8, n=3; 1122 and 1158, n=2 unconformable
JGB–457A	6° 57' 32.95''	72° 55' 44.00''	Monzogranite	Santa Bárbara Monzogranite	195.1 ± 1.9	392, n=1
GR–6719	7° 10' 32.46''	72° 49' 32.68''	Monzogranite	Santa Bárbara Monzogranite	196.8 ± 2.0	224–221, n=2 unconformable; 474, n=1 unconformable
GZ–6821	6° 55' 14.09''	72° 54' 19.44''	Monzogranite	Santa Bárbara Monzogranite	198.0 ± 2.7	238.4–213.3, n=4; 395.6–380.8, n=3; 427.9–417.8, n=3; 470–447.4, n=3
GR–6718	7° 7' 53.82''	72° 51' 2.68''	Monzogranite	Santa Bárbara Monzogranite	203.8 ± 2.7	
GR–6717	7° 10' 7.27''	72° 51' 46.08''	Monzogranite (minor body)	Santa Bárbara Monzogranite	190.6 ± 1.5	425.2, n=1 unconformable; 208–202.9; n=3
LMC–059A	7° 10' 44.67''	72° 52' 12.58''	Syenogranite (dike)	Santa Bárbara Monzogranite	200.7 ± 2.0	628 ± 26, n=1
AMC–0127	6° 56' 10.40''	72° 54' 6.56''	Pheno-dacite (dike)	Santa Bárbara Monzogranite	204.0 ± 2.3	267, n=1

Table 3. LA–ICP–MS U–Pb zircon ages of granitoid bodies from the SM *(continued).*

Sample	Latitude N	Longitude W	Classification	Unit	Age (Ma)	Inherited ages (Ma)
AMC–0145	6° 26' 4.14''	72° 52' 37.30''	Quartz-trachyte of Kfs (dike)	Alto de Los Cacaos Rhyolite	205.2 ± 2.6	279 ± 2.8, n=1; 410 ± 4.4, n=1; 429 ± 8.3, n=1; 454 ± 7.5, n=1; 464 ± 4.2, n=1;1681 ± 67, n=1
GR–6729	6° 26' 37.39''	72° 51' 22.91''	Pheno dacite	San Joaquín Rhyolite	201.0 ± 2.1	390 ± 20, n=1; 446 ± 8, n=1; 1630 ± 170, n=1 unconformable
MIA–641	6° 27' 33.24''	72° 48' 4.01''	Porphyritic rhyolite (dike)	El Uvo Rhyolite	197.2 ± 1.6	218.2 ± 4.0, n=2; 1168 ± 25, n=1
LMC–088	8° 8' 36.39''	73° 26' 32.93''	Granodiorite	San Martín Tonalite	198.0 ± 2.8	
TCR–395A	7° 55' 41.64''	73° 23' 44.50''	Metatonalite	San Martín Tonalite	198.9 ± 1.8	
LMC–090B	8°5′3.51''	73° 26' 26.86''	Phenodacite (dike)	San Martín Tonalite	196.6 ± 2.5	999 ± 26, n=1
TCR–363	7° 12' 51.61''	72° 53' 55.78''	Granodiorite	Páramo Rico Tonalite	206.84 ± 0.98	

Source: Data from Arango et al. (2016); Correa–Martínez et al. (2016, 2018); Rodríguez et al. (2017b, 2017c, 2017d, 2018c); Zapata et al. (2016b, 2017b).

4.1.5. Inherited Ages

The inherited zircon cores of the granitoids from the SM yield ages ranging from 1873.1 ± 105 (Mesoproterozoic) to approximately 220 Ma (Early Triassic) (Figure 8; Table 3).

Inherited ages of approximately 1800 and 1600 Ma are found in zircon cores of the Mogotes Batholith, Pescadero Granite, and El Uvo and San Joaquín Rhyolites. Rare inherited cores with ages ranging from 850 to 635 Ma (Cryogenian) and from 635 to 542 Ma (Ediacaran) are found in the Mogotes Batholith, Pescadero Granite, and Santa Bárbara Monzogranite. A set of Early, Middle, and Late Ordovician ages is found in the Mogotes Batholith; La Corcova, Santa Bárbara, and Rionegro Monzogranites; and the San Joaquín Rhyolite (Figure 8).

Permian ages ranging from 290 to 262 Ma, as well as Triassic to Carnian ages, occur in inherited zircon cores from the Mogotes Batholith and La Corcova, Santa Bárbara, and Rionegro Monzogranites.

4.1.6. Age of the Basement in the NW zone

A U–Pb zircon age from an amphibolite of the amphibolite and migmatite unit in the northwest part of the SM yielded a metamorphic age of ca. 897 ± 28 Ma, a Th/U ratio <0.2, and inherited ages of 1120 ± 58 Ma (n = 4) and 1421 ± 40 Ma (n = 16) (Figure 9).

4.2. Upper Magdalena Valley

The Jurassic magmatism in the UMV is represented by batholiths, stocks, and volcano–sedimentary units that are distributed on the eastern edge of the Central Cordillera and on the western edge of the Eastern Cordillera of Colombia. All of the units were grouped according to their current spatial positions, compositions, and ages into the western and eastern plutons (Rodríguez et al., 2015a, 2018a).

The western plutons are located between the western Avirama and the eastern Betania–El Agrado Faults. They are composed of the Anchique Quartz Monzonite (Arango et al., 2015a; Cossio et al., 1994), San Cayetano Quartz Monzonite (Bermúdez et al., 2015; Carvajal et al., 1983, 1993), Los Naranjos Quartz Monzonite (Rodríguez & Fuquen, 1989; Rodríguez et al., 2015b; Velandia et al., 2001b), Páez Quartz Monzodiorite (Zapata et al., 2015), El Astillero Quartz Monzodiorite (Rodríguez et al., 2015c; Velandia et al., 2001b), and Las Minas Monzonite (Arango et al., 2015b; Velandia et al., 2001b) (Figure 10).

The eastern plutons are located between the Betania–El Agrado and Algeciras Faults. This group is represented by the Algeciras Monzogranite (Ferreira et al., 1998, 2002; Rodríguez et al., 2015d), Teruel Quartz Latite (Arango et al., 2015c), Garzón Granite (Rodríguez et al., 2015e; Velandia et al., 2001b), Altamira Monzogranite (Arango et al., 2015d), Sombrerillo Quartz Monzonite (Rodríguez et al., 2018a), and Mocoa Monzogranite (Arango et al., 2015e) (Figure 10).

4.2.1. Petrography

The western plutons consist of quartz monzonites, quartz monzodiorites, quartz diorites, and some monzogranites (Figure 11). They range from quartz monzonites in the north to quartz monzodiorites in the south and consist of Pl + Kfs + Qtz (<20%) ± Hbl ± Bt ± Cpx ± Opx with opaques, apatite, zircon, and titanite as accessory minerals. The eastern plutons include monzogranite rocks with slight lithological variations between syenogranites and granodiorites (Figure 11), which consist of Kfs + Pl + Qtz (>20%) + Bt ± Hbl ± Cpx with opaques, apatite, zircon, titanite ± allanite as accessory minerals.

The modal quartz contents differ markedly between the two groups. The quartz contents of the western plutons are generally lower than 20%, whereas the eastern plutons of the UMV contain rocks with quartz contents higher than 20%. Mafic minerals are commonly found in higher modal quantities in the western plutons, particularly hornblende, biotite, clinopyroxene, and subordinate orthopyroxene. Mafic minerals occur in lower ratios in the eastern plutons and include biotite and hornblende with or without clinopyroxene and completely lacking orthopyroxene.

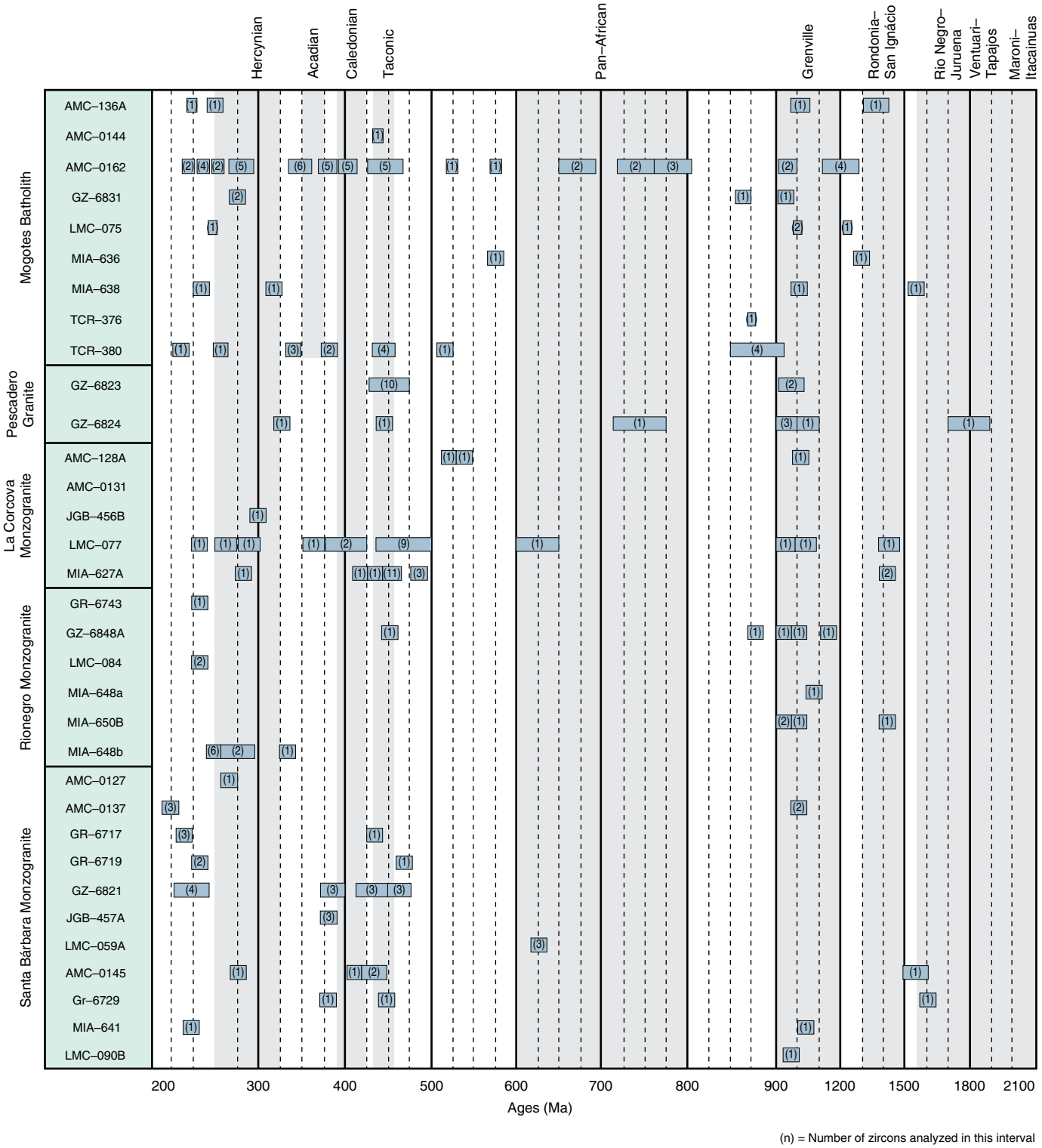

Figure 8. Ages of inherited zircons in samples of granitoids from the SM (data sources: Arango et al., 2016; Correa–Martínez et al., 2016, 2018; Rodríguez et al., 2017b, 2017c, 2017d, 2018c; Zapata et al., 2016b, 2017b).

Both groups of plutons are intruded by dikes of basic to intermediate compositions, including andesites, microdiorites, and basalts, as well as acidic dikes such as rhyolites, dacites, and aplitic monzogranites.

Texturally, the western plutons range from equigranular to inequigranular and commonly show micrographic intergrowths. The eastern plutons are inequigranular with bimodal crystals of alkaline feldspar.

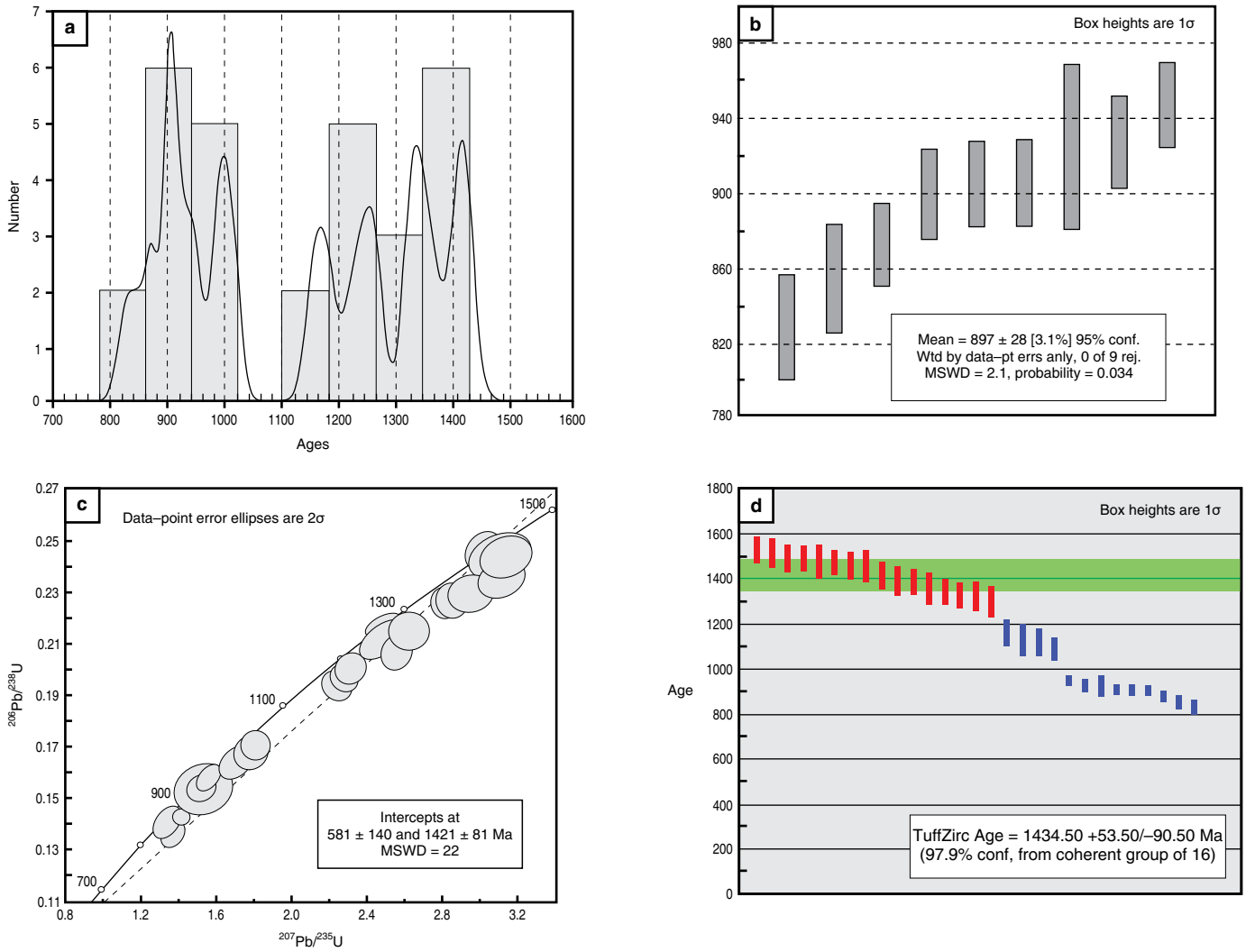

Figure 9. Age and inheritance of amphibolite sample MIA-661 from the Aguachica–Ocaña road. **(a)** Probability density diagram; **(b)** weighted average age diagram; **(c)** concord diagram; **(d)** tuffzirc age diagram.

The volcanic units include the Saldaña Formation and the Pitalito Vulcanites (Rodríguez et al., 2016b, 2018a). The former is located in the Central Cordillera and the serranía de Las Minas near the western plutons. The latter is located near the western edge of the Eastern Cordillera near the eastern plutons (Figure 10). They consist of andesitic to rhyolitic lava flows, tuffs, and agglomerates.

4.2.2. Geochemistry

Whole–rock geochemical analyses were performed on 72 samples from the eastern and western plutons (Rodríguez et al., 2018a). Data sources include Arango et al. (2015a, 2015b, 2015c, 2015d, 2015e); Bermúdez et al. (2015); Bustamante et al. (2010); Rodríguez et al. (2015a, 2015b, 2015c, 2015d, 2015e, 2016b); and Zapata et al. (2015) (see Table 1, Supplementary Information).

The eastern plutons are grouped in the TAS diagram (Figure 12a) in the field of granites, although a few rocks from the Algeciras and Altamira Monzogranites are alkali feldspar granites. The western plutons tend to have more basic compositions, varying between quartz diorites and quartz monzodiorites. Some rocks from the Páez Quartz Monzodiorite reach the granite field, which is consistent with the petrographic data (Figures 11, 12a).

The Jurassic granitoids of the UMV show decreases in TiO_2, Al_2O_3, MgO, CaO, and P_2O_5 and increases in K_2O and Na_2O with increasing SiO_2. The rocks in the A (Al_2O_3), F (FeO), M (MgO) (AFM) diagram range from tholeiitic to more differentiated calc–alkaline rocks (Figure 12b) and mostly plot within the field of the high–K, calc–alkaline series (Figure 12c). These rocks transition from metaluminous in the western granitoids to peraluminous in the eastern granitoids (Figure 12d), with A/CNK ratios ranging from 0.5 to 1.2 and A/NK ratios ranging from 1 to 2.8, suggesting magmatic differentiation.

The eastern granitoids are high–K calc–alkaline, and some rocks are shoshonitic (Figure 12c), with SiO_2 contents ranging

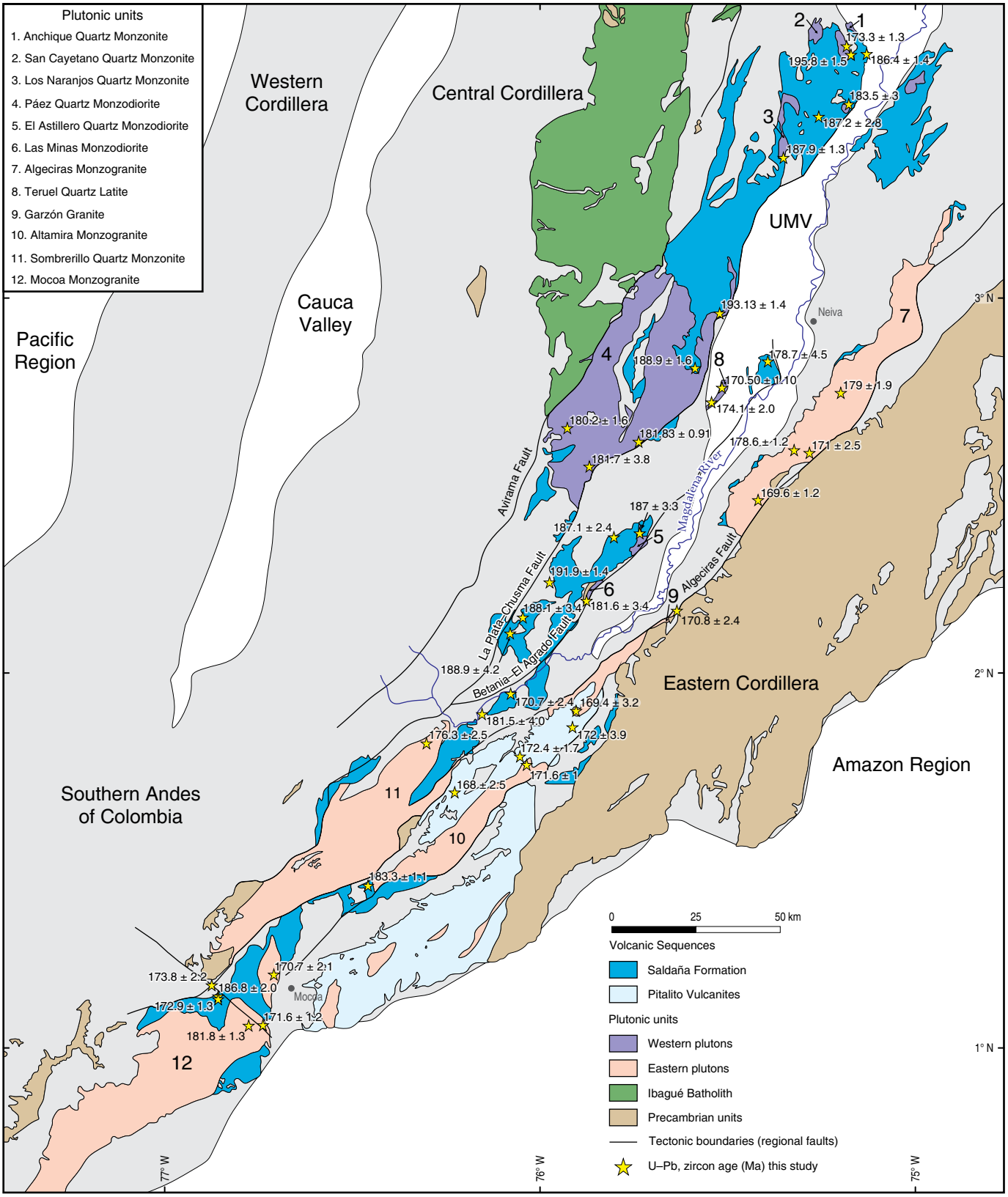

Figure 10. Locations and U–Pb ages of Jurassic plutons and volcanic rocks associated with the UMV (taken from Rodríguez et al., 2018a).

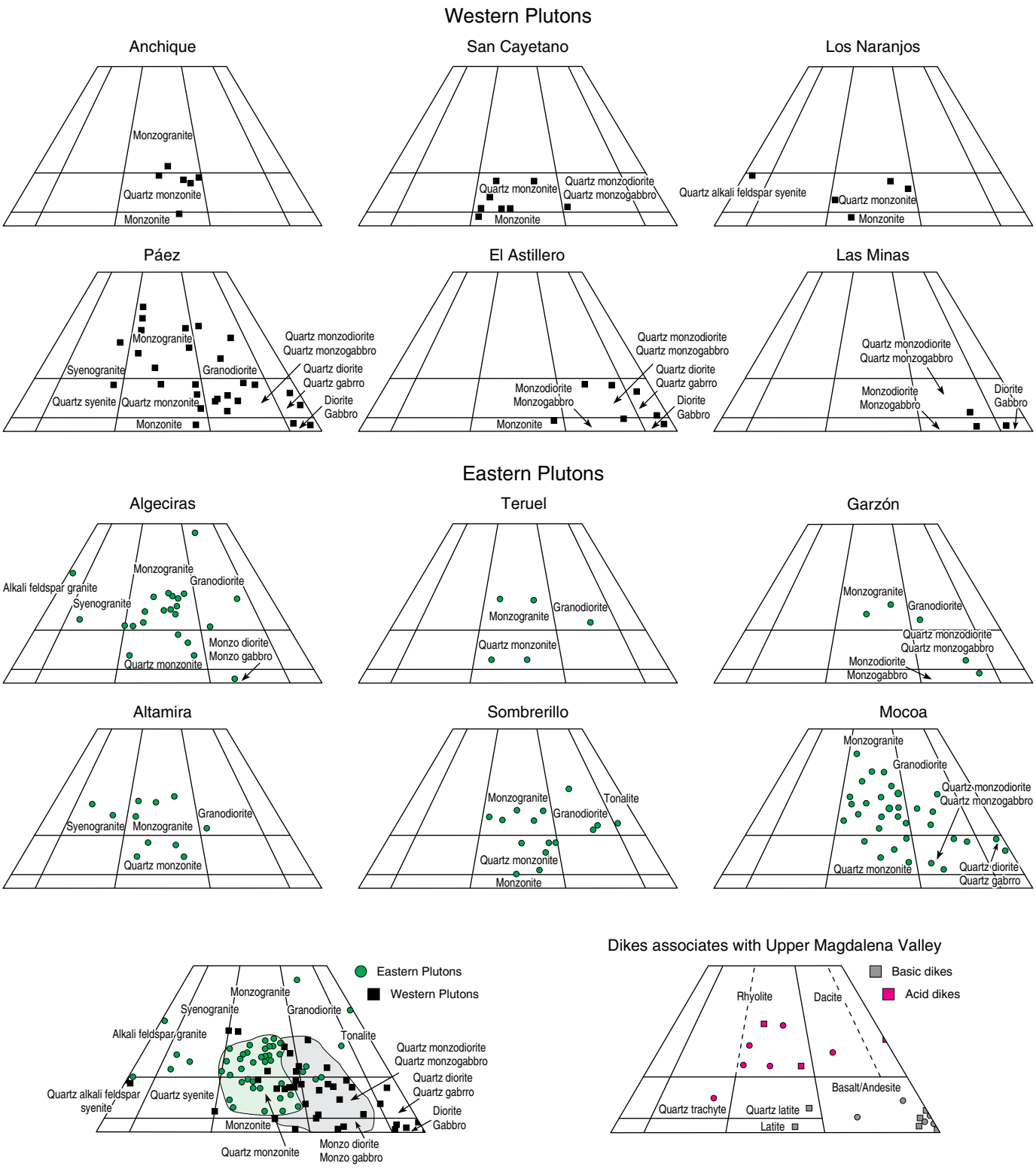

Figure 11. Modal compositions of Jurassic granitoids from the Upper Magdalena Valley (UMV) of Streckeisen (1974). Western plutons are shown in black, and eastern plutons are shown in green. Data sources: Arango et al. (2015a, 2015b, 2015c, 2015d, 2015e); Bermúdez et al. (2015); Rodríguez et al. (2015a, 2015b, 2015c, 2015d, 2015e, 2018a); Zapata et al. (2015).

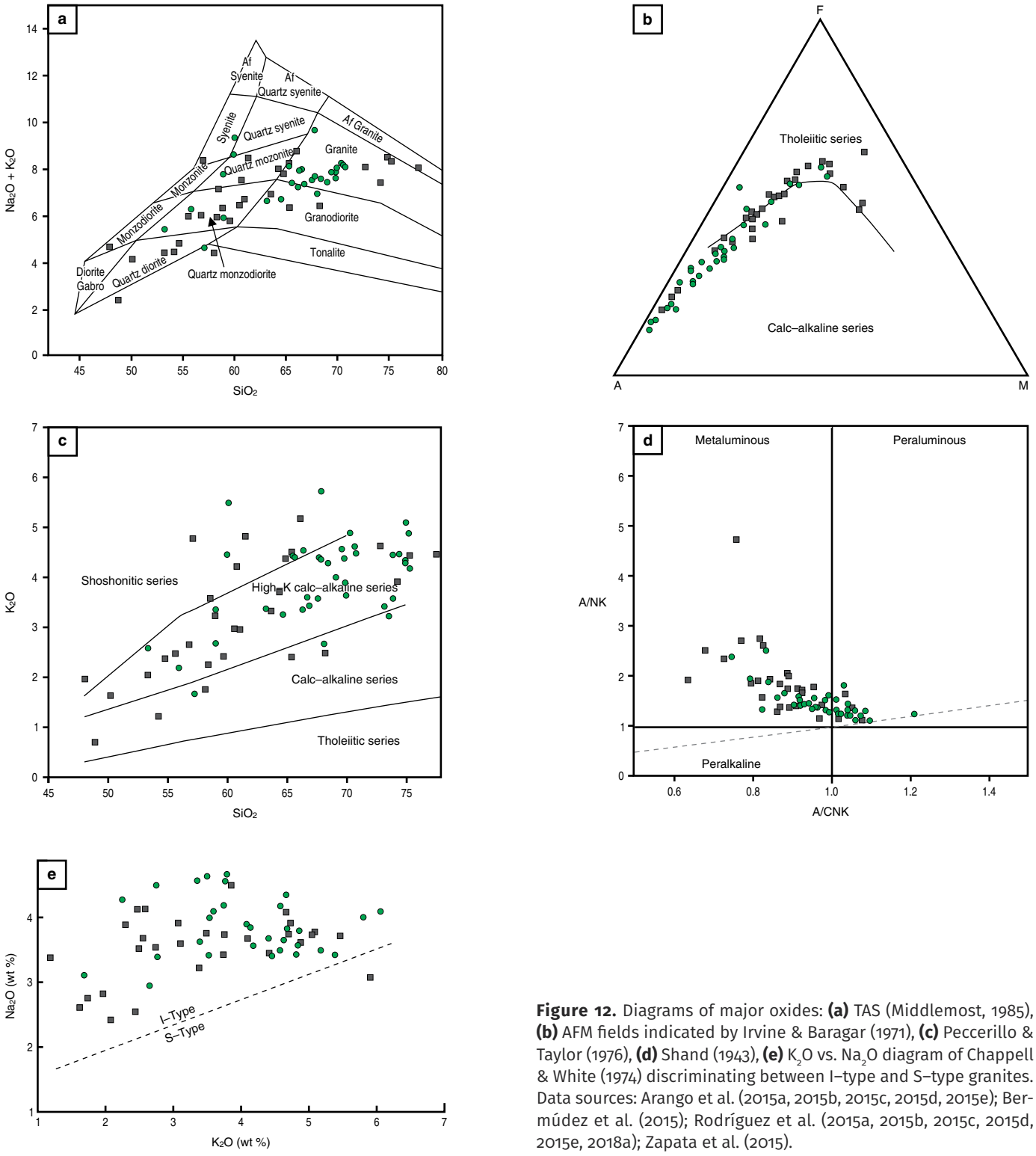

Figure 12. Diagrams of major oxides: **(a)** TAS (Middlemost, 1985), **(b)** AFM fields indicated by Irvine & Baragar (1971), **(c)** Peccerillo & Taylor (1976), **(d)** Shand (1943), **(e)** K_2O vs. Na_2O diagram of Chappell & White (1974) discriminating between I–type and S–type granites. Data sources: Arango et al. (2015a, 2015b, 2015c, 2015d, 2015e); Bermúdez et al. (2015); Rodríguez et al. (2015a, 2015b, 2015c, 2015d, 2015e, 2018a); Zapata et al. (2015).

from 53% to 78%, Na_2O contents ranging from 2.8% to 4.7%, and K_2O contents ranging from 2.1% to 5% (Figure 12e). They have low Fe_2O_3 contents ranging from 0.5% to 10.4% and MgO contents ranging from 0.18 to 6.4%. The western plutons vary between tholeiitic to calc–alkaline in the AFM diagram (Figure 12b) and are calc–alkaline (Figure 12c), with low SiO_2 contents ranging from 47.6% to 74.8% (average of 61%), low Na_2O contents ranging from 2.4% to 4.2%, with most values near 3.30%, and higher Fe_2O_3 (6.21%) and MgO (3.39%) contents. The TiO_2 content is usually less than 1%.

The western plutons have a predominantly metaluminous character (Figure 12d), with mean Al_2O_3 contents of 15.5% wt

and lower ($CaO + Na_2O + K_2O$) contents of 11.7% wt. Some silica–enriched rocks reach the peraluminous series. The western plutons range from metaluminous, with Al_2O_3 contents of 15.34% wt and ($CaO + Na_2O + K_2O$) contents of 10.86% wt, to peraluminous in the rocks from the Garzón Granite and in most samples from the Altamira Monzogranite, with A/NK (1.74) > A/CNK (1.46).

Both groups of plutons of the UMV have markedly negative Nb, Ti, and P anomalies and positive anomalies and high values of Cs, Ba, Th, Sr, K, Pb, and Rb. These characteristics are typical of magmas that are generated in continental margin arc environments (Pearce et al., 1984; Pearce, 1996) with gradual depletion from LILE to HFSE (Figure 13).

The K_2O versus CaO ratios allow the differentiation between the high–K calc–alkaline granitoids (KCG) of the eastern plutons and the arc calc–alkaline granitoids (ACG) of the western plutons, according to the classification of Barbarin (1999). This suggests a mixed component (mantle and crust contributions) in the origin of these groups of granitoids. KCG are associated with crustal melting with a minor mantle contribution, whereas the mantle fraction prevails over the crustal component in ACG.

The (Ba/Sr) and (K/Rb) ratios are higher in the eastern bodies, with values of 3.29 and 34.92, respectively, that are associated with plagioclase crystallization (Green, 1980) and the ease of Ba replacement by K, indicating higher alkali enrichment. In contrast, the western plutons have values of 1.93 and 31.42, respectively.

The patterns of the chondrite–normalized rare earth elements (REE) (McDonough & Sun, 1995) of most of the samples are subparallel in both groups of plutons, with negative slopes and patterns similar to those of rocks generated in subduction environments above the subducted plate, including enrichment in light rare earth elements (LREE) and depletion in heavy rare earth elements (HREE) (Figure 14). Most samples have slightly positive Eu anomalies, with mean ratios of Eu/Eu* = 1.22 in the western plutons and Eu/Eu* = 1.14 in the eastern plutons; some of the samples had ratios of Eu/Eu* < 1 (Table 4).

The $(La/Yb)_n$ ratios range from 10 to 26 in the eastern plutons, with most values between 10 and 15, except in the Sombrerillo Quartz Monzonite, where they range from 4.8 to 7.3. In the western plutons, $(La/Yb)_n < 10$ in most samples, and a few rocks have values between 10 and 20 (e.g., 900642, 900643, 900752, 900673). These values are consistent and lower than those of the eastern plutons, suggesting decreased magmatic differentiation and decreased crustal contribution. The sums of the contents of the rare earth elements (∑ REE) range from 62.3 to 338 in the eastern plutons and from 36.7 to 252 in the western plutons (Table 4).

Both groups of plutons show characteristics of continental arc (Figure 15a, 15b), I–type (cordilleran) (Figure 15c), magnesian (oxidizing magmas) (Figure 15d) granites with greater enrichments in SiO_2 in the eastern plutons.

4.2.3. Geochronology

Forty samples of rocks and saprolites of granitoids and volcanic rocks from the UMV were dated using the U–Pb zircon LA–ICP–MS method. The samples correspond to the Anchique Quartz Monzonite, San Cayetano Quartz Monzonite, Los Naranjos Quartz Monzonite, Páez Quartz Monzodiorite, El Astillero Quartz Monzodiorite, Las Minas Monzonite, Algeciras Monzogranite, Teruel Quartz Latite, Garzón Granite, Altamira Monzogranite, Sombrerillo Quartz Monzonite, Mocoa Monzogranite, Saldaña Formation, and Pitalito Vulcanites (data sources: Arango et al., 2015a, 2015b, 2015c, 2015d, 2015e; Bermúdez et al., 2015; Rodríguez et al., 2015a, 2015b, 2015c, 2015d, 2015e, 2018a; Zapata et al., 2015). The locations of the samples are shown in Figure 10, and the ages are presented in Table 5.

The ages reported for the eastern and western plutons show clustering according to the spatial position of the bodies in the UMV, and the different age groups identify at least three magmatic pulses. The western plutons record a main magmatic pulse between 193 and 186 Ma with some ages between 182 and 178 Ma. The eastern plutons indicate narrow crystallization ages ranging from 173 to 169 Ma with some inherited and crystallization ages ranging from 182 to 179 Ma. The latter age range suggests an intermediate magmatic event that is present both in the western and eastern plutons, which likely occurred during the migration of magmatism within the arc (Rodríguez et al., 2018a).

The ages of the volcanic units in the UMV match the spatial distribution of the ages of both the western and eastern plutons. The Saldaña Formation is exposed near the western plutons and has crystallization ages ranging from 188.9 ± 4.2 to 186 ± 2.0 Ma with some intermediate ages of approximately 183 Ma, which is similar to those obtained in the western plutons (Rodríguez et al., 2016b). The Pitalito Vulcanites are located near the eastern plutons and have ages ranging from 172.4 ± 1.7 to 168 ± 2.5 Ma with intermediate ages of approximately 183–178 Ma, similar to those obtained in the eastern plutons (Table 5).

Zircons from Jurassic granitoids and volcanic rock samples from the UMV have rare inherited cores (Table 5), which suggest that they are derived from the Neoproterozoic basement that outcrops in the UMV, including the Garzón Group, the Mancagua and Guapotón Gneisses, and Las Minas Metamorphites. The metamorphic and inherited ages are similar to those found in zircon cores of the Jurassic granitoids and volcanic rocks (MIA–538, GZ–6774, GR–6611B, GR–6636, and JGB–355; data sources: Arango et al., 2015a, 2015b, 2015c, 2015d, 2015e; Bermúdez et al., 2015; Rodríguez et al., 2015a, 2015b, 2015c, 2015d, 2015e, 2018a; Zapata et al., 2015). These zircons may have been inherited from the Paleozoic sedimentary rocks that overlie the Precambrian crystalline basement. A second group of inherited ages of 183–181 Ma is interpreted to repre-

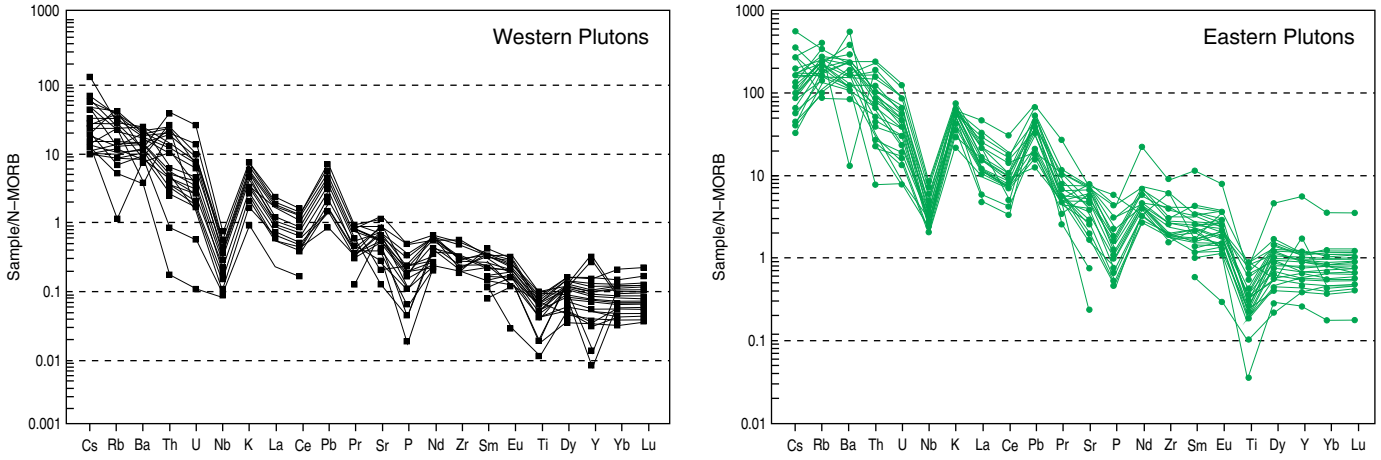

Figure 13. N–MORB–normalized trace element diagrams (Sun & McDonough, 1989) for both groups of plutons from the Upper Magdalena Valley (UMV). Data sources: Arango et al. (2015a, 2015b, 2015c, 2015d, 2015e); Bermúdez et al. (2015); Rodríguez et al. (2015a, 2015b, 2015c, 2015d, 2015e, 2018a); Zapata et al. (2015). Gray shading indicates the general pattern of trace elements of the arc.

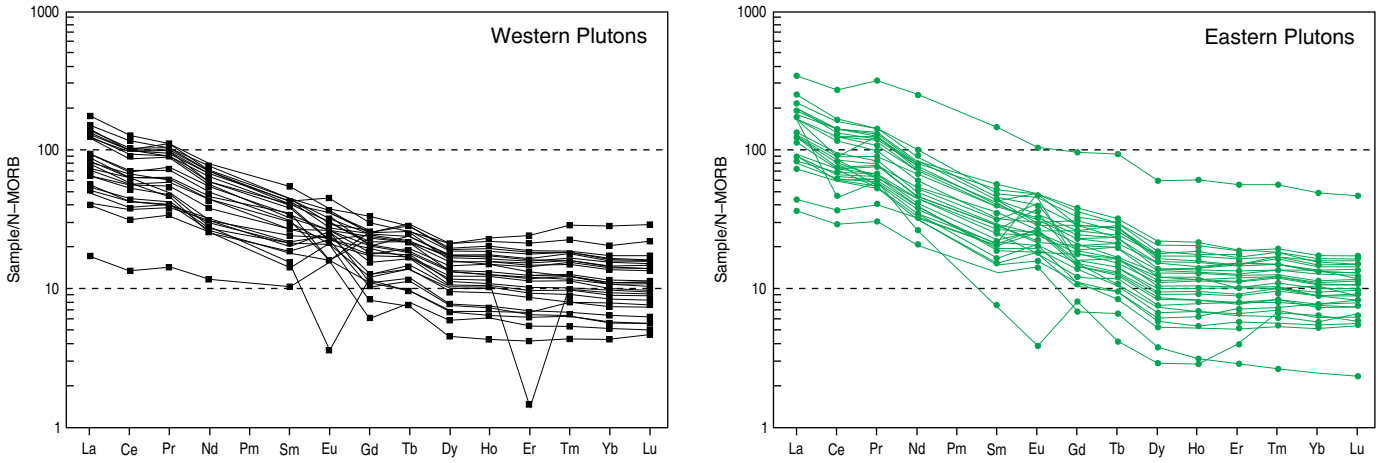

Figure 14. Chondrite–normalized rare earth element diagram (Nakamura, 1974) for both groups of plutons from the Upper Magdalena Valley (UMV). Data sources: Arango et al. (2015a, 2015b, 2015c, 2015d, 2015e); Bermúdez et al. (2015); Rodríguez et al. (2015a, 2015b, 2015c, 2015d, 2015e; 2018a); Zapata et al. (2015).

sent zircons or zircon cores that were inherited from previous pulses of magmatism in the same arc, which were assimilated or reincorporated in subsequent pulses in the magmatic chamber.

4.3. Northern Block of the Ibagué Batholith (NBIB)

The northern section of the Ibagué Batholith is called the "northern block of the Ibagué Batholith (NBIB)" in this paper. This block is bounded by the Ibagué Fault to the south and by the Otú–Pericos Fault to the east, and it is located southwest of the town of Armero to the Ibagué Fault line on the eastern flank of the Central Cordillera of Colombia (Figures 1, 16). Two intrusives, the Anzoátegui Metatonalite to the west and the Ibagué Tonalite to the east, have been identified in this block. They are separated by a block of metamorphic rocks that consists of schists, gneisses, quartzites, and amphibolites (Tierradentro Gneisses and Amphibolites sensu Barrero & Vesga, 1976).

The Anzoátegui Metatonalite has an irregular elongated shape that is approximately 55 km long and 27 km wide (Figure 16). It is in intrusive and locally faulted contact on the east and west with the Tierradentro Gneisses and Amphibolites. The granitoid shows mineral orientation and local development of gneissic structures (Figure 17a). The Ibagué Tonalite is elongated in the N–S direction and is approximately 78 km long and 19 km wide. It is covered by alluvial deposits and alluvial fans to the east and intrudes the metamorphic strip of Tierradentro Gneisses and Amphibolites to the west (Figure 16). It has a granular texture and an isotropic (Figure 17b) to locally oriented structure near the contact with the metamorphic block (Figures 16, 17). Both plutons are intruded by andesitic and dacitic dikes.

Table 4. Chondrite–normalized rare earth element diagram (Nakamura, 1974) for granitoids from the UMV.

IGM	UNIT	Eu/Eu*	(La/Yb)n	(La/Sm)n	(Ce/Yb)n	(Ce/Sm)n	(Eu/Yb)n	∑REE
			Western Plutons					
CB0007A*	Las Minas Monzodiorite	0.9	6.92	2.92	5.53	2.33	1.77	116.6
900752	Las Minas Monzodiorite	1.26	11.23	2.84	9.12	2.31	4.14	219.53
900643	Anchique Quartz Monzonite	1.08	15.05	4.29	11.23	3.2	2.83	204.95
900642	Anchique Quartz Monzonite	1.02	15.99	4.29	11.65	3.13	2.77	252.38
900647	Los Naranjos Quartz Monzonite	1.21	5.04	2.1	4.35	1.81	2.24	145.26
900651	Los Naranjos Quartz Monzonite	0.93	5.71	2.72	4.65	2.22	1.49	145.53
900650	Los Naranjos Quartz Monzonite	0.95	8.16	2.94	6.34	2.28	2.03	217.48
900641	Los Naranjos Quartz Monzonite	0.89	6.54	2.99	4.86	2.22	1.46	224.33
900649	Los Naranjos Quartz Monzonite	0.82	9.15	3.51	7.03	2.69	1.65	240.88
900823	San Cayetano Quartz Monzonite	1.07	9.11	3.04	6.27	2.09	2.57	197.82
900827	San Cayetano Quartz Monzonite	0.72	9.17	3.52	6.36	2.44	1.52	201.28
900825	San Cayetano Quartz Monzonite	0.69	8.04	3.08	6.06	2.32	1.43	201.81
900826	San Cayetano Quartz Monzonite	0.51	4.95	3.88	3.69	2.89	0.55	222.14
900824	San Cayetano Quartz Monzonite	0.89	8.52	2.57	6.22	1.88	2.3	237.3
900719	El Astillero Quartz Monzodiorite	1.1	6.2	2.62	4.88	2.07	2.25	132.55
900721	El Astillero Quartz Monzodiorite	1.11	7.57	2.95	5.73	2.23	2.43	142.48
900720	El Astillero Quartz Monzodiorite	0.94	6.58	2.72	4.92	2.04	1.89	163.41
900678	Páez Quartz Monzodiorite	1.97	3.33	1.7	2.63	1.34	3.01	36.68
900683	Páez Quartz Monzodiorite	1.63	7.06	2.16	5.55	1.7	3.96	74.86
900725	Páez Quartz Monzodiorite	1.13	9.79	3.12	7.28	2.32	2.77	89.79
900738	Páez Quartz Monzodiorite	1.14	4.06	1.68	3.71	1.54	2.32	91.87
900658	Páez Quartz Monzodiorite	1.46	6.61	2.25	5.15	1.75	3.28	92.17
900679	Páez Quartz Monzodiorite	1.27	5.72	2.4	4.71	1.98	2.29	94.39
900665	Páez Quartz Monzodiorite	1.28	6.05	2.53	5.07	2.12	2.32	98.43
900664	Páez Quartz Monzodiorite	1.73	10.36	3.28	8.26	2.62	4.04	108.23
900673	Páez Quartz Monzodiorite	1.96	18.86	5.8	13.14	4.04	4.87	108.29
900737	Páez Quartz Monzodiorite	0.27	11.35	5.72	8.05	4.06	0.47	119.76
900681	Páez Quartz Monzodiorite	1.28	7.68	2.41	6.62	2.08	3.07	120.75
900722	Páez Quartz Monzodiorite	0.97	8.07	2.89	6.52	2.33	2.28	138.87
900730	Páez Quartz Monzodiorite	0.6	5.71	2.97	4.4	2.29	1	161.17
900667	Páez Quartz Monzodiorite	1.1	8.05	3.12	6.2	2.4	2.12	228.64
			Eastern Plutons					
900718	Altamira Monzogranite	0.89	12.49	5.52	7.03	3.11	1.74	165.9
900734	Altamira Monzogranite	0.83	12.29	4	6.56	2.14	2.1	226
900745	Altamira Monzogranite	0.51	26.95	23.21	7.1	6.12	0.61	127.1
900749	Altamira Monzogranite	0.68	10.37	4.38	7.33	3.09	1.38	186.4
CB0005*	Altamira Monzogranite	1.49	14.81	2.73	11.77	2.17	5.82	62.28
900691	Altamira Monzogranite	1.2	17.65	7.28	10.92	4.51	2.35	166.6
900692	Altamira Monzogranite	1.03	13.09	4.13	10.17	3.21	2.54	250.2
900694	Altamira Monzogranite	1.54	20.56	6.69	14.41	4.69	3.81	147.1
900697	Altamira Monzogranite	1.13	14.75	4.49	10.71	3.26	3.03	331.7
900699	Altamira Monzogranite	1.1	16.77	5.43	11.25	3.65	2.68	338
900703	Altamira Monzogranite	1.44	14.9	7.54	9.13	4.62	2.35	139.1

Table 4. Chondrite–normalized rare earth element diagram (Nakamura, 1974) for granitoids from the UMV *(continued).*

IGM	UNIT	Eu/Eu*	(La/Yb)n	(La/Sm)n	(Ce/Yb)n	(Ce/Sm)n	(Eu/Yb)n	∑REE
900704	Altamira Monzogranite	1.15	15.28	5.13	10.6	3.56	2.74	230.4
900706	Altamira Monzogranite	1.04	15.95	5.22	10.36	3.39	2.45	269.3
900708	Altamira Monzogranite	1.03	14.89	5.03	10.34	3.49	2.38	283.1
900709	Altamira Monzogranite	1.03	12.93	4.37	9.4	3.18	2.34	287.8
900711	Altamira Monzogranite	1.24	17.54	6	11.57	3.96	3.11	119.6
900715	Garzón Granite	1.17	14.9	4.74	10.51	3.35	3.11	134.5
900716	Garzón Granite	1.43	11.14	3.77	8.01	2.71	3.25	182.7
900698	Teruel Quarz Latite	1.83	13.54	4.88	9.09	3.27	3.97	177.5
900712	Teruel Quarz Latite	1.7	12.13	4.38	8.41	3.04	3.65	196.4
900713	Teruel Quarz Latite	2.67	21.89	5.99	13.81	3.78	8.35	159.9
900781	Mocoa Monzogranite	1.05	10.35	2.9	7.88	2.21	3.09	272.2
900782	Mocoa Monzogranite	1.1	9.28	3.11	7	2.34	2.72	267.5
900784	Mocoa Monzogranite	1.02	11.28	4.67	8.17	3.39	2.04	188.2
900785	Mocoa Monzogranite	1.14	11.83	4.71	7.92	3.15	2.41	176.5
900813	Mocoa Monzogranite	1.06	11.88	5.35	7.9	3.56	1.99	162.1
900815	Mocoa Monzogranite	0.86	10.75	4.9	7.29	3.32	1.59	172
900816	Mocoa Monzogranite	1.4	12.38	4.14	8.5	2.84	3.46	137.3
900818	Mocoa Monzogranite	1.52	10.99	3.82	8.53	2.97	3.67	127.4
900819	Mocoa Monzogranite	1.36	12.72	4.97	8.46	3.31	2.95	155.3
900820	Mocoa Monzogranite	1.46	9.78	4.27	6.8	2.97	2.83	126.8
900821	Mocoa Monzogranite	1.18	9.65	4.44	6.53	3	2.17	158.9
900822	Mocoa Monzogranite	0.83	11.39	4.18	8.97	3.29	1.92	285.8
900764	Sombrerillo Quartz Monzonite	1.35	4.84	1.89	4.1	1.6	2.94	93.44
900765	Sombrerillo Quartz Monzonite	0.86	5.5	2.55	4.45	2.06	1.57	170
900766	Sombrerillo Quartz Monzonite	1.01	6.37	2.54	5.23	2.08	2.13	137.4
900768	Sombrerillo Quartz Monzonite	1.4	7.28	2.57	5.98	2.11	3.27	202.1
900768	Sombrerillo Quartz Monzonite	1.15	6.54	2.49	5.47	2.08	2.4	165.3
900768	Sombrerillo Quartz Monzonite	0.89	6.25	2.94	5.16	2.43	1.62	149
900808	Sombrerillo Quartz Monzonite	0.92	5.57	2.79	4.64	2.33	1.54	147.8
900810	Sombrerillo Quartz Monzonite	0.88	7.07	2.38	5.54	1.86	2.11	664.9

Source: Data from Arango et al. (2015a, 2015b, 2015c, 2015d, 2015e); Bermúdez et al. (2015); Rodríguez et al. (2015a, 2015b, 2015c, 2015d, 2015e, 2018a); Zapata et al. (2015).
n—normalized to chondrite values of Nakamura (1974).

4.3.1. Petrography

The Anzoátegui Metatonalite consists of metatonalites and metagranodiorites (Figure 18; Table 6) with polycrystalline quartz in polygonal to sutured mosaics (Figure 17c, 17d), which resulted from metamorphic recrystallization. The rocks are equigranular to inequigranular, medium–grained, white or gray with black spots, and have mineral orientation in most outcrops. Locally, the rocks lack mineral orientation and are isotropic. Plagioclase is zoned from oligoclase to sodic andesine (An28 to An34) based on the symmetrical zone albite twin method of Michel–Lévy. Orthoclase is rare and varies to interstitial microcline. The rocks contain mafic minerals such as biotite, which is usually altered to slightly oriented chlorite, and hornblende with clinopyroxene cores. Opaque minerals, apatite, zircon, and titanite are accessory minerals.

The Ibagué Tonalite consists of tonalites, subordinate quartz diorites and granodiorites (Figure 18; Table 7). It is white or gray with black spots and has an equigranular texture. The rocks are composed of anhedral quartz, oligoclase to sodic andesine plagioclase, and occasional interstitial orthoclase. It contains mafic minerals such as hornblende and biotite that are partly altered to chlorite, and it contains accessory minerals such as zircon, apatite, titanite, and opaque minerals (Figure 17e, 17f).

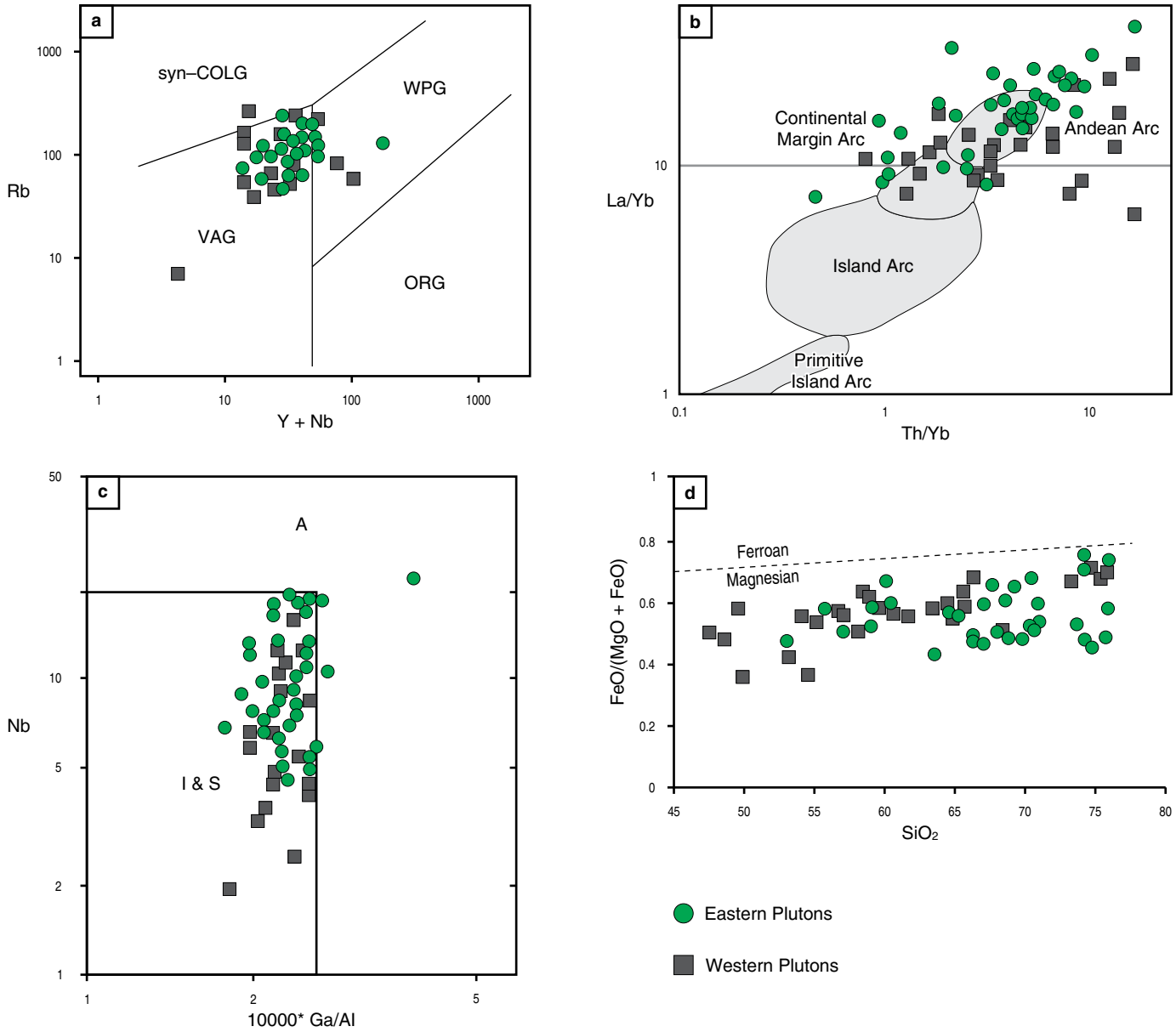

Figure 15. Geotectonic discrimination diagrams: **(a)** Y+Nb vs. Rb diagram of Pearce et al. (1984), **(b)** La/Yb vs. Th/Yb diagram of Condie (1989), **(c)** (Ga/al*10,000) vs. Nb diagram of Whalen et al. (1987), **(d)** FeO/(FeO + MgO) vs. SiO_2 diagram of Frost et al. (2001). Data sources: Arango et al. (2015a, 2015b, 2015c, 2015d, 2015e); Bermúdez et al. (2015); Rodríguez et al. (2015a, 2015b, 2015c, 2015d, 2015e, 2018a); Zapata et al. (2015).

4.3.2. Geochemistry

Whole–rock chemical analyses were performed on 3 rocks from the Anzoátegui Metatonalite and 4 rocks from the Ibagué Tonalite (Table 8). In addition, 8 sets of data from Bustamante et al. (2016) were compiled (see Table 1, Supplementary Information). The samples from both plutons have SiO_2 contents ranging from 50.3% to 67.8%. The K_2O contents range from 0.84% to 3.3% with values from 1% to 2% in most samples. CaO ranges from 3.35% to 9.8%, and TiO_2 is <1% except in sample JGB–492 (1.4% TiO_2). The plutons cluster in the field of tonalites and granodiorites in the TAS diagram, with some reaching the field of quartz diorites and quartz monzodiorites (Figure 19a), which is consistent with the petrographic data. The samples show decreases in TiO_2, MgO, and CaO and an increase in K_2O with increasing SiO_2.

The rocks plot in the field of the calc–alkaline series (Figure 19b, 19c). These rocks are mostly metaluminous (Figure 19d) with A/CNK ratios ranging from 0.7 to 1.05 and A/NK ratios ranging from 1.4 to 3, which indicates a low contribution of crustal material to the magma during the formation of the plutons.

Table 5. LA–ICP–MS U–Pb zircon ages of granitoid bodies and volcanic rocks from the UMV.

Sample	Latitude N	Longitude W	Classification	Unit	Age (Ma)	Inherited ages (Ma)
Western Plutons						
MIA–438	3° 33' 46.184"	75° 08' 26.761"	Monzonite	Anchique Quartz Monzonite	183.5 ± 3	
MIA–440	3° 39' 47.772"	75° 06' 20.693"	Monzonite	Anchique Quartz Monzonite	186.4 ± 1.4	
JGB–357	3° 41' 17.677"	75° 10' 51.437"	Quartz monzonite with px	San Cayetano Quartz Monzonite	173.3 ± 1.3	
JGB–356	3° 39' 52.894"	75° 10' 16.665"	Quartz monzonite with px	San Cayetano Quartz Monzonite	195.8 ± 1.5	
JGB–345	3° 21' 58.505"	75° 20' 38.041"	Monzodiorite	Los Naranjos Quartz Monzonite	187.9 ± 1.3	
GR–6634	2° 39' 57.305"	75° 55' 35.226"	Granodiorite	Páez Quartz Monzodiorite	180.2 ± 1.6	
GR–6639	2° 37' 45.611"	75° 44' 07.812"	Tonalite	Páez Quartz Monzodiorite	181.83 ± 0.91	
GR–6645	2° 15' 07.848"	75° 58' 19.470"	Granite	Páez Quartz Monzodiorite	191.9 ± 1.4	
MIA–454	2° 56' 37.242"	75° 30' 41.603"	Monzodiorite	Páez Quartz Monzodiorite	193.13 ± 1.4	
MIA–499	2° 32' 51.609"	75° 49' 56.785"	Quartz monzodiorite	Páez Quartz Monzodiorite	181.7 ± 3.8	
GR–6625	2° 20' 19.440"	75° 44' 44.618"	Monzodiorite	El Astillero Quartz Monzodiorite	187 ± 3.3	
MIA–482	2° 11' 43.395"	75° 51' 27.021"	Quartz monzodiorite	Las Minas Monzodiorite	181.6 ± 3.4	
Eastern Plutons						
GR–6585	2° 36' 17.331"	75° 19' 09.103"	Aplite in granodiorite	Algeciras Monzogranite	178.6 ± 1.2	
GR–6586	2° 35' 59.239"	75° 16' 49.980"	Granodiorite	Algeciras Monzogranite	171 ± 2.5	
GR–6589	2° 28' 22.946"	75° 24' 58.344"	Granite	Algeciras Monzogranite	169.6 ± 1.2	
GZ–6750	2° 45' 36.701"	75° 11' 48.824"	Quartz monzonite	Algeciras Monzogranite	179 ± 1.9	
MIA–458	2° 46' 25.626"	75° 30' 46.993"	Quartz monzonite	Teruel Quartz Latite	170.50 ± 1.10	181.1 ± 1.70
MIA–460	2° 44' 08.778"	75° 32' 25.933"	Quartz monzonite	Teruel Quartz Latite	174.1 ± 2.0	
GR–6619	2° 10' 01.284"	75° 36' 36.632"	Granite	Garzón Granite	170.8 ± 2.4	
GR–6652	1° 44' 56.859"	76° 01' 25.944"	Granite	Altamira Monzogranite	171.6 ± 1	
JGB–390	1° 50' 36.121"	75° 54' 31.726"	Granite	Altamira Monzogranite	172 ± 3.9	
MIA–478	1° 53' 05.855"	75° 53' 44.793"	Monzogranite	Altamira Monzogranite	169.4 ± 3.2	
GZ–6780	1° 10' 04.832"	76° 51' 39.289"	Quartz monzodiorite	Sombrerillo Quartz Monzonite	173.8 ± 2.2	
MIA–512	1° 48' 42.758"	76° 17' 34.195"	Granodiorite	Sombrerillo Quartz Monzonite	176.3 ± 2.5	
MIA–525	1° 54' 17.460"	76° 08' 48.014"	Monzogranite Saprolite	Sombrerillo Quartz Monzonite	181.5 ± 4.0	
GR–6672	1° 04' 17.186"	76° 44' 12.719"	Quartz monzodiorite	Mocoa Monzogranite	171.6 ± 1.2	
MIA–538	1° 04' 08.328"	76° 46' 16.618"	Granitic saprolite	Mocoa Monzogranite	181.8 ± 1.3	939 ± 40
MIA–543	1° 12' 06.116"	76° 40' 54.752"	Granitic saprolite	Mocoa Monzogranite	170.7 ± 2.1	
Volcanic Rocks						
GR–6611B	2° 48' 40.70"	75° 35' 22.34"	Phenotrachyte	Saldaña Formation	188.9 ± 1.6	923 ± 24, n=1
GR–6636	2° 19' 46.38"	75° 48' 47.34"	Andesite	Saldaña Formation	187.1 ± 2.4	510, n=1; 1960, n=1
GR–6664	1° 26' 0.53"	76° 26' 47.05"	Andesite	Saldaña Formation	183.3 ± 1.1	
MIA–504	2° 7' 48.30"	76° 4' 7.02"	Andesite	Saldaña Formation	188.9 ± 4.2	
MIA–519	2° 9' 24.95"	76° 0' 59.55"	Andesite	Saldaña Formation	188.1 ± 3.4	
GR–6579	3° 28' 55.25"	75° 14' 42.79"	Lithic tuff	Saldaña Formation	187.2 ± 2.8	
GZ–6775	1° 6' 43.10"	76° 50' 5.32"	Crystal tuff	Saldaña Formation	186.8 ± 2.0	
GZ–6774	1° 5' 35.28"	76° 50' 20.90"	Crystal tuff	Saldaña Formation	172.9 ± 1.3	223.48 ± 9.5, n=1 and 906.3 ± 21.1, n=1
JGB–355	2° 48' 59.55"	75° 21' 46.52"	Tuff	Pitalito Vulcanites	178.7 ± 4.5	980–1060, n=4; 1460, n=1; 1570, n=1; 1630, n=1; 2770, n=1
GR–6649	1° 45' 42.92"	76° 2' 25.09"	Phenocryst andesite	Pitalito Vulcanites	172.4 ± 1.7	183.30 +0.30/-3.30, n=20

Table 5. LA–ICP–MS U–Pb zircon ages of granitoid bodies and volcanic rocks from the UMV *(continued)*.

Sample	Latitude N	Longitude W	Classification	Unit	Age (Ma)	Inherited ages (Ma)
GZ–6766	1° 57' 1.26"	76° 3' 20.24"	Dacite	Pitalito Vulcanites	170.7 ± 2.4	
GZ–6769	1° 40' 54.67"	76° 13' 7.69"	Rhyolite	Pitalito Vulcanites	168 ± 2.5	

Source: Data from Arango et al. (2015a, 2015b, 2015c, 2015d, 2015e); Bermúdez et al. (2015); Rodríguez et al. (2015a, 2015b, 2015c, 2015d, 2015e, 2018); Zapata et al. (2015).

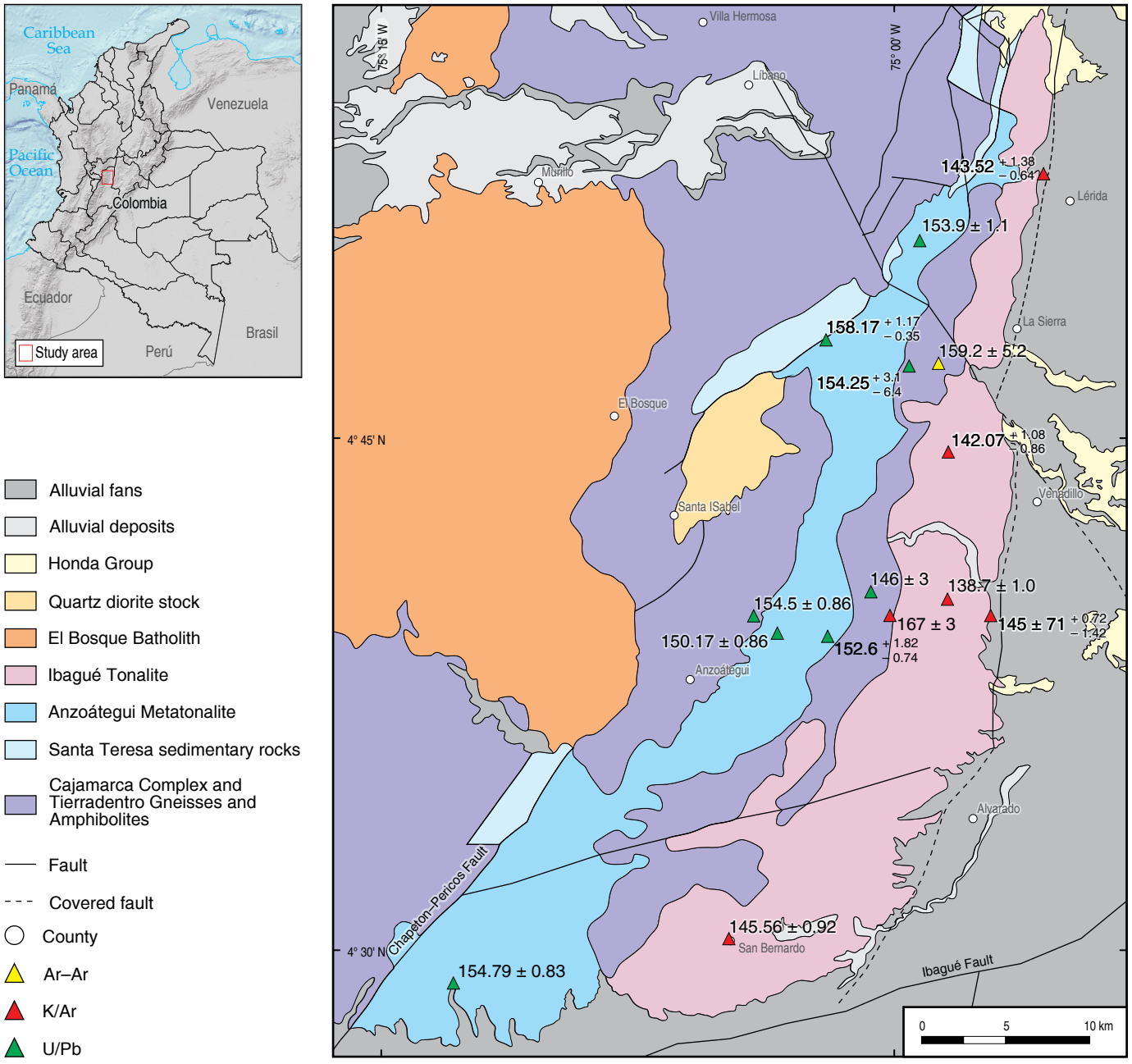

Figure 16. Geological map and U–Pb zircon ages of the Anzoátegui Metatonalite and Ibagué Tonalite. The K–Ar data are from Vesga & Barrero (1978) and McCourt et al. (1984), the Ar–Ar data are from Villagómez et al. (2011), and the U–Pb data are from Bustamante et al. (2016) and this study.

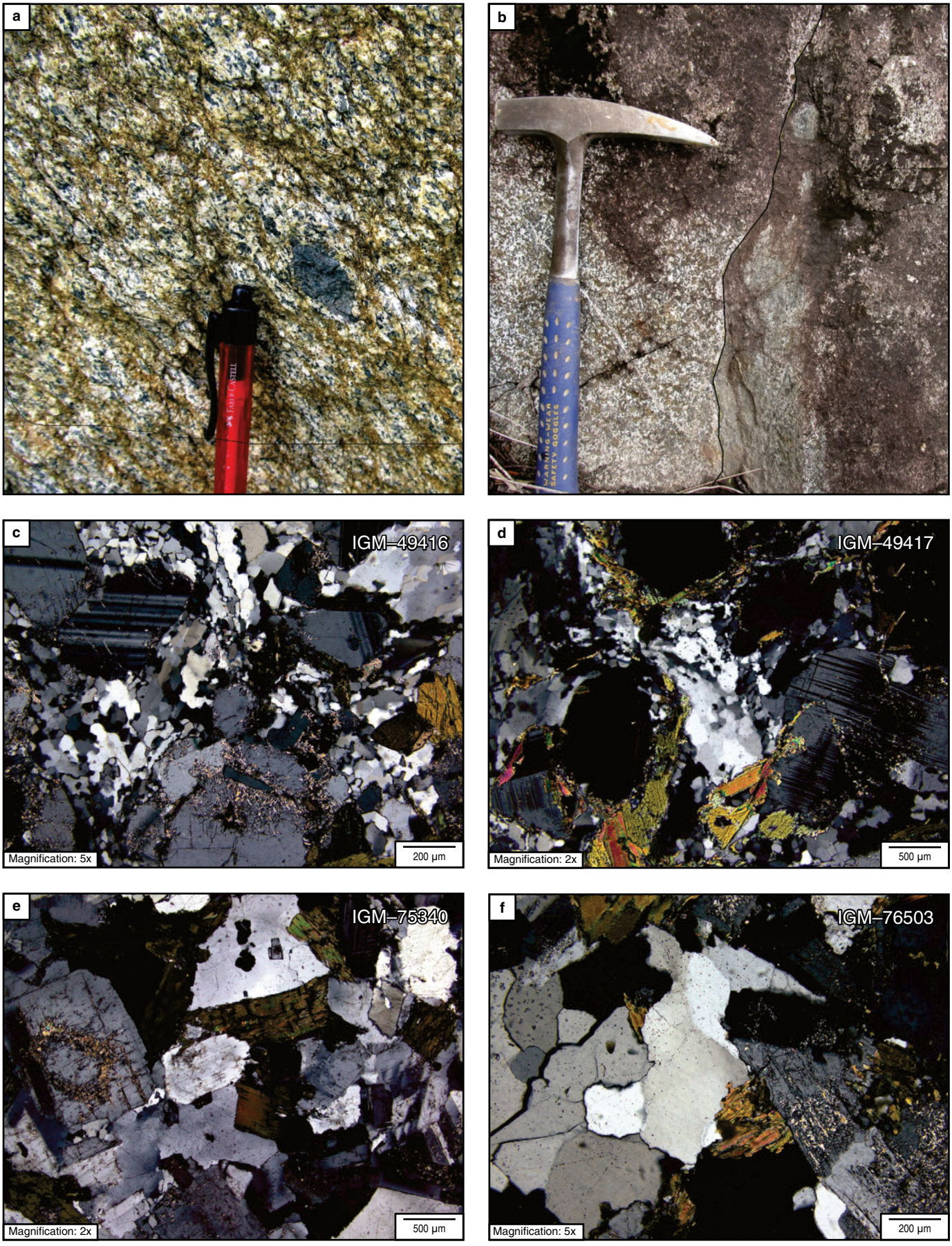
a
b
c
IGM–49416
Magnification: 5x
200 µm
d
IGM–49417
Magnification: 2x
500 µm
e
IGM–75340
Magnification: 2x
500 µm
f
IGM–76503
Magnification: 5x
200 µm

Figure 17. (a) Macroscopic view of the Anzoátegui Metatonalite (IGM–49416, IGM–49417) with mineral orientation and enclaves. **(b)** Ibagué Tonalite with schist xenolith and granular texture. **(c), (d)** microscopic views of the Anzoátegui Metatonalite (IGM–49416, IGM–49417). **(e), (f)** microscopic views of the Ibagué Tonalite (IGM–75340, IGM–76503).

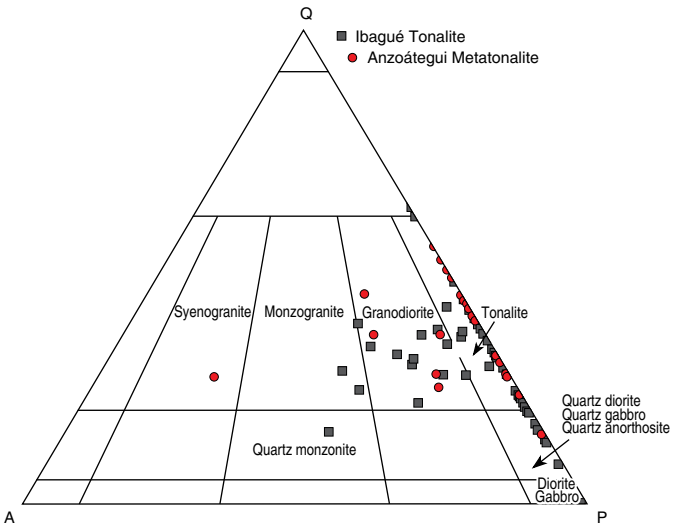

Figure 18. Modal compositions of the Anzoátegui Metatonalite and Ibagué Tonalite in the NBIB. Quartz, Alkali feldspar, Plagioclase, Feldspathoid (QAPF) diagrams of Streckeisen (1974).

Both tonalitic plutons show markedly negative Nb, Ti, Ce, and P anomalies and positive anomalies and high values of Cs, Ba, Th, Sr, K, Pb, and Rb, similar to the patterns of continental margin magmatic arcs (Pearce, 1996) with gradual depletion from LILE to HFSE (Figure 19e).

Based on the values of Nakamura (1974), the patterns of the chondrite–normalized REE for both plutons are subparallel with negative slopes and are similar to patterns for rocks that are generated in subduction environments above the subducted plate, with enrichment in LREE and depletion in HREE (Figure 19f). These results are consistent with those of Bustamante et al. (2016). They have negative Eu anomalies with Eu/Eu* ratios ranging from 0.52 to 0.93, indicating plagioclase fractionation at the source (Table 9). The $(La/Yb)_n$ ratios range from 3.9 to 10.9 with no major differences in the $(La/Sm)_n$, $(Ce/Yb)_n$, $(Ce/Sm)_n$, and $(Eu/Yb)_n$ ratios between the two plutons (Table 9).

In the tectonic environment discrimination diagrams, the samples from both intrusives plot within continental margin arcs of calc–alkaline affinity (Figure 20a) and within I–type granites (Figure 20b).

4.3.3. Geochronology

Eight rocks from the NBIB were dated, including three samples from the Anzoátegui Metatonalite, two from the Ibagué Tonalite, and three from the Tierradentro Gneisses and Amphibolites (Table 10).

4.3.3.1. Igneous Ages

The following samples from the Anzoátegui Metatonalite were dated: one tonalite (GOE–1088) with a weighted mean age of 154.79 ± 0.83 Ma (n = 91, MSWD = 3.1, and Th/U ratios ranging from 0.3 to 1.3); one metatonalite (LMC–104) with a U–Pb weighted mean age of 153.9 ± 1.1 Ma (n = 39, MSWD = 2.5, and Th/U ratios ranging from 0.43 to 0.9); and one metagranodiorite (AMC–0153) with a U–Pb zircon weighted mean age of 159.91 ± 0.69 Ma (n = 67, MSWD = 1.4, and Th/U ratios ranging from 0.31 to 1.24) (Figure 21). These ages represent magmatic crystallization ages based on the concentric structures of the zircons in CL images and the Th/U ratios.

Two samples from the Ibagué Tonalite were dated, including a granodiorite (MIG–076) with a U–Pb weighted mean age of 145.52 ± 0.82 (n = 67, MSWD = 4.5, and Th/U ratios ranging from 0.34 to 1.1; Figure 21) and a tonalite (JPZ–001A) with a U–Pb zircon weighted mean age of 138.48 ± 0.95 Ma (n = 53, MSWD = 2.2, and Th/U ratios ranging from 0.45 to 0.88). These ages represent magmatic crystallization ages based on the concentric structures of the zircons in CL images and the Th/U ratios.

4.3.3.2. Basement Ages

Three samples from the Tierradentro Gneisses and Amphibolites unit were dated, including two amphibolites from the metamorphic strip that separates the two intrusive bodies (AMC–0171 and MIG–074) and one sample from a metamorphic strip west of the Anzoátegui Metatonalite (AMC–0152). The results are shown in Figure 22. AMC–0171 corresponds to an amphibolite with a weighted mean age from zircon edges of 167.3 ± 3.0 Ma (n = 11, MSWD = 3.2, and Th/U ratios ranging from 0.012 to 0.048), in which the individual ages range from 174.6 Ma to 161.3 Ma. These are interpreted as metamorphic ages. AMC–0171 shows inheritances from the Mesoproterozoic (n = 1), Neoproterozoic (1141 to 728 Ma; n = 9), Cambrian (n = 5), Devonian (n = 4), Permian (264.7 Ma; n = 1), Triassic (223 Ma to 240 Ma; n = 3), and Early Jurassic (187.1 ± 3.8 Ma; n = 9). The structures of the zircons are complex and are characterized by abundant inherited cores and metamorphic overgrowths. MIG–074 also corresponds to an amphibolite, and the analyzed zircons were concentrated from a saprolite. Thirty–two consistent analyses indicate a median age of 154.5 +3.1/–6.4 Ma, which is interpreted as a magmatic crystallization age based on the concentric, zoned structures of the zircons in the CL images and the Th/U ratios ranging from 0.25 to 3.9. This sample yielded the following ages from inherit-

Table 6. Modal compositions of rocks from the Anzoátegui Metatonalite.

Anzoátegui Metatonalite															
IGM	**Sample**	**Longitude W**	**Latitude N**	**Qtz**	**Pl**	**Kfs**	**Cpx**	**Hbl**	**Bt**	**Op**	**Ap**	**Zrn**	**Ttn**	**Ep**	**Classification**
49277	GB–1422	74° 58' 14.24''	4° 51' 11.38''	7	41	Tr	Tr	33	19		Tr	Tr	Tr	Tr	Quartz diorite
901079	LMC–104	74° 59' 3.23''	4° 50' 36.88''	18	45	10		15	12	Tr	Tr	Tr		Tr	Granodiorite
77804	PM–8221	75° 9' 13.61''	4° 33' 21.50''	26.3	57.7	12.4	Tr	2.1	1.5	Tr	Tr	Tr	Tr		Metagranodiorite
49668	DMT–5474	75° 2' 54.50''	4° 38' 5.88''	25.4	31.7	14.3	1.6	7.9	12.7	Tr			4.8		Metagranodiorite
77805	PM–8224	75° 9' 27.27''	4° 33' 46.22''	31	49.6	7	Tr	3.1	9.3	Tr	Tr	Tr	Tr		Metagranodiorite
49444	VW–4539	75° 1' 35.44''	4° 43' 20.10''	17.5	13	34.8	Tr	18.8	Tr				5.8	Tr	Metagranodiorite
49644	IB–167	75° 2' 12.49''	4° 40' 10.28''	25.3	22.3	10	Tr	38.7	Tr						Metagranodiorite
48469	GB–1104	74° 57' 0.70''	4° 52' 41.64''	21.8	51.5	Tr	Tr	16.5	8	1.5	0.25	0.25	0.25	Tr	Metatonalite
48473	GB–1114	74° 56' 13.30''	4° 52' 29.66''	22.5	33.3	Tr	Tr	24.3	5	1.4		3.6	6.8		Metatonalite
49304	HP–3214	75° 0' 8.98''	4° 45' 24.89''	21	33	Tr	Tr	15	5		Tr		Tr	7	Metatonalite
49243	PM–6028	75° 0' 24.49''	4° 48' 37.56''	19	51	Tr	Tr	0	13		Tr	Tr	Tr	4	Metatonalite
49416	PM–6388	75° 2' 21.72''	4° 41' 58.99''	24	53	Tr	Tr	10	8		Tr	Tr	3	Tr	Metatonalite
49417	PM–6391	75° 2' 32.10''	4° 41' 56.37''	35	39	Tr	Tr	9	16		Tr	Tr	1	Tr	Metatonalite
48470	GB–1105	74° 56' 55.50''	4° 52' 40.02''	31.5	50.5	Tr	Tr	12.5	4	0.75	0.35	0.2	0.2	Tr	Metatonalite
48471	GB–1109	74° 56' 30.51''	4° 52' 37.12''	33.5	47	Tr	Tr	8	10.5	0.6	0.3		0.1	Tr	Metatonalite
68436	PM–7124	75° 3' 20.60''	4° 35' 58.24''	27.3	26.1	Tr	Tr	33	10.2	Tr		3.4			Metatonalite
49673	DMT–5519	75° 3' 41.81''	4° 37' 33.26''	26.7	28	Tr	Tr	22.7	6.7	Tr	0		2.7	4	Metatonalite
901072	JPZ–004	75° 2' 40.24''	4° 39' 4.03''	29.2	37.5			25	2.8	1.4	2.8		1.4		Metatonalite
49425	VW–4349	75° 2' 57.19''	4° 47' 7.19''	39	33.7				26	Tr			1.3		Metatonalite
49298	HP–3169	74° 59' 17.87''	4° 49' 27.62''	18	61	Tr	Tr	14	5		Tr	Tr	0	Tr	Tonalite
49301	HP–3195	74° 58' 47.30''	4° 50' 41.88''	16	44	Tr	Tr	25	15		Tr	Tr		Tr	Tonalite
49643	IB–643	75° 3' 13.15''	4° 40' 6.29''	20	44.1	Tr	Tr	22	10.2		1.7		1.7		Tonalite
49647	IB–187	75° 4' 10.95''	4° 36' 49.60''	26.5	42.2	Tr	4.8	21.7	0	Tr			2.4	2.4	Tonalite
49646	IB–180	75° 4' 58.59''	4° 36' 15.03''	22.9	31.3	Tr	Tr	31.3	0	1	2		7.3	4.2	Tonalite

Tr—Traces of accessory mineral.

ed cores: a crystal with Neoproterozoic ages of 1084.6 Ma (n = 1) and 987.9 Ma (n = 1), a concordant age of 207.6 Ma (n = 1), and a discordant age of 187 Ma (n = 1). Sample AMC–0152, which was collected from an amphibolite, yielded a weighted mean age of 154.5 ± 3.6 Ma (n = 13, MSWD = 6.3, and Th/U ratio <0.2). The zircons are homogeneous, and some have luminescent borders and rounded ends (Figure 22). They are interpreted as metamorphic zircons.

5. Discussion

5.1. SM, UMV, and NBIB Basements

Our interpretation of the distribution of metamorphic basement related to the Jurassic magmatism in Colombia is shown in Figure 1b, which shows three basement units. These include an Early Neoproterozoic basement, which corresponds to the Andaquí Terrane and most of the Chibcha Terrane based on Restrepo & Toussaint (1989); a Paleozoic basement, which corresponds to most of the Norte de Santander, Santander, Floresta, and Quetame Terranes, according to Etayo–Serna et al. (1983); and an Ordovician and Mesozoic basement, which includes most of the Tahamí Terrane as described by Restrepo & Toussaint (1989), the Tierradentro Gneisses and Amphibolites (previously included in the Chibcha Terrane by Restrepo & Toussaint, 1989), and the Anacona Terrane (Martens et al., 2014; Restrepo et al., 2009).

In the SM, Late Triassic – Early Jurassic arc magmatic rocks were emplaced in a variable metamorphic basement. In the extreme northern part of the SM, the basement is represented by Neoproterozoic migmatitic amphibolites (dated at approximately 945 ± 40 Ma K–Ar by Goldsmith et al. (1971) and at approximately 897 ± 28 Ma U–Pb in this study; coordinates 8° 17' 21" N, 73° 24' 56" W). The Neoproterozoic data are correlated with those reported by Ibañez–Mejia et al. (2011) in units of the Putumayo Orogen (Garzón Massif, Las Minas Migmatites,

Table 7. Modal compositions of rocks from the Ibagué Tonalite.

Ibagué Tonalite																
IGM	Sample	Longitude N	Latitude W	Qtz	Pl	Kfs	Cpx	Hbl	Bt	Chl	Op	Ap	Zrn	Ttn	Ep	Classification
49280	GB–1462	4° 45' 14.72"	74° 56' 59.48"	15	57	Tr	Tr	12	16	Tr				Tr	Tr	Quartz diorite
49290	GB–1517	4° 38' 58.92"	74° 59' 2.94"	19	65	Tr	Tr	5	11	Tr		Tr	Tr			Quartz diorite
76501	HC–748	4° 34' 42.36"	74° 59' 46.41"	15.6	64.35	Tr	Tr	11.9	7.92	Tr	Tr				Tr	Quartz diorite
77741	HC–946	4° 30' 37.55"	75° 4' 17.57"	17.5	42.97	4.94	Tr	19.4	15.2	Tr	Tr	Tr	Tr	Tr	Tr	Quartz diorite
49291	HP–3140	4° 47' 52.18"	74° 58' 1.65"	14	60	Tr	Tr	17	9	Tr			Tr		Tr	Quartz diorite
49295	HP–3159	4° 48' 46.26"	74° 57' 27.98"	16	57	Tr	Tr	6	14	Tr					7	Quartz diorite
49241	PM–6021	4° 47' 27.57"	74° 56' 25.25"	12	65	Tr	Tr	5	12	Tr	4	Tr		Tr		Quartz diorite
49242	PM–6034	4° 46' 59.54"	74° 56' 55.39"	15	63	Tr	Tr	8	14	Tr		Tr	Tr	Tr	Tr	Quartz diorite
49246	PM–6050	4° 44' 13.20"	74° 56' 51.29"	10	68	Tr	Tr	13	9	Tr	Tr	Tr	Tr	Tr	Tr	Quartz diorite
49256	PM–6105	4° 40' 47.73"	74° 57' 48.46"	13	65	Tr	Tr	17	5	Tr		Tr			Tr	Quartz diorite
49248	PM–6260	4° 44' 6.24"	74° 58' 28.29"	14	53	Tr	7	17	9	Tr	Tr	Tr	Tr		Tr	Quartz diorite
49258	PM–C15	4° 40' 50.92"	74° 58' 46.21"	15	59	Tr	1Tr	15	1	Tr		Tr		Tr	Tr	Quartz diorite
75339	VW–4851	4° 28' 54.65"	75° 6' 44.52"	10	64	Tr	Tr	18.5	7	Tr	0.5	Tr	Tr	Tr	Tr	Quartz diorite
76502	HC–760	4° 33' 47.05"	74° 59' 24.93"	5.6	61.7			17	8.1	Tr	Tr	Tr			1.5	Quartz diorite
49274	GB–1401	4° 50' 16.20"	74° 56' 13.78"	19	54	17	Tr	0	9	Tr	1		Tr		Tr	Quartz monzodiorite
49310	HP–3273	4°45´42.29"	74° 58' 15.60"	0	75	Tr	Tr	25	Tr	Tr		Tr	Tr		Tr	Diorite
49492	JV–4342	4° 54' 40.83"	74° 56' 18.33"	15	40	Tr	Tr	44	Tr	Tr	1				Tr	Diorite
49281	GB–1471	4° 45' 8.12"	74° 58' 8.26"	26	50	Tr	Tr	12	12	Tr		Tr	Tr	Tr	Tr	Granodiorite
76503	HC–779	4° 33' 34.02"	74° 59' 31.07"	13	39.9	32.5	Tr	Tr	11.4	Tr	Tr	Tr		0.2		Granodiorite
77765	HC–980	4° 32' 8.59"	75° 9' 11.56"	33.5	36.6	19.5	Tr	Tr	9.3	Tr	0.5	Tr	Tr	0.6	Tr	Granodiorite
48533	IV–3656	4° 55' 16.63"	74° 56' 24.38"	30.4	53.8	6.9	Tr	Tr	7.9		0.5	Tr	0.5	0	Tr	Granodiorite
77793	PM–8167	4° 28' 20.30"	75° 6' 47.55"	29.5	44.5	9.43	Tr	8.68	6.32	Tr	0.8	Tr	0	0.75	Tr	Granodiorite
901080	LMC–105	4° 50' 42.37"	74° 56' 42.27"	26	47	13			12	Tr	2	Tr	0		Tr	Granodiorite
48534	IV–3656–A	4° 55' 16.63"	74° 56' 24.38"	22.7	37.1	12.8	Tr	19.8	0	Tr	2.1	1.5	1.3	2.7	Tr	Granodiorite
68438	PM–7131–A	4° 35' 49.90"	75° 1' 53.65"	14.3	27	7.9	Tr	25.4	11.1	Tr	1.6	3.2		9.5	Tr	Granodiorite
76499	HC–728	4° 35' 42.32"	74° 58' 56.85"	22.4	50.9	9.69	Tr	10.6	5.73	Tr	0.4		Tr	0.2	Tr	MetaGranodiorite
68440	DMT–6059	4° 35' 55.79"	75° 1' 26.41"	26.1	36.2	17.4	Tr	5.8	8.7	Tr	1.4	Tr		4.3	Tr	MetaGranodiorite
77795	PM–8174	4° 29' 26.88"	75° 4' 40.51"	28.6	45.2	Tr	Tr	9.5	14.3		2.4	Tr		0	Tr	MetaTonalite
48537	JV–3660	4° 54' 54.04"	74° 56' 0.99"	24.8	52.2	Tr	Tr	15.7	3.6	TR	1.22	1.5	Tr	1		MetaTonalite
901098	MIG–076	4° 30' 9.62"	75° 4' 37.45"	17.5	62.7			7.2	11.4		1.2	Tr	Tr	0	Tr	MetaTonalite
49303	HP–3207	4° 45' 44.21"	74° 58' 41.07"	30	44	Tr	Tr	5	10	Tr		Tr	Tr	3	8	MetaTonalite
49305	HP–3220	4° 45' 21.53"	74° 59' 23.71"	29	18	Tr	Tr	7	9	Tr		Tr		2	Tr	MetaTonalite
76493	PM–7977	4° 34' 40.07"	74° 59' 54.19"	17	59	Tr	Tr	9	15	Tr	Tr	Tr	Tr	0	Tr	MetaTonalite
77794	PM–8171	4° 29' 1.41"	75° 5' 36.26"	48.6	32.4	Tr	Tr	8.2	2.7		2.7			5.4		MetaTonalite
49275	GB–1405	4° 50' 8.67"	74° 56' 47.52"	22	44	26	Tr	Tr	8	Tr					Tr	Monzogranite
49294	HP–3152	4° 48' 52.68"	74° 56' 30.87"	22	34	23	Tr	7	11	Tr		Tr			3	Monzogranite
48474	GB–1118	4° 52' 23.18"	74° 55' 51.87"	17.1	43.8	Tr	Tr	22.9	0	5.2	2.9		2.4	1	Tr	Tonalite
49276	GB–1409	4° 50' 9.27"	74°57' 28.08"	30	58	Tr	Tr	0	12	Tr	Tr	Tr	Tr		Tr	Tonalite
49288	GB–1502	4° 39' 1.00"	74° 57' 21.08"	22	50	Tr	Tr	11	17	Tr		Tr				Tonalite
49289	GB–1507	4° 38' 38.81"	74° 58' 4.52"	16	55	Tr	Tr	10	19			Tr		Tr	Tr	Tonalite
48507	HP–2761	4° 53' 10.38"	74° 55' 45.93"	29.5	49.5	3	Tr	11.5	4.5	Tr	1	0.25	0.25	0.5	Tr	Tonalite
49293	HP–3149	4° 48' 49.44"	74° 56' 24.06"	18	33	Tr	Tr	39	10	Tr		Tr	Tr		Tr	Tonalite
49302	HP–3200	4° 46' 7.90"	74° 57' 31.02"	25	56	Tr	Tr	10	9	Tr		Tr	Tr	Tr	Tr	Tonalite
49306	HP–3225	4° 42' 0.21"	74° 59' 16.31"	22	55	Tr	Tr	9	17	Tr		Tr	Tr		Tr	Tonalite
48536	IV–3659	4° 55' 0.71"	74° 56' 5.22"	24.8	38.1	5.4	Tr	14.9	3.5	6.9	1		1			Tonalite
49322	JV–4075	4° 54' 21.80"	74° 56' 9.71"	19	52	Tr	Tr	21	8	Tr		Tr	Tr	Tr	Tr	Tonalite
49244	PM–6047	4° 44' 10.30"	74° 56' 32.47"	15.9	40.7	Tr	Tr	23.4	0	7.5	3.3		1.9		2.8	Tonalite
49257	PM–6110	4° 40' 49.33"	74° 58' 14.42"	22	56	Tr	Tr	13	9	Tr		Tr	Tr		Tr	Tonalite
49259	PM–6122	4° 40' 16.37"	74° 59' 15.53"	27	45	Tr	Tr	15	13	Tr		Tr	Tr	Tr	Tr	Tonalite
49452	VW–4620	4° 54' 23.89"	74° 56' 31.94"	23	50	Tr	Tr	27	0		Tr	Tr				Tonalite
75338	VW–4850	4° 28' 54.65"	75° 6' 44.52"	20	64.6	Tr	Tr	1.4	13	Tr	1	Tr	Tr	Tr	Tr	Tonalite
75340	VW–4852	4° 28' 54.65"	75° 6' 44.52"	25	60	2	Tr	2.5	9	Tr	1.5	Tr	Tr	Tr	Tr	Tonalite

Table 7. Modal compositions of rocks from the Ibagué Tonalite *(continued).*

Ibagué Tonalite																
IGM	**Sample**	**Longitude N**	**Latitude W**	**Qtz**	**Pl**	**Kfs**	**Cpx**	**Hbl**	**Bt**	**Chl**	**Op**	**Ap**	**Zrn**	**Ttn**	**Ep**	**Classification**
49287	GB–1501	4° 38' 57.11''	74° 57' 8.42''	18	67			9	6			Tr				Tonalite
49267	PM–6145	4° 46' 20.78''	74° 57' 8.00''	20	54			15	11	Tr	Tr	Tr	Tr		Tr	Tonalite
49498	JV–4375	4° 55' 40.46''	74° 55' 31.35''	26.7	36	Tr	Tr	25.3	Tr		Tr				Tr	Tonalite
48535	IV–3658	4° 55' 6.40''	74° 56' 8.63''	33.7	45.2	3.1	Tr	3.8	12.7	Tr	1	0.5	Tr			Tonalite
49230	PM–5977	4° 51' 34.68''	74° 55' 51.00''	27.3	47.7	Tr	Tr	15.9	6.8	Tr	2.3		Tr		Tr	Tonalite
49635	PM–6551	4° 36' 17.29''	75° 1' 18.65''	25.7	30	Tr	Tr	30	8.6	Tr					Tr	Tonalite
901070	JPZ–001–A	4° 40' 11.16''	74° 58' 26.37''	23.1	44.6			24.6	6.2		Tr		Tr	1.5		Tonalite
48529	IV–3643	4° 56' 4.78''	74° 56' 47.49''	25.3	44.2	3.2	Tr	21.4	0	Tr	1.1	0.7			Tr	Tonalite

Tr—Traces of accessory mineral.

Los Mangos Granulite–Dibulla Gneiss) and correspond to the Andaquí Terrane and to the eastern edge of the Chibcha Terrane according to Restrepo & Toussaint (1989). Toward the SM core, the metamorphic basement consists of schists and gneisses with Early Ordovician metamorphic ages (Bucaramanga Gneiss, Silgará Schists, orthogneiss bodies) (Rodríguez et al., 2017b; van der Lelij, 2013; van der Lelij et al., 2016; Zuluaga et al., 2017) and pre–kinematic and post–kinematic Paleozoic plutons, which together form a terrain that has been related to the Famatinian Orogeny (Mantilla–Figueroa et al., 2016; van der Lelij, 2013; van der Lelij et al., 2016; Zuluaga et al., 2017) that has been identified along the western continental margin of South America from Chile to Venezuela. The boundary between the Neoproterozoic basement terrane and the terrane that forms the Santander Famatinian Orogen likely corresponds to a branch of the Bucaramanga Fault (Figure 2), although this is not well established due to mapping problems. The relationships between the Jurassic plutons and volcanic rocks and the basement remain unclear. Apparently, the compositions and ages of the plutons vary from the Neoproterozoic basement to the Ordovician basement, although further studies are necessary to document these characteristics in detail.

The Jurassic igneous rocks of the UMV block have a Neoproterozoic metamorphic basement (Garzón Group, Mancagua and Guapotón Gneisses, Las Minas Metamorphites), which is similar to the rocks of similar ages at serranía de San Lucas (San Lucas Gneiss) and Sierra Nevada de Santa Marta (Los Mangos Granulite) as well as those outcropping at serranía de Cocinas in Upper Guajira (Jojoncito Gneiss) and in the NW part of the SM (migmatitic amphibolites). Paleozoic sedimentary rocks (Mudstones and Granadillo Limestones, La Jagua Paleozoic, El Hígado Formation, and La Batalla Limestones and Sandstones at the UMV), blocks of Permian granitoids that formed in a continental margin arc environment (La Plata Granite at the UMV, Nechí Gneiss at serranía de San Lucas, and mylonitic granitoids in the Sierra Nevada de Santa Marta), and Upper Triassic limestones (Payandé Formation at the UMV) have been identified over the metamorphic basement.

The results of this study show that the metamorphic basement of the NBIB corresponds to the Tierradentro Gneisses and Amphibolites unit, which as U–Pb metamorphic ages of 167–154 Ma (Middle to Late Jurassic). This unit was interpreted by Bustamante et al. (2017) as Permian – Triassic. Our new U–Pb data indicate that the Tierradentro Gneisses and Amphibolites are geochronologically correlated with the metamorphic rocks of the Cajamarca Complex, in which Blanco–Quintero et al. (2014) found Jurassic metamorphic ages. Thus, the basement corresponds to a Jurassic metamorphic block that likely developed during its accretion to the continental margin and whose boundaries with adjacent terranes have not been established.

Based on current geological knowledge (Rodríguez–García et al., 2019), we propose that to the south, the Ibagué Fault borders the Jurassic orogen and the Chibcha Terrane (or Putumayo Orogen), which is composed of Permian granitoids, Triassic limestones (Payandé Formation), and Middle Jurassic plutons with no metamorphic involvement. To the east, the suture with the Chibcha Terrane is covered by alluvial fans; to the west, the tectonic boundary with the Tahamí Terrane is unknown; and to the north, its limit is unknown because its length within the Central Cordillera of Colombia has not yet been determined. The terrane that constitutes the Jurassic orogen likely represents a collision between the Chibcha and Tahamí Terranes between 166 and 154 Ma. Furthermore, La Cocha–Río Téllez Complex (described by Zapata et al., 2017a) is part of this terrane.

5.2. Characteristics of Jurassic Magmatism in the SM, UMV, and NBIB

5.2.1. Magmatism

The fact that the magmatism in the three blocks (SM, UMV, and NBIB) is of Jurassic age does not imply that they developed from a single arc and that the basement units were amalgamated and in similar geotectonic positions throughout Jurassic time. The differences in the composition, crystallization age,

Table 8. Major and trace elements of the Anzoátegui Metatonalite and Ibagué Tonalite in the NBIB.

Sample	JGB–492	JPZ–004	LMC–104	*CI11A	GOE–1001	JPZ–001–A	LMC–105	MIG–076	*CI2	*CI9B	*CI13	*CI15	*CI5B	*CI7	*CI10
wt%															
SiO2	50.3	61.1	59	61.2	65.6	58	64.6	61.3	67.8	57.8	61.7	58.9	64.3	63.7	57.2
Al2O3	16.7	15.4	15.6	16.1	15.7	17.4	15.4	17.2	15.6	17.9	16.4	16.8	15.8	17.9	17.2
Fe2O3	9.8	6.1	6.8	6.3	4.5	6.5	4.3	5.6	3.6	6.9	5.5	6	4.8	4.6	6.7
MgO	6.3	4	3.5	3.6	2.2	3.8	1.8	2.8	1.4	3.9	3	3.7	2.1	1.8	4.2
MnO	0.2	0.1	0.1	0.1	0.1	0.1	0.1	0.1	0	0.1	0.1	0.1	0.1	0.1	0.1
CaO	9.8	5	4.2	6.1	4.9	6.3	3.3	5.2	3.4	7.2	5.4	6.7	4	5.9	5.3
K2O	1.2	2.2	3.3	2	1.7	1.6	1.2	1.8	2.3	0.8	1.8	1.4	1.9	1.3	1.1
Na2O	2.8	3.6	2.6	3.9	3.4	3.5	5.4	3.4	4.1	4	3.8	3.6	4.7	3.7	4.3
P2O5	0.2	0.2	0.2	0.2	0.2	0.2	0.1	0.2	0.1	0.2	0.1	0.2	0.1	0.1	0.2
TiO2	1.4	0.7	0.8	0.7	0.5	0.8	0.6	0.7	0.5	0.8	0.7	0.7	0.6	0.5	0.9
LOI	1.2	1.5	3.7	0.6	1.2	1.8	3.1	1.6	1.5	0.8	1.3	0.8	2.2	0.6	2.2
SUM	99.9	99.8	99.6	100.7	99.9	99.9	99.9	99.9	98.8	100.4	99.8	98.1	98.3	99.7	97.1
ppm															
Ba	308.5	741.6	1254.5	804	499.4	441.3	185.3	638.3	488.5	318	475	292.2	525.8	674.2	285.5
Ce	36.9	44	49.3	49.8	45.5	29.9	42.8	48.9	47.3	27.4	44.9	33.6	36.1	25.2	39.2
Ga	26.7	23	22.2	17.8	21.5	25.5	21.4	24.3	17.4	17.9	16.6	18.9	16.8	18.8	17.7
La	16.7	23.6	26	23.5	26.2	15	22.3	27.4	24.4	12.8	18.8	13.4	19	12.7	16
Nb	6.3	5.3	7.3	5.9	5.4	4.7	7.4	4.8	7.6	6	8	7.3	8.6	4.9	7.6
Nd	26.7	27.5	25.8	21.7	22.1	17.5	23.6	25.2	21.9	13.8	26.1	16.7	19.6	9.9	21.9
Rb	39.1	68.2	111.7	43.7	37.9	50.7	50.3	38.4	45.3	12.2	41	36	43.6	52.3	21.7
Sr	629.2	680.5	362.7	704	747.1	595.3	441.5	826	305.6	503.6	458	402.4	514.4	420.5	438.8
Th	0.8	6.5	5.7	3.3	7.5	2.9	8.1	5.5	6.5	1.3	8.3	5.1	8.8	4.5	3.2
U	0.3	1.3	1.6	0.9	1.7	0.9	1.9	1	3	0.3	5	1.4	2.7	0	0
V	290.9	135.4	144.2	172	84.1	141.3	78.9	105.3	75.7	172	138	166.5	101.4	63.6	178.3
Y	29.3	17.3	21	18.6	17.4	21.3	23.7	19.4	18.8	17.3	31.3	24.2	23.5	12.2	29.5
Zr	94.1	151.6	194.1	182.1	113.5	104.4	185	136.1	166.9	112.5	151	130.6	202	134	182
Cu	11.8	49.6	23.7	63.9	7.8	28.7	14.4	6.9	5.9	23.9	52.6	27.3	3.3	6.6	36.6
Ni	1.6	2.1	1.7	10.3	1.9	1.8	1.9	1.7	2.2	10.1	7.3	13.5	7.1	4.3	11.5
Pb	3.1	3.8	7.5	1.3	4.2	5.2	<2.0	3.1	4.2	0.4	2.3	6.7	2.5	5.9	4.6
Zn	125	87.9	76.9	37	60.1	94.4	59.4	77.6	17.2	22	32	72.6	37	71.3	79.4

* Data from Bustamante et al. (2016)

LOI: loss on ignition

and evolutionary development of the arcs suggest independent and non–correlative magmatic events.

The lithological compositions of the SM plutons are primarily monzogranitic to syenogranitic without key compositional variations or spatial migration throughout the period of arc activity (25 to 30 Ma) (Figure 23a, 23d). The Jurassic magmatism in the UMV was quartz monzodioritic–quartz monzonitic in its initial stages and changed to monzogranitic after 20 to 27 Ma of arc evolution. Its spatial migration is reflected in the ages and positions of the plutons and volcanic products in the UMV (Figure 23b, 23e). The compositions of the Jurassic magmatic rocks of the NBIB indicate no changes in the compositions of the plutons, which are predominantly tonalitic with minor variations to quartz dioritic and granodioritic (Figure 23c, 23f) and show a migration of the magmatism from west to east over a time period of 15 to 20 Ma.

The Jurassic magmatic rocks in the three blocks (SM, UMV, NBIB) are sub–alkaline. In the SM, the plutonic rocks are more differentiated and are characterized by minor lithological variations (Figure 23g). They have higher Al_2O_3 and SiO_2 contents and belong to the high–K calc–alkaline series of peraluminous affinity (Figure 23j). In the UMV, the arc development had greater magmatic differentiation, which is clearly observed in the AFM diagram (Figure 23h). It began with rocks that were

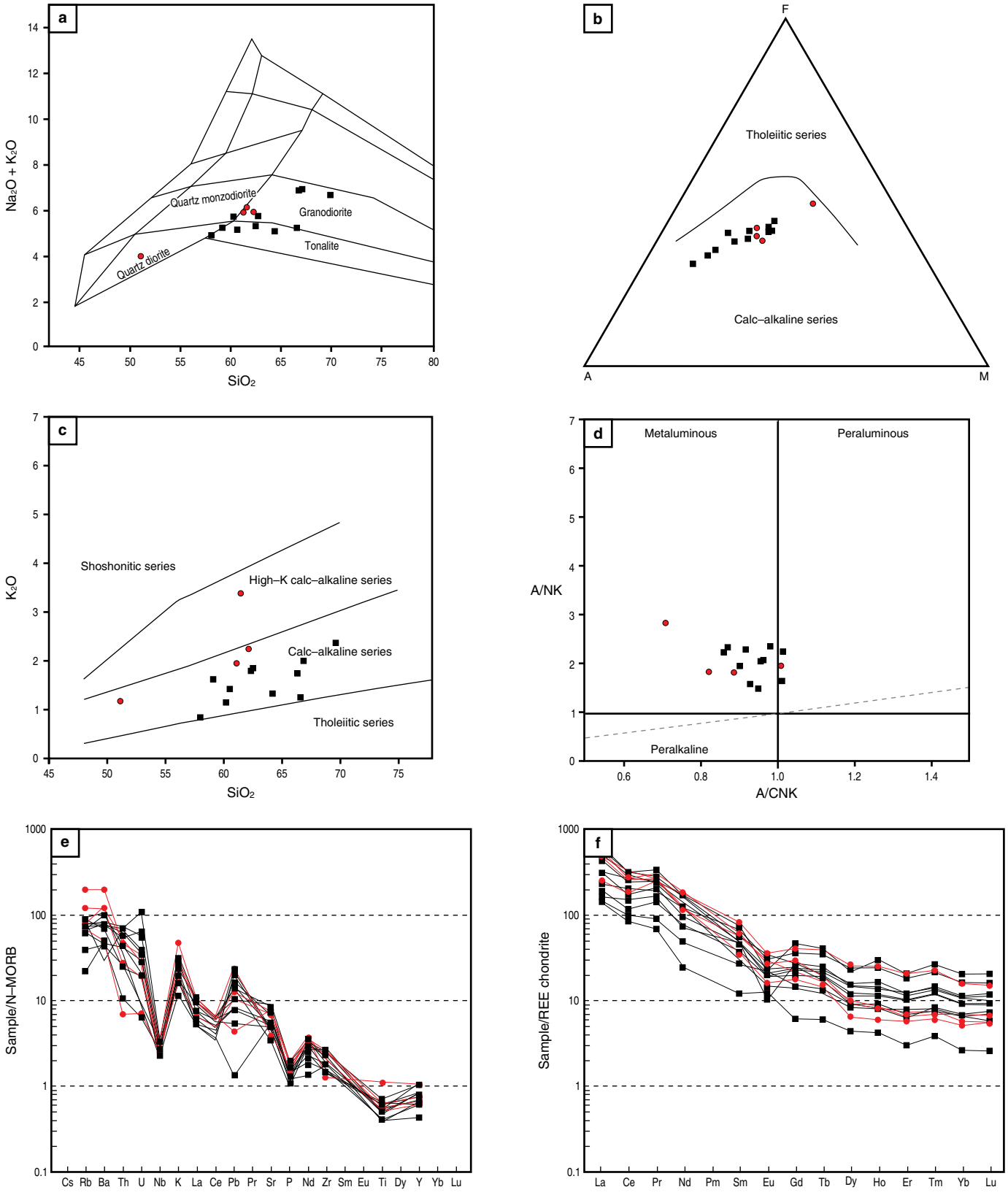

Figure 19. Diagrams of major oxides and multi–element diagrams. **(a)** TAS (Middlemost, 1985). **(b)** AFM fields indicated by Irvine & Baragar (1971). **(c)** diagram of Peccerillo & Taylor (1976). **(d)** diagram of Shand (1943). **(e)** N–MORB–normalized multi–element diagram (Sun & McDonough, 1989). **(f)** chondrite–normalized rare earth elements (Nakamura, 1974) diagram. The Ibagué Tonalite is shown in black, and the Anzoátegui Metatonalite is shown in red.

Table 9. Chondrite–normalized rare earth element diagram (Nakamura, 1974) for the Anzoátegui Metatonalite and Ibagué Tonalite.

Sample	Unit	Eu/Eu*	$(La/Yb)_n$	$(La/Sm)_n$	$(Ce/Yb)_n$	$(Ce/Sm)_n$	$(Eu/Yb)_n$
JGB–492	Anzoátegui Metatonalite	0.78	3.97	1.76	3.35	1.48	1.48
JPZ–004	Anzoátegui Metatonalite	0.8	9.41	2.87	6.7	2.04	2.18
LMC–104	Anzoátegui Metatonalite	0.93	8.21	3.31	5.94	2.39	1.93
GOE–1001	Ibagué Tonalite	0.8	10.97	4.14	7.27	2.74	1.78
JPZ–001–A	Ibagué Tonalite	0.84	4.78	2.32	3.63	1.76	1.46
LMC–105	Ibagué Tonalite	0.52	6.52	3.02	4.78	2.22	0.97
MIG–076	Ibagué Tonalite	0.82	10.24	3.74	6.96	2.54	1.89

n: normalized to chondrite values of Nakamura (1974).

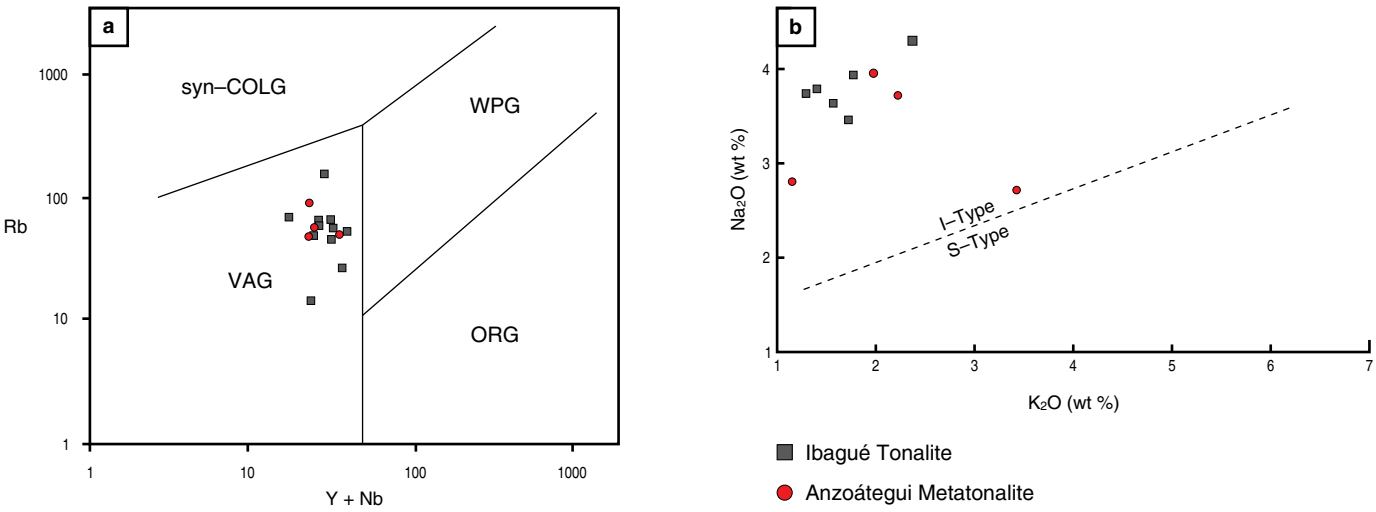

Figure 20. Geotectonic discrimination diagrams: **(a)** Pearce et al. (1984), **(b)** K_2O vs. Na_2O diagram of Chappell & White (1974) discriminating between I–type and S–type granites.

Table 10. LA–ICP–MS U–Pb zircon ages in the NBIB.

Sample	Longitude W	Latitude N	Classification	Unit	Age (Ma)
GOE–1088	75° 12' 47,8''	4° 29' 5.46''	Tonalite	Anzoátegui Metatonalite	154.79 ± 0.83
AMC–0153	75° 2' 56.93''	4°38´56.20¨	Metagranodiorite	Anzoátegui Metatonalite	150.17 ± 0.86
LMC–104	74° 59' 3.23''	4° 50' 36.88''	Metatonalite	Anzoátegui Metatonalite	153.9 ± 1.1
JPZ–001A	74° 58' 26.37''	4° 40' 11.16''	Tonalite	Ibagué Tonalite	138.7 ± 1.0
MIG–076	75° 4' 37.45''	4° 30' 9.62''	Granodiorite	Ibagué Tonalite	145.56 ± 0.92
MIG–O74	74° 59' 21.96''	4° 46' 58.24''	Amphibolite	Tierradentro Gneisses and Amphibolite	154.25 +3.1/-6.4
AMC–0152	75° 3' 54.37''	4° 39' 29.16''	Amphibolite	Tierradentro Gneisses and Amphibolite	154.5 ± 3.6
AMC–0171	75° 0' 41.5''	4° 40' 29.5''	Amphibolite	Tierradentro Gneisses and Amphibolite	167.0 ± 3.0

poor in quartz (<20%) and had a higher content of ferromagnesian minerals, which is reflected in the high content of total FeO and MgO. The arc gradually became enriched in quartz–rich rocks (>20%) of the high–K calc–alkaline series and subordinate shoshonitic series throughout its evolution, starting with metaluminous rocks and changing to granitic peraluminous rocks as its composition varied over time (Figure 23k). This was accompanied by a decrease in the A/NK ratios and an increase in the A/CNK ratios. In the NBIB, the rocks have lower alkali ($Na_2O + K_2O$) values, and the differentiation within the

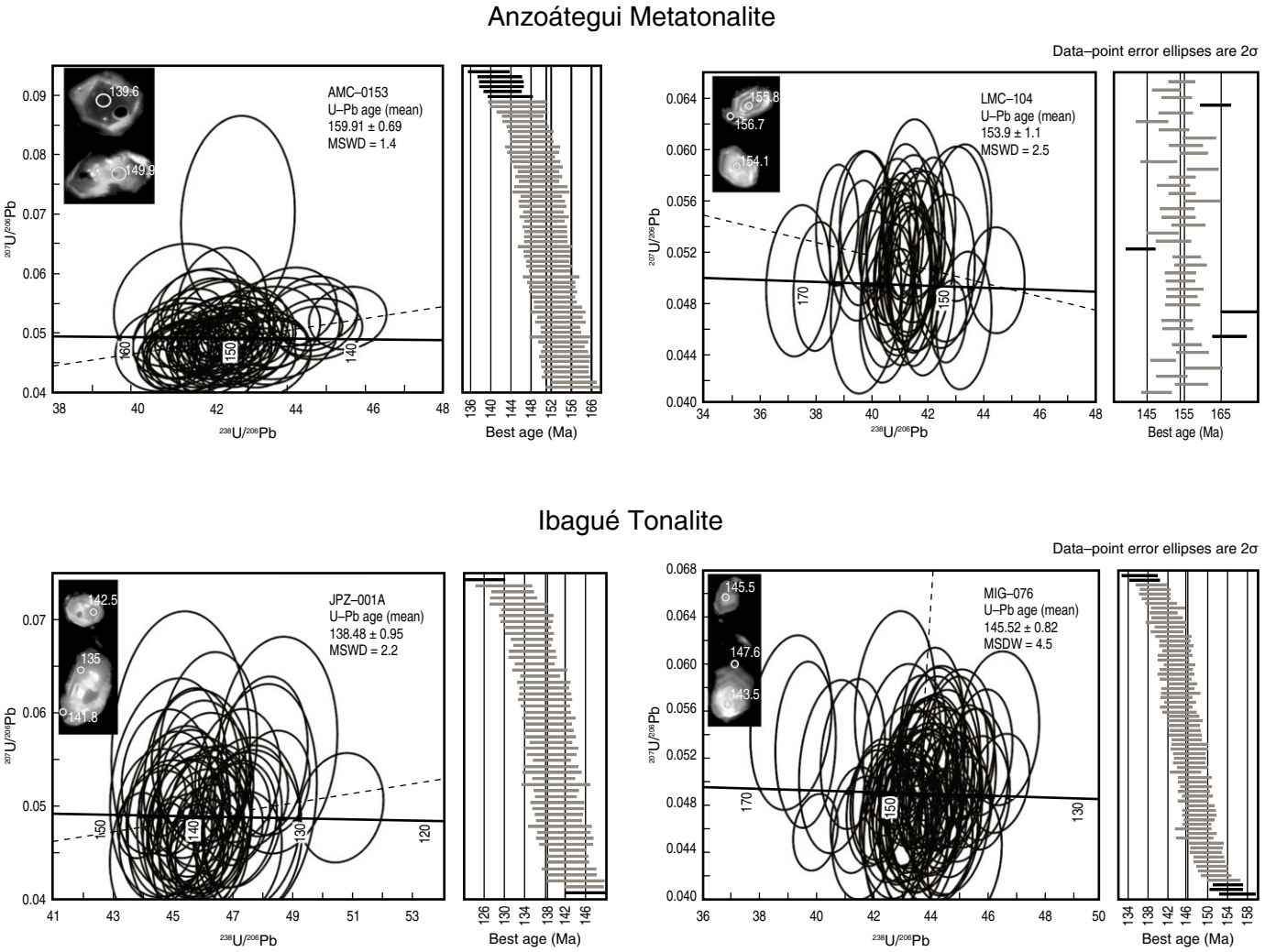

Figure 21. Geochronological results of the Anzoátegui Metatonalite (AMC–0153, LMC–104) and the Ibagué Tonalite (JPZ–001A, MIG–076). CL images of zircons representative of each sample.

arc is lower than in the UMV and SM (Figure 23i) with intermediate SiO_2 values, quartz contents >20% in most rocks, and lower total FeO and MgO contents than rocks with similar SiO_2 contents in the SM and UMV. They correspond to the normal calc–alkaline series and are metaluminous with higher A/NK ratios than those in the SM and UMV (Figure 23j, 23k, 23l).

A comparison of the patterns of N–MORB–normalized trace elements (Figure 24; Sun & McDonough, 1989) and chondrite–normalized rare earth elements (based on the values in Nakamura, 1974) of Triassic and Jurassic plutons from the SM, UMV, and NBIB shows that they are similar to rocks generated in continental margin arcs (Figure 24). However, the data from different arcs have different trace element distribution patterns and negative Nb, Ti, and P anomalies. The high anomalous values of Rb, Ba, Th, and Pb, albeit nonparallel, suggest that they correspond to different magmatic arc events or to different arcs. The magmatic arc of the SM is characterized by nonparallel REE patterns compared to rocks with similar SiO_2 contents. The data have different intersecting patterns in the same pluton, different HREE enrichments, minor or major LREE enrichments, and negative or no Eu anomalies (Figure 7). There are also different U–Pb zircon ages for each pattern and different $(La/Yb)_n$ values, suggesting multi–pulse plutons with different crustal contributions. This characteristic is not observed in the Jurassic arc rocks of the UMV and NBIB, where the rocks in each of these areas have similar compositions and ages. The REE and trace element patterns are parallel with LREE enrichments in the eastern plutons of the UMV, which are related to greater K contents and major rock differentiation (Figure 14).

The lack of analytical results of Ta and Y (see Table 1, Supplementary Information) limits the interpretation of the tectonic

Figure 22. Geochronological results of the Tierradentro Gneisses and Amphibolites; photomicrographs showing microscopic views and CL images of representative zircons.

Tierradentro Gneisses and Amphibolites

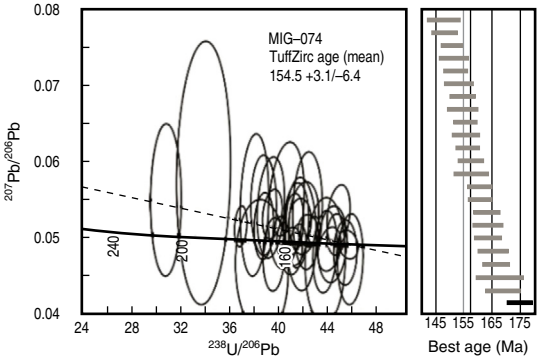

Data–point error ellipse are 2σ

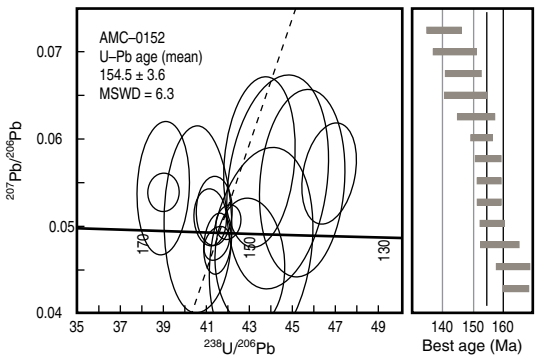

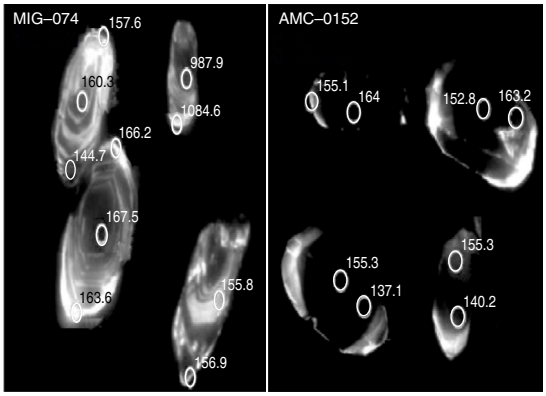

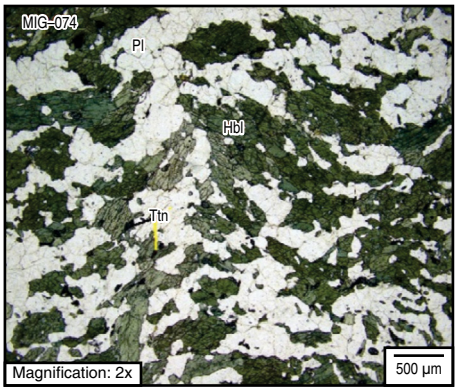

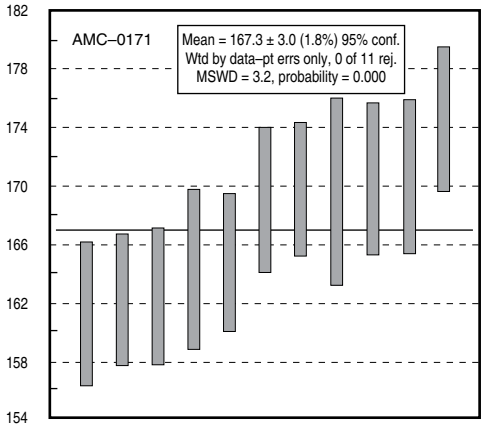

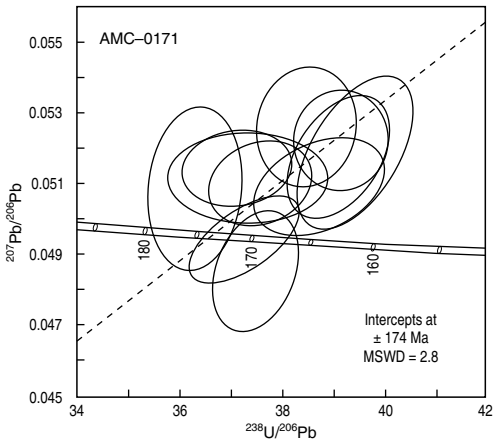

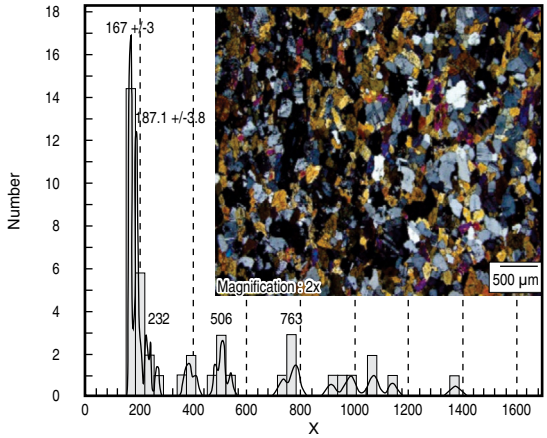

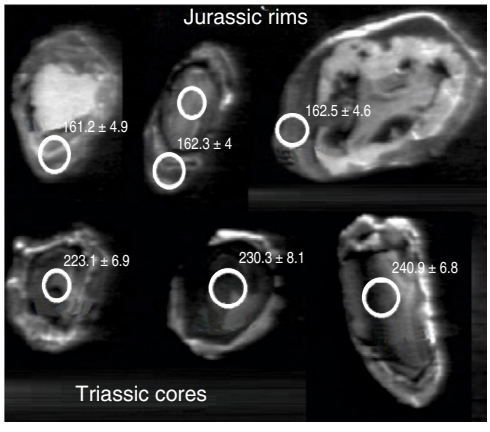

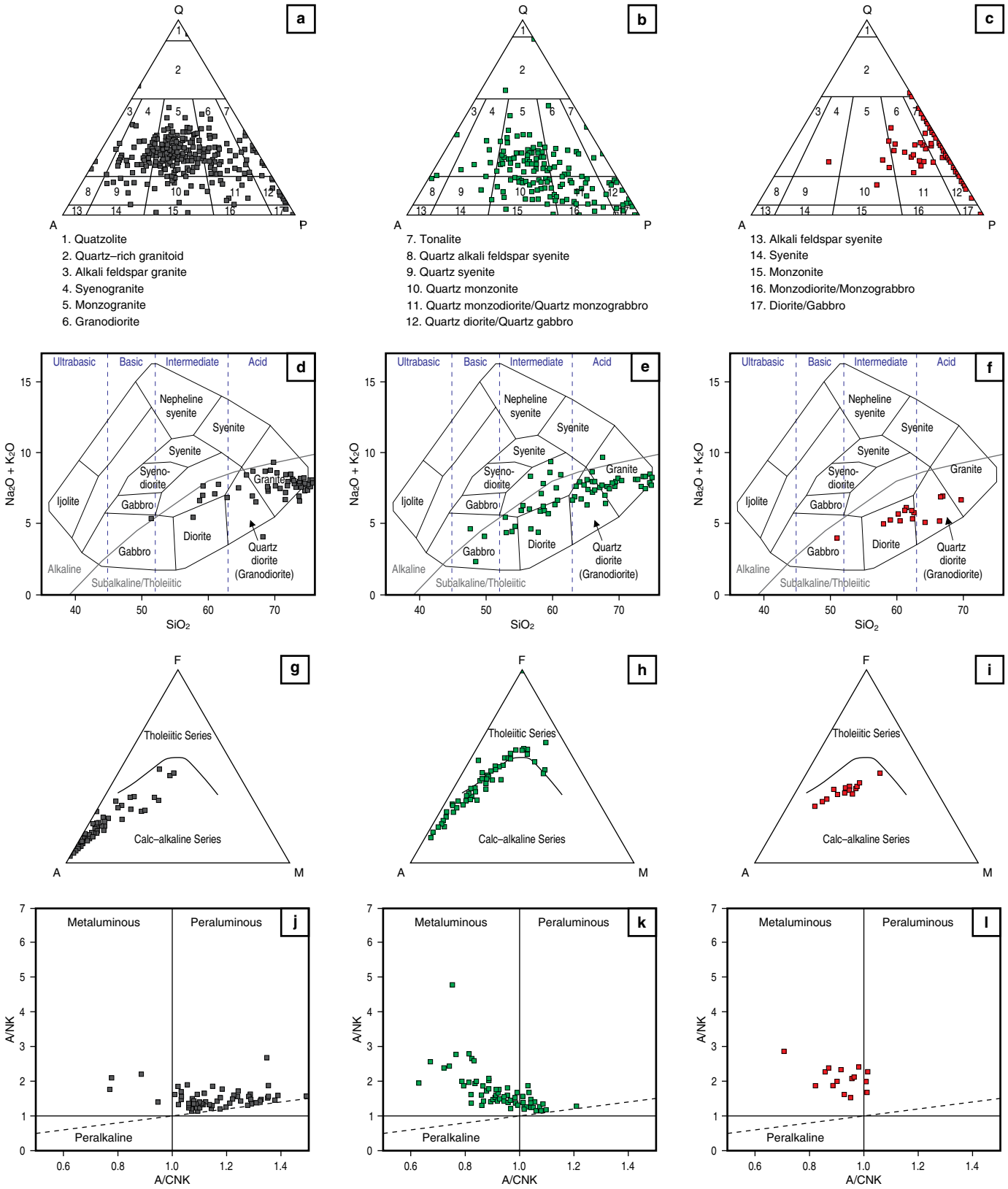

Figure 23. Compositional and geochemical characteristics of the Jurassic arc plutons. SM (black) period of arc activity (25 to 30 Ma); UMV (green) period of arc activity (20 to 27 Ma), and NBIB (red) period of arc activity (15 to 20 Ma). **(a)**, **(b)**, **(c)** Streckeisen diagrams (1979) for the rocks of the SM, UMV, and NBIB, respectively. **(d)**, **(e)**, **(f)** TAS diagrams (Cox et al., 1979) for the rocks of the SM, UMV, and NBIB, respectively. **(g)**, **(h)**, **(i)** AFM diagrams (Irvine & Baragar, 1971) for the rocks of the SM, UMV, and NBIB, respectively. **(j)**, **(k)**, **(l)** Alumina saturation index diagrams (Shand, 1943) for the rocks of the SM, UMV, and NBIB, respectively.

environment and the discrimination between volcanic arc granites and post–collisional granites. According to the diagrams of Pearce (1982) and Pearce et al. (1984), the samples plot within the field of volcanic arc granites (Figures 24, 25a). The UMV and SM plutons have slightly higher Rb values than those of the NBIB within the field of volcanic arcs. The samples of van der Lelij (2013) in the SM and Bustamante et al. (2016) in the NBIB plot within the volcanic arcs field in the discrimination diagram of Harris et al. (1986) (Figure 25b).

Magmatic activity occurred during different time intervals in each block. In the SM, the arc initiated at approximately 214 Ma, and most magmatic activity occurred from 203 to 197 Ma. It lasted for approximately 30 Ma and continued until 184 Ma (Figure 26). In the UMV, the magmatic arc activity started at approximately 195 Ma and included three periods of formation of plutons and volcanic rocks at 187, 182, and 172 Ma. These are reflected in the ages of the western and eastern plutons and the associated volcanic rocks and in the spatial migration of the arc. The magmatism lasted for approximately 27 Ma and ended at approximately 168 Ma (Figure 26). In the NBIB, we interpret that the arc had two periods of magmatic activity. The first period occurred from 158 to 152 Ma, and it generated the Anzoátegui Metatonalite, which was syntectonically emplaced during metamorphism of the Tierradentro Gneisses and Amphibolites and the Cajamarca Complex. The second period occurred from 145 to 138 Ma, when the Ibagué Tonalite intruded after the metamorphic event.

5.2.2. Inheritances

Inherited zircon cores in plutonic and volcanic rocks provide valuable information about the relationship between crustal basement and arc magmatism. The highest numbers of inheritances were found in granitoids of the SM, whereas inheritances are rare in the UMV and NBIB granitoids.

The xenocrysts and inherited zircon cores in the Late Triassic – Early Jurassic plutons in the SM show several inherited populations. These include a minor Paleoproterozoic to Neoproterozoic population, a major Ordovician to Devonian population, and a moderate Permian – Triassic population (Figure 27).

Inherited Paleoproterozoic ages have also been found in basement units such as the Bucaramanga Gneiss, the Silgará Schists, the Chicamocha Schists, and the San Pedro Phyllites. Cordani et al. (2005) and Mantilla–Figueroa et al. (2016) suggest that these zircons were possibly derived from the Rio Negro Juruena, Rondonian, and Sunsás units in the Amazonian Craton. A second group of inherited zircon cores in the Triassic – Jurassic granitoids yielded ages ranging from 1200 to 1000 Ma. These ages have also been reported in the Chicamocha Schists, San Pedro Phyllites, and Silgará Schists (Cardona et al., 2016; Mantilla–Figueroa et al., 2016) and could be related to both the Amazonian Craton (Cordani et al., 2005; Mantilla–Figueroa et al., 2016) and to the pericratonic magmatic arc of the Colombo Oaxaquian Terrane (Ibañez–Mejia et al., 2011). Inherited ages ranging from 1000 to 850 Ma have been identified in inherited cores in the Silgará Schists (Cardona et al., 2016; Mantilla–Figueroa et al., 2016) and in the Santa Rosita Monzogranite (Zapata et al., 2017b) and could be related to the Grenville Orogeny (Cordani et al., 2005) or to the Putumayo Orogeny (Ibañez–Mejia et al., 2011). Finally, Mantilla–Figueroa et al. (2016) related the zircons inherited from the Proterozoic, which have ages ranging from 850 to 540 Ma, to the Brasiliano/Pan–African Orogeny. They are present in units that are currently buried under the basin and in some intrusive bodies, such as the Ediacaran San José del Guaviare Nepheline Syenite (Arango et al., 2012), which are the possible source of these inherited cores.

Ordovician inherited zircon cores have been found in several Late Triassic – Jurassic granitoids. This group of zircons likely represents the crystallization age of the Ordovician pre–, syn–, and post–tectonic plutons associated with the Famatinian Orogeny in the Santander Massif (Mantilla–Figueroa et al., 2012; Restrepo–Pace & Cediel, 2010) and Floresta Massif (Horton et al., 2010) and the metamorphic age of the Bucaramanga Gneiss related to the Famatinian Orogeny. Silurian inherited zircon cores may be derived from plutons related to continental arc magmatism that developed on the western margin of Gondwana during this time period (van der Lelij et al., 2016). The Devonian and Carboniferous inherited zircon cores may also be related to magmatic bodies of the SM.

Middle and Lower Triassic and Permian ages ranging from 262 to 290 Ma have been reported for small intrusive bodies in the SM, serranía de Perijá, and Mérida Andes (van der Lelij, 2013; van der Lelij et al., 2016). They occur in inherited zircon cores in the Mogotes Batholith and La Corcova, Santa Bárbara, and Rionegro Monzogranites. These ages are common in the metamorphic basement of the Central Cordillera associated with the Tahamí Terrane (Restrepo et al., 2011; Rodríguez et al., 2016a; Spikings et al., 2015; Villagómez et al., 2011; Vinasco et al., 2006), in the Permian arc that developed on the western margin of the Chibcha Terrane (Cardona et al., 2010; Rodríguez et al., 2017a) in the Central Cordillera, and in the serranía de San Lucas and Sierra Nevada de Santa Marta. They also occur in small intrusive bodies east of Pamplona, where a U–Pb age of 265.2 ± 4.5 Ma was determined in granodiorite intruding metamorphic rocks that are similar to the Bucaramanga Gneiss, which were mapped and identified as granodiorites and granites (Ward et al., 1973).

In summary, the Late Triassic – Early Jurassic plutons of the SM contain abundant inherited zircons of crustal origin that are correlated with the ages of inherited and primary zircons of metasedimentary, metaigneous, and igneous units that form the SM basement, such as the Bucaramanga Gneiss, Silgará Schists,

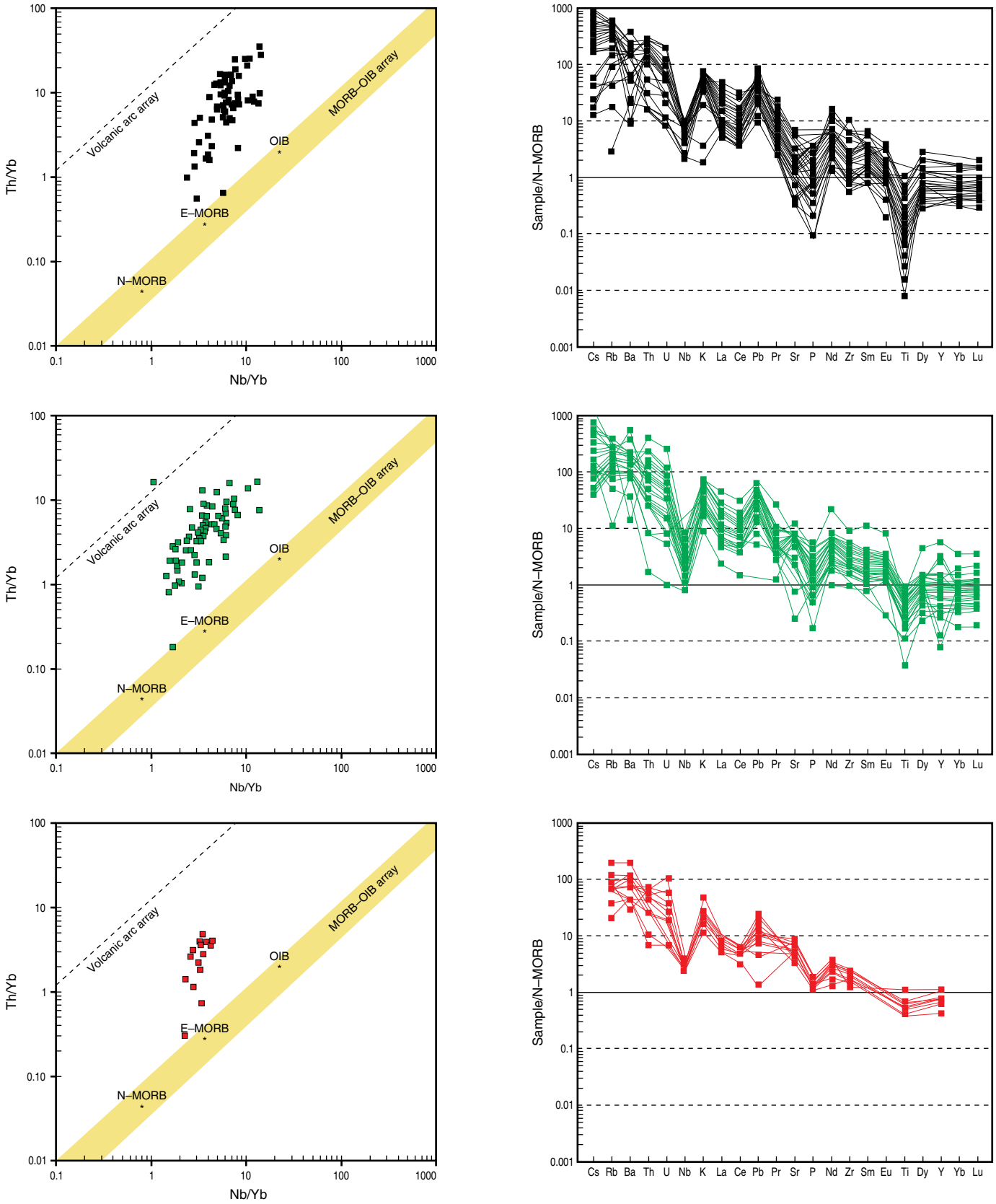

Figure 24. Multi–element diagrams and tectonic discrimination diagrams (Pearce, 1982) for plutonic bodies from the SM, UMV, and NBIB blocks. Samples from the SM are shown in black, samples from the UMV are shown in green, and samples from the NBIB are shown in red.

and Paleozoic pre– and post–kinematic orthogneissic and plutonic bodies, among others. The probability density diagram of the inherited ages (Figure 27) of the granitoids is similar to the results of inherited zircons from the Silgará Formations reported by Cardona et al. (2016) and Mantilla–Figueroa et al. (2016), which range from the Mesoproterozoic to the Devonian.

The geochemical characteristics and the quantity of inherited zircons suggest different degrees of crustal melting, which implies a high heat gradient in the arc that melted the continental basement rocks and incorporated them into the magma (Figure 27). In line with the crustal melting phenomenon and advanced magmatic differentiation in the SM, the plutons have a peraluminous affinity and dual classification as I– and S–type granites, which could result from the melting of basement metasedimentites in some pulses but not in others.

In the UMV, inheritance is limited to a few inherited zircon cores with Mesoproterozoic to Neoproterozoic and Jurassic ages. The former ages suggest a contribution of the Amazonian Craton to the oldest cores and of metamorphic basement of the Chibcha Terrane (Putumayo Orogen), whereas the Jurassic inheritances are related to previous periods of magmatic activity within the same arc.

No record of inheritance was found in the Anzoátegui Metatonalite and in the Ibagué Tonalite of the NBIB.

5.3. Evolutionary Model

The Triassic – Jurassic magmatic histories of the SM, UMV, and NBIB blocks are represented by different lithological, geochemical, and geochronological data that differentiate them. Furthermore, these rocks were emplaced in metamorphic basement units of different ages. Therefore, the correlations between Jurassic magmatic events and the regional models from a single arc model described previously are less valid (Bustamante et al., 2010, 2016; Leal–Mejía, 2011; Spikings et al., 2015; Villagómez et al., 2015; Zapata et al., 2016a). We propose a model involving several arcs that developed in different geotectonic positions that were emplaced in different metamorphic terranes with unique compositional, geochronological, and evolutionary characteristics without any similarity that would allow their correlation.

Figure 28 shows the evolutionary model proposed to explain the genesis of the Late Triassic – Early Cretaceous igneous activity in Colombia.

5.3.1. ca. 214 to 195 Ma

During this time period, we propose that an active subduction zone was located along the NW edge of Gondwana that generated a magmatic arc that is current recorded in the Santander Massif. This arc mainly intrudes the Famatinian Orogen (Bucaramanga Gneiss, Silgará Formation, orthogneisses, and post–tectonic granites) and, to a lesser extent, part of the Neoproterozoic basement that outcrops NW of the Santander Massif. Between ca. 194 to 189 Ma, the arc axis migrated toward the ocean (Spikings et al., 2015), and a possible clockwise rotation of the continental plate occurred.

5.3.2. ca. 195 to 168 Ma

Extension of the continental margin began during this period, causing the formation of back–arc basins, similar to the interpretation of Toussaint (1995). Arc volcanism, plutonism, and sedimentation occurred concurrently. Volcano–sedimentary sequences formed, including the Saldaña Formation and Pitalito Vulcanites in the UMV, the Noreán Formation in the Middle Magdalena Valley and on the eastern flank of serranía de San Lucas, La Quinta Formation in serranía de Perijá, La Caja de Ahorros Ignimbrite and Los Clavos Ignimbrite in the Sierra Nevada de Santa Marta, and sedimentary rocks such as the Jordán and Girón Formations in the SM. Plutonism generated, in approximately chronological order, the western plutons in the UMV and the Norosí Batholith in serranía de San Lucas, the plutons in the SNSM, the intermediate plutons between the western and eastern plutons in the UMV, the eastern plutons of the UMV, and plutons of the same age in the Sierra Nevada de Santa Marta.

5.3.3. ca. 167 to ca. 138 Ma

This interval is divided into three time periods. The first event was the collision of allochthonous terranes with the continental margin between ca. 167 and ca. 154 Ma with consequent metamorphism that formed the metamorphic assemblage of Tierradentro Gneisses and Amphibolites (this study) in the NBIB (167–154 Ma), the SW section of the Cajamarca Complex (158 and 147 Ma; Blanco–Quintero et al., 2014), and La Cocha–Río Téllez Complex (163 Ma; Zapata et al., 2017a). The second event, which lasted from ca. 158 to 150 Ma, included syntectonic arc magmatism that produced the Anzoátegui Metatonalite in the NBIB. The third event, which lasted from ca. 145 to ca. 138 Ma, was the post–tectonic magmatism that generated the Ibagué Tonalite in the NBIB.

Alternative hypotheses to explain the arc magmatism during this period include: (1) Genesis of the arc at another paleolatitude and transport to the current position along regional faults, and (2) the creation of different volcanic fronts in a supra–subduction system. However, in the latter, the spatial position with respect to the trench and the westward migration coeval with terrane accretion on the western margin of the Neoproterozoic basement appear to be problematic.

Due to the lack of geological data about the central section of the batholith, its corresponding model is unknown. The geochronological data available in the literature for the southern section (Páez Quartz Monzodiorite) (Leal–Mejía, 2011; Zapata

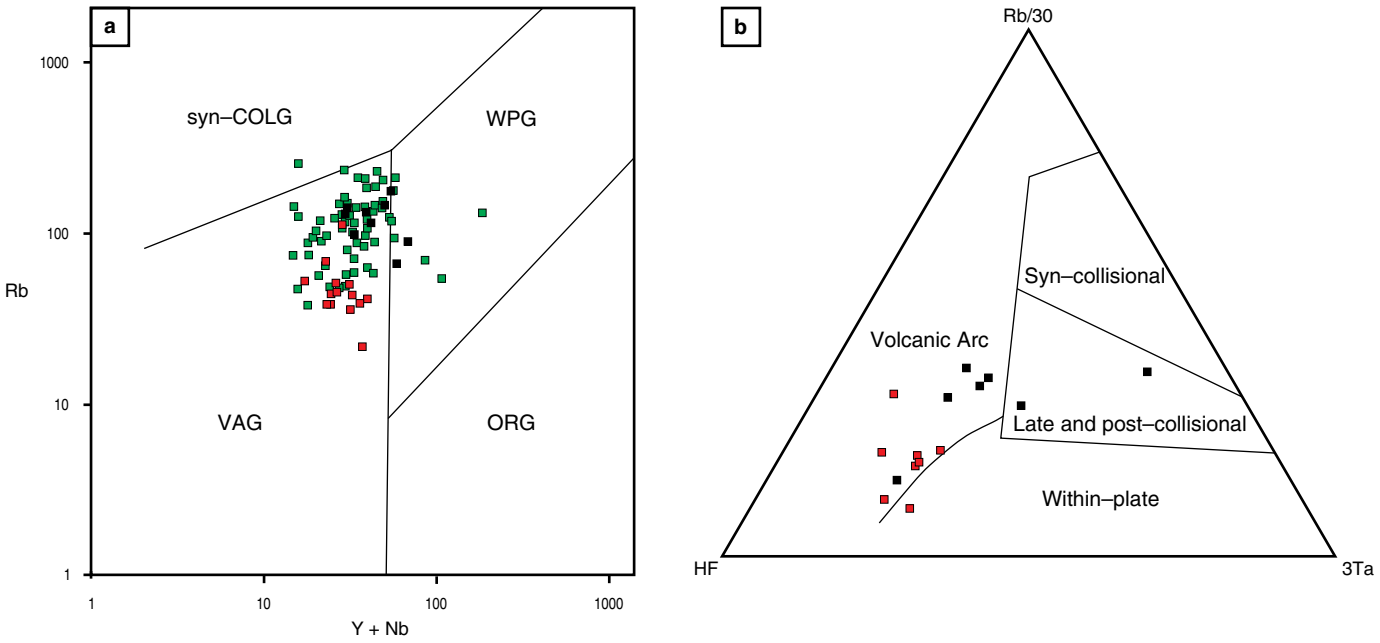

Figure 25. Tectonic discrimination diagrams: **(a)** Pearce et al. (1984), **(b)** Harris et al. (1986). Diagrams for plutonic bodies from the SM, UMV, and NBIB blocks. Samples from the SM are shown in black, samples from the UMV are shown in green, and samples from the NBIB are shown in red.

et al., 2015) suggest a correlation with the western plutons of the UMV (Zapata et al., 2015). Conversely, some data from the central section of the Ibagué Batholith indicate its heterogeneity and inclusion of Permian (Villagómez et al., 2011; preliminary results from the "Jurassic Magmatism of Colombia" project of the SGC) and Jurassic bodies ranging from 170 to 150 Ma (Villagómez et al., 2011; Leal–Mejía, 2011). Future studies will make it possible to understand this section of the batholith and correlate it with the other Jurassic units.

6. Conclusions

The compositional characteristics and crystallization ages of the Late Triassic and Jurassic igneous units in the Santander Massif, Upper Magdalena Valley, and northern block of the Ibagué Batholith have no common features that make it possible to correlate the magmatism associated with each block.

The Triassic and Jurassic magmatic rocks in Colombia were emplaced during different orogens. The Late Triassic – Jurassic plutons of the Santander Massif were emplaced into metamorphic and igneous units related to the Famatinian or Quetame–Caparonensis Orogeny, which occurred in the Early Ordovician (480–465 Ma). North of the massif, several plutons (Rionegro Monzogranite and San Martín Tonalite) were emplaced into Neoproterozoic basement, which is associated with the Chibcha Terrane or Putumayo Orogen (approximately 990 Ma), although the boundary between the orogens in the northern SM remains unclear. The Early Jurassic – Middle Jurassic plutons and volcanic rocks in the Upper Magdalena Valley were emplaced into basement consisting of Neoproterozoic metamorphic rocks, Paleozoic sedimentary rocks and Permian arc rocks related to the Chibcha Terrane or Putumayo Orogen. The Jurassic magmatic rocks associated with the northern block of the Ibagué Batholith were emplaced syn–tectonically and post–tectonically into metamorphic rocks related to a Late Jurassic orogen that includes units such as the Tierradentro Gneisses and Amphibolites, part of the Cajamarca Complex, and La Cocha–Río Téllez Complex. We suggest that this orogen should be called the Tierradentro Terrane, which borders the Chibcha Terrane to the east and the Tahamí Terrane to the west, although the tectonic borders between these three terranes are unknown.

Late Triassic – Jurassic magmatism occurred in several subduction zones that were active at different times, likely through the westward migration of the subduction zone. This generated different continental margin arcs that evolved independently in the three tectonic blocks (Santander Massif, Upper Magdalena Valley, and northern block of the Ibagué Batholith).

In the Santander Massif, arc magmatism lasted for approximately 30 Ma (from 214 to 184 Ma) and included multiple pulses of different–aged monzogranitic magmatism that generated batholitic bodies and stocks. The magmatism involved major crustal melting, represented by I– and S–type peraluminous granitoids. In the Upper Magdalena Valley, arc magmatism lasted for approximately 30 Ma (197 to 167 Ma) and included three large magmatic pulses (187, 182, and 172 Ma), starting with the formation of metaluminous monzodioritic stocks and batholiths

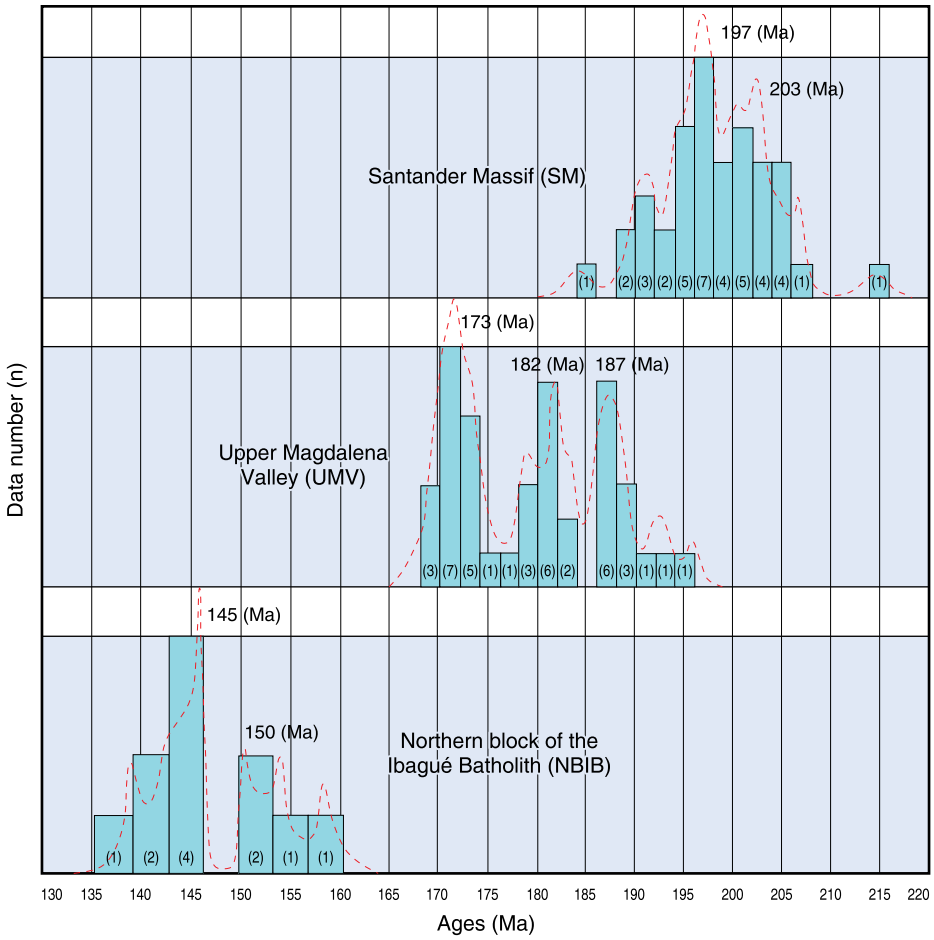

Figure 26. Frequency diagrams of U–Pb zircon ages for Triassic – Jurassic magmatic bodies of the SM, UMV, and NBIB.

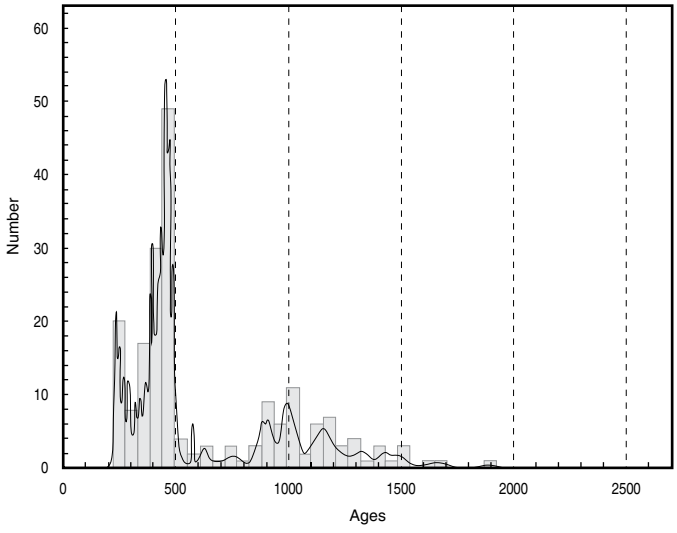

Figure 27. Probability density diagram of 200 xenocrysts and inherited zircon cores related to 41 U–Pb ages of SM plutons.

and ending with the emplacement of I–type metaluminous and peraluminous batholiths and monzogranitic stocks. The spatial migration of the arc is recorded in the composition of the igneous rocks. In the northern block of the Ibagué Batholith, the arc lasted for 20 Ma (from 158 to 138 Ma) and contained at least two magmatic pulses (154 and 144 Ma) that formed I–type metaluminous plutons with tonalitic compositions. The arc migrated from west to east without a record of compositional changes during arc activity. The first pulse (Anzoátegui Metatonalite), which occurred from 158 to 151 Ma, is interpreted as syntectonic with the metamorphism based on the similarity of the ages of the metamorphic rocks and the development of metamorphic structures. The second pulse (Ibagué Tonalite), which occurred from 145 to 138 Ma, is interpreted as post–tectonic based on the isotropic structure of the rocks.

The large number of inheritances found in the Triassic – Jurassic granitoids of the SM, which have Mesoproterozoic, Neoproterozoic, Cambrian, Ordovician, Silurian, Devonian, Carboniferous, Permian, and Upper and Lower Triassic ages,

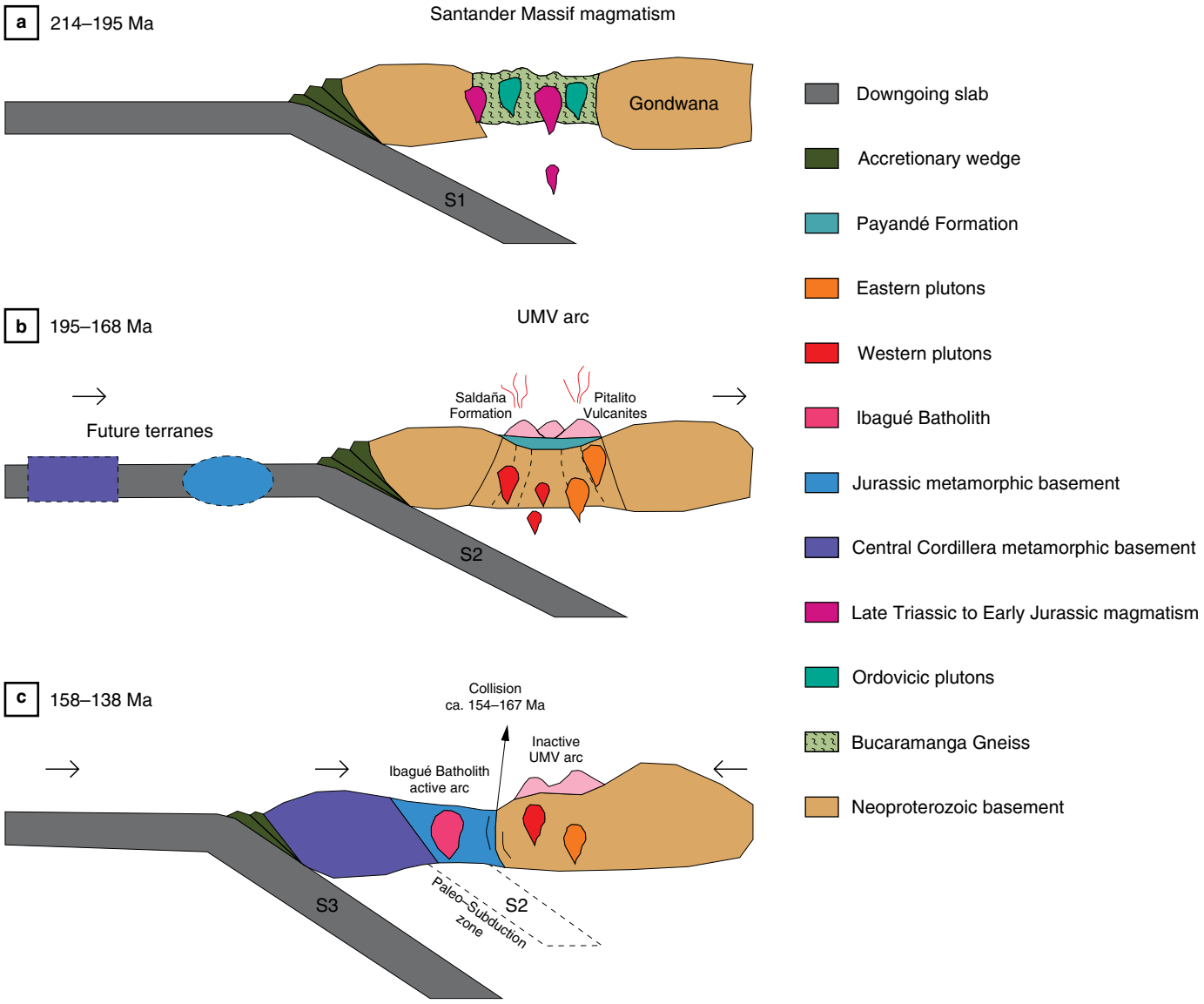

Figure 28. Geologic model of the evolution of the Santander Massif (SM), Upper Magdalena Valley (UMV), and northern block of the Ibagué Batholith (NBIB) during the Late Triassic – Early Cretaceous at: **(a)** 214–195 Ma, **(b)** 195–168 Ma, **(c)** 158–138 Ma.

suggests magmatism that assimilated crustal material from the basement and included most of the units preceding the magmatic event of the Triassic – Jurassic arc.

Acknowledgments

The authors acknowledge the Servicio Geológico Colombiano for the support in developing the "Magmatismo Jurásico en Colombia" project as well as geologists Tomás CORREA, Lina María CETINA, Milton OBANDO, Ángela RINCÓN, and María Isabel GIRALDO, who helped with the sampling. We thank Diego RAMÍREZ for editing the text. Special thanks are given to the staff of the Laser Ablation Geochronology Laboratory, SGC, for conducting the U–Pb zircon dating of the samples reported in this study.

References

Álvarez, A.J. 1983. Geología de la cordillera Central y el occidente colombiano y petroquímica de los intrusivos granitoides mesocenozoicos. Boletín Geológico, 26(2): 1–175. Bogotá.

Arango, M.I., Zapata, G. & Martens, U. 2012. Caracterización petrográfica, geoquímica y edad de la Sienita Nefelínica de San José del Guaviare. Boletín de Geología, 34(1): 15–26.

Arango, M.I., Rodríguez, G., Bermúdez, J.G. & Zapata, G. 2015a. Cuarzomonzonita de Anchique. Catálogo de unidades li-

toestratigráficas de Colombia. Servicio Geológico Colombiano, 26 p. Medellín.

Arango, M.I., Rodríguez, G., Bermúdez, J.G. & Zapata, G. 2015b. Monzodiorita de Las Minas. Catálogo de unidades litoestratigráficas de Colombia. Servicio Geológico Colombiano, 26 p. Medellín.

Arango, M.I., Rodríguez, G., Zapata, G. & Bermúdez, J.G. 2015c. Cuarzolatita de Teruel. Catálogo de unidades litoestratigráficas de Colombia. Servicio Geológico Colombiano, 25 p. Medellín.

Arango, M.I., Rodríguez, G., Zapata, G. & Bermúdez, J.G. 2015d. Monzogranito de Altamira. Catálogo de unidades litoestratigráficas de Colombia. Servicio Geológico Colombiano, 31 p. Medellín.

Arango, M.I., Rodríguez, G., Zapata, G. & Bermúdez, J.G. 2015e. Monzogranito de Mocoa. Catálogo de unidades litoestratigráficas de Colombia. Servicio Geológico Colombiano, 41 p. Bogotá.

Arango, M.I., Rodríguez, G., Zapata, G. & Correa, A.M. 2016. Monzogranito de Rionegro. Catálogo de unidades litoestratigráficas de Colombia. Servicio Geológico Colombiano, 128 p. Medellín.

Arias, A. & Morales, C.J. 2003. Memoria explicativa: Mapa geológico generalizado del departamento del Cesar. Scale 1:250 000. Ingeominas, 93 p. Bogotá.

Arias–Tauta, A. & Vargas–Higuera, R. 1978. Memoria explicativa: Geología de las planchas 86 Ábrego y 97 Cáchira. Scale 1:100 000. Boletín Geológico, 23(2): 3–38. Bogotá.

Aspden, J.A., McCourt, W.J. & Brook, M. 1987. Geometrical control of subduction–related magmatism: The Mesozoic and Cenozoic plutonic history of western Colombia. Journal of the Geological Society, 144(6): 893–905. https://doi.org/10.1144/gsjgs.144.6.0893

Barbarin, B. 1999. A review of the relationships between granitoid types, their origins and their geodynamic environments. Lithos, 46(3): 605–626. https://doi.org/10.1016/S0024-4937(98)00085-1

Barrero, D. & Vesga, C.J. 1976. Mapa geológico del cuadrángulo K–9 Armero y mitad sur del J–9 La Dorada. Scale 1:100 000. Ingeominas. Bogotá.

Bayona, G., Rapalini, A. & Costanzo–Álvarez, V. 2006. Paleomagnetism in Mesozoic rocks of the northern Andes and its implications in Mesozoic tectonics of northwestern South America. Earth, Planets and Space, 58(10): 1255–1272. https://doi.org/10.1186/BF03352621

Bayona, G., Jiménez, G., Silva, C., Cardona, A., Montes, C., Roncancio, J. & Cordani, U. 2010. Paleomagnetic data and K–Ar ages from Mesozoic units of the Santa Marta Massif: A preliminary interpretation for block rotation and translations. Journal of South American Earth Sciences, 29(4): 817–831. https://doi.org/10.1016/j.jsames.2009.10.005

Bermúdez, J.G., Arango, M.I., Rodríguez–García, G. & Zapata–García, G. 2015. Cuarzomonzonita de San Cayetano. Catálogo de unidades litoestratigráficas de Colombia. Servicio Geológico Colombiano, 37 p. Medellín.

Blanco–Quintero, I.F., García–Casco, A., Toro, L.M., Moreno, M., Ruiz, E.C., Vinasco, C.J., Cardona, A., Lázaro, C. & Morata, D. 2014. Late Jurassic terrane collision in the northwestern margin of Gondwana (Cajamarca Complex, eastern flank of the Central Cordillera, Colombia). International Geology Review, 56(15): 1852–1872. https://doi.org/10.1080/00206814.2014.963710

Bustamante, C., Cardona, A., Bayona, G., Mora, A., Valencia, V., Gehrels, G. & Vervoort, J. 2010. U–Pb LA–ICP–MS geochronology and regional correlation of Middle Jurassic intrusive rocks from the Garzón Massif, Upper Magdalena Valley and Central Cordillera, southern Colombia. Boletín de Geología, 32(2): 93–109.

Bustamante, C., Archanjo, C.J., Cardona, A. & Vervoort, J.D. 2016. Late Jurassic to early Cretaceous plutonism in the Colombian Andes: A record of long–term arc maturity. Geological Society of America Bulletin, 128(11–12): 1762–1779. https://doi.org/10.1130/B31307.1

Bustamante, C., Archanjo, C.J., Cardona, A., Bustamante, A. & Valencia, V.A. 2017. U–Pb ages and Hf isotopes in zircons from parautochthonous Mesozoic terranes in the western margin of Pangea: Implications for the terrane configurations in the northern Andes. The Journal of Geology, 125(5): 487–500. https://doi.org/10.1086/693014

Cardona, A., Valencia, V., Garzón, A., Montes, C., Ojeda, G., Ruiz, J. & Weber, M. 2010. Permian to Triassic I to S–type magmatic switch in the northeast Sierra Nevada de Santa Marta and adjacent regions, Colombian Caribbean: Tectonic setting and implications within Pangea paleogeography. Journal of South American Earth Sciences, 29(4): 772–783. https://doi.org/10.1016/j.jsames.2009.12.005

Cardona, A., Valencia, V.A., Lotero, A., Villafañez, Y. & Bayona, G. 2016. Provenance of middle to late Palaeozoic sediments in the northeastern Colombian Andes: Implications for Pangea reconstruction. International Geology Review, 58(15): 1914–1939. https://doi.org/10.1080/00206814.2016.1190948

Carvajal, C.A., Fuquen, J.A., Gómez, L.A. & Núñez, A. 1983. Memoria explicativa: Cartografía geológica y prospección geoquímica regional de la plancha 282 Chaparral. Ingeominas, 88 p. Bogotá.

Carvajal, C.A., Fuquen, J.A. & Gómez, L.A. 1993. Geología de la plancha 282 Chaparral. Scale 1:100 000. Ingeominas. Bogotá.

Cediel, F., Shaw, R.P. & Cáceres, C. 2003. Tectonic assembly of the northern Andean Block. In: Bartolini, C., Buffler, R.T. & Blickwede, J. (editors), The circum–Gulf of Mexico and the Caribbean: Hydrocarbon habitats, basin formation, and plate tectonics. American Association of Petroleum Geologists, Memoir 79, p. 815–848. Tulsa, USA.

Chappell, B.W. & White, A.J.R. 1974. Two contrasting granite types. Pacific Geology, 8: 173–174.

Clavijo, J. 1994. Memoria explicativa: Mapa geológico generalizado del departamento de Norte de Santander. Scale 1:250 000. Ingeominas, Internal report 2182, 47 p. Bucaramanga.

Clavijo, J., Mantilla, L., Pinto, J., Bernal, L. & Pérez, A. 2008. Evolución geológica de la serranía de San Lucas, norte del Valle Medio del Magdalena y noroeste de la cordillera Oriental. Boletín de Geología, 30(1): 45–62.

Cochrane, R., Spikings, R., Gerdes, A., Winkler, W., Ulianov, A., Mora, A. & Chiaradia, M. 2014. Distinguishing between in–situ and accretionary growth of continents along active margins. Lithos, 202–203: 382–394. https://doi.org/10.1016/j.lithos.2014.05.031

Condie, K.C. 1989. Plate tectonics and crustal evolution. Third edition, Pergamon Press, 476 p. Oxford.

Cordani, U.G., Cardona, A., Jiménez, D., Liu, D. & Nutman, A.P. 2005. Geochronology of Proterozoic basement inliers in the Colombian Andes: Tectonic history of remnants of a fragmented Grenville belt. In: Vaughan, A.P.M., Leat, P.T. & Pankhurst, R.J. (editors), Terrane processes at the margins of Gondwana. Geological Society of London, Special Publication 246, p. 329–346. https://doi.org/10.1144/GSL.SP.2005.246.01.13

Correa–Martínez, A.M., Rodríguez, G., Arango, M.I., Zapata, G. & Bermúdez, J.G. 2016. Batolito de Mogotes. Catálogo de unidades litoestratigráficas de Colombia. Servicio Geológico Colombiano, 110 p. Medellín.

Correa–Martínez, A.M., Rodríguez, G., Bermúdez, J.G., Arango, M.I. & Zapata, G. 2018. Riolitas del Alto Los Cacaos. Catálogo de unidades litoestratigráficas de Colombia. Servicio Geológico Colombiano, 54 p. Medellín.

Cossio, U., Rodríguez, G. & Rodríguez, M.A. 1994. Memoria explicativa: Geología de la plancha 283 Purificación, departamento del Tolima. Scale 1:100 000. Ingeominas, 108 p. Bogotá.

Cox, K.G., Bell, J.D. & Pankhurst, R.J. 1979. The interpretation of igneous rocks. George Allen & Unwin, 464 p. London.

Daconte, R. & Salinas, R. 1980a. Memoria explicativa: Geología de las planchas 66 Miraflores y 76 Ocaña. Scale 1:100 000. Ingeominas, 105 p. Bucaramanga.

Daconte, R. & Salinas, R. 1980b. Geología de la plancha 66 Miraflores. Scale 1:100 000. Ingeominas. Bucaramanga.

Daconte, R. & Salinas, R. 1980c. Geología de la plancha 76 Ocaña. Scale 1:100 000. Ingeominas. Bucaramanga.

Dörr, W., Grösser, J.R., Rodríguez, G.I. & Kramm, U. 1995. Zircon U–Pb age of the Paramo Rico tonalite–granodiorite, Santander Massif (Cordillera Oriental, Colombia) and its geotectonic significance. Journal of South American Earth Sciences, 8(2): 187–194. https://doi.org/10.1016/0895-9811(95)00004-Y

Etayo–Serna, F., Barrero, D., Lozano, H., Espinosa, A., González, H., Orrego, A., Ballesteros, I., Forero, H., Ramírez, C., Zambrano–Ortiz, F., Duque–Caro, H., Vargas, R., Núñez, A., Álvarez, J., Ropaín, C., Cardozo, E., Galvis, N., Sarmiento, L., Alberts, J.P., Case, J.E., Singer, D.A., Bowen, R.W., Berger, B.R., Cox, D.P. & Hodges, C.A. 1983. Mapa de terrenos geológicos de Colombia. Publicaciones Geológicas Especiales del Ingeominas 14(1), p. 1–235. Bogotá.

Feininger, T., Barrero, D. & Castro, N. 1972. Geología de parte de los departamentos de Antioquia y Caldas–subzona II–B. Boletín Geológico, 20(2): 1–173.

Ferreira, P., Núñez, A. & Rodríguez, M.A. 1998. Geología de la plancha 323 Neiva. Scale 1:100 000. Ingeominas. Bogotá.

Ferreira, P., Núñez, A. & Rodríguez, M.A. 2002. Memoria explicativa: Levantamiento geológico de la plancha 323 Neiva. Scale 1:100 000. Ingeominas. 100 p. Bogotá.

Forero–Suárez, A. 1990. The basement of the Eastern Cordillera, Colombia: An allochthonous terrane in northwestern South America. Journal of South American Earth Sciences, 3(2–3): 141–151. https://doi.org/10.1016/0895-9811(90)90026-W

Frost, B.R., Barnes, C.G., Collins, W.J., Arculus, R.J., Ellis, D.J. & Frost, C.D. 2001. A geochemical classification for granitic rocks. Journal of Petrology, 42(11): 2033–2048. https://doi.org/10.1093/petrology/42.11.2033

García, C.A. & Ríos, C.A. 1999. Metamorfismo y metalogenia asociada del Macizo de Santander, cordillera Oriental, Colombia. Proyecto de investigación 1102–05–083–95, Informe final, unpublished. Universidad Industrial de Santander. 191 p. Bucaramanga.

Gendall, I.R., Quevedo, L.A., Sillitoe, R.H., Spencer, R.M., Puente, C.O., León, J.P. & Povedo, R.R. 2000. Discovery of a Jurassic porphyry copper belt, Pangui area, southern Ecuador. SEG Newsletter, 43(1): 8–15.

Goldsmith, R., Marvin, R.F. & Mehnert, H.H. 1971. Radiometric ages in the Santander Massif, Eastern Cordillera, Colombian Andes. United States Geological Survey, Professional Paper, 750–D: D41–D49.

Gómez, J., Montes, N., Nivia, Á. & Diederix, H., compiladores. 2015a. Geological Map of Colombia 2015. Scale 1:1 000 000. Servicio Geológico Colombiano, 2 sheets. Bogotá.

Gómez, J., Montes, N.E., Alcárcel, F.A. & Ceballos, J.A. 2015b. Catálogo de dataciones radiométricas de Colombia en ArcGIS y Google Earth. In: Gómez, J. & Almanza, M.F. (editors), Compilando la geología de Colombia: Una visión a 2015. Servicio Geológico Colombiano, Publicaciones Geológicas Especiales 33, p. 63–419. Bogotá.

González, H. 1980. Geología de las planchas 167 Sonsón y 187 Salamina. Scale 1:100 000. Boletín Geológico, 23(1): 1–174.

Green, T.H. 1980. Island arc and continent–building magmatism: A review of petrogenetic models based on experimental petrology and geochemistry. Tectonophysics, 63(1–4): 367–385. https://doi.org/10.1016/0040-1951(80)90121-3

Hall, R.B., Álvarez, J. & Rico, H. 1972. Geología de parte de los departamentos de Antioquia y Caldas (Sub–Zona II–A). Boletín Geológico, 20(1): p. 1–85.

Harris, N.B.W., Pearce, J.A. & Tindle, A.G. 1986. Geochemical characteristics of collision–zone magmatism. In: Coward, M.P. & Ries, A.C. (editors), Collision tectonics. Geological Soci-

ety of London, Special Publication 19, p. 67–81. https://doi.org/10.1144/GSL.SP.1986.019.01.04

Horton, B.K., Saylor, J.E., Nie, J., Mora, A., Parra, M., Reyes–Harker, A. & Stockli, D.F. 2010. Linking sedimentation in the northern Andes to basement configuration, Mesozoic extension, and Cenozoic shortening: Evidence from detrital zircon U–Pb ages, Eastern Cordillera, Colombia. Geological Society of America Bulletin, 122(9–10): 1423–1442. https://doi.org/10.1130/B30118.1

Ibañez–Mejia, M., Ruiz, J., Valencia, V., Cardona, A., Gehrels, G.E. & Mora, A. 2011. The Putumayo Orogen of Amazonia and its implications for Rodinia reconstructions: New U–Pb geochronological insights into the Proterozoic tectonic evolution of northwestern South America. Precambrian Research, 191(1–2): 58–77. https://doi.org/10.1016/j.precamres.2011.09.005

Irvine, T.N. & Baragar, W.R.A. 1971. A guide to the chemical classification of the common volcanic rocks. Canadian Journal of Earth Sciences, 8(5): 523–548. https://doi.org/10.1139/e71-055

Jiménez–Mejía, D.M., Juliani, C. & Cordani, U.G. 2006. P–*T*–*t* conditions of high–grade metamorphic rocks of the Garzón Massif, Andean basement, SE Colombia. Journal of South American Earth Sciences, 21(4): 322–336. https://doi.org/10.1016/j.jsames.2006.07.001

Kennan, L. & Pindell, J.L. 2009. Dextral shear, terrane accretion and basin formation in the northern Andes: Best explained by interaction with a Pacific–derived Caribbean Plate? In: James, K.H., Lorente, M.A. & Pindell, J.L. (editors), The origin and evolution of the Caribbean Plate. Geological Society of London, Special Publication 328, p. 487–531. https://doi.org/10.1144/SP328.20

Kroonenberg, S.B. & Diederix, H. 1982. Geology of south–central Huila, uppermost Magdalena Valley, Colombia. A preliminary note. Guide Book 21 Annual Field Trip. Colombian Society Petroleum Geologists and Geophysicists, 39 p. Bogotá.

Le Maitre, R.W., Streckeisen, A., Zanettin, B., Le Bas, M.J., Bonin, B., Bateman, P., Bellieni, G., Dudek, A., Efremova, S., Keller, J., Lameyre, J., Sabine, P.A., Schmid, R., Sørensen, H. & Woolley, A.R., editors. 2002. Igneous rocks: A classification and glossary of terms. Recommendations of the International Union of Geological Sciences Subcommission on the systematics of igneous rocks. Cambridge University Press, 236 p. Cambridge, UK. https://doi.org/10.1017/CBO9780511535581

Leal–Mejía, H. 2011. Phanerozoic gold metallogeny in the Colombian Andes: A tectono–magmatic approach. Doctoral thesis, Universitat de Barcelona, 989 p. Barcelona.

Ludwig, K.R. 2012. User´s manual for Isoplot 3.75. A geochronological toolkit for Microsoft Excel. Berkeley Geochronology Center Special Publication 5, 75 p. Berkeley, USA.

Mantilla–Figueroa, L.C., Bissig, T., Cottle, J.M. & Hart, C.J.R. 2012. Remains of early Ordovician mantle–derived magmatism in the Santander Massif (Colombian Eastern Cordillera). Journal of South American Earth Sciences, 38: 1–12. https://doi.org/10.1016/j.jsames.2012.03.001

Mantilla–Figueroa, L.C., Bissig, T., Valencia, V. & Hart, C.J.R. 2013. The magmatic history of the Vetas–California mining district, Santander Massif, Eastern Cordillera, Colombia. Journal of South American Earth Sciences, 45: 235–249. https://doi.org/10.1016/j.jsames.2013.03.006

Mantilla–Figueroa, L.C., García–Ramírez, C.A., Valencia, V.A. 2016. Propuesta de escisión de la denominada 'Formación Silgará' (Macizo de Santander, Colombia), a partir de edades U–Pb en zircones detríticos. Boletín de Geología, 38(1): 33–50. https://doi.org/10.18273/revbol.v38n1-2016002

Marshall, J.D. 1988. Cathodoluminescence of geological materials. Unwin Hyman, 146 p. Boston.

Martens, U., Restrepo, J.J., Ordoñez–Carmona, O. & Correa–Martínez, A.M. 2014. The Tahamí and Anacona Terranes of the Colombian Andes: Missing links between South American and Mexican Gondwana margins. The Journal of Geology, 122(5): 507–530. https://doi.org/10.1086/677177

Maya, M. & González, H. 1995. Unidades litodémicas en la cordillera Central de Colombia. Boletín Geológico, 35(2–3): 43–57.

McCourt, W.J., Aspden, J.A. & Brook, M. 1984. New geological and geochronological data from the Colombian Andes: Continental growth by multiple accretion. Journal of the Geological Society, 141(5): 831–845. https://doi.org/10.1144/gsjgs.141.5.0831

McDonough, W.F. & Sun, S.S. 1995. The composition of the Earth. Chemical Geology, 120(3–4): 223–253. https://doi.org/10.1016/0009-2541(94)00140-4

Meschede, M. & Frisch, W. 1998. A plate–tectonic model for the Mesozoic and early Cenozoic history of the Caribbean Plate. Tectonophysics, 296(3–4): 269–291. https://doi.org/10.1016/S0040-1951(98)00157-7

Middlemost, E.A.K. 1985. Magmas and magmatic rocks: An introduction to igneous petrology. Addison–Wesley Longman Ltd., 266 p. London & New York.

Mojica, J. & Villarroel, C. 1984. Contribución al conocimiento de las unidades paleozoicas del área de Floresta (cordillera Oriental colombiana; departamento de Boyacá) y en especial al de la Formación Cuche. Geología Colombiana, (13): 55–79.

Mojica, J., Villarroel, C., Cuerda, A. & Alfaro, M. 1988. La fauna de graptolites de la Formación El Hígado (Llanvirniano?–Llandeiliano). Serranía de Las Minas, Valle Superior del Magdalena, Colombia. V Congreso Geológico Chileno. Memoirs, II, p. 189–202. Santiago de Chile.

Mojica, J., Kammer, A. & Ujueta, G. 1996. El Jurásico del sector noroccidental de Suramérica y guía de la excursión al Valle Superior del Magdalena (Nov. 1–4/95), regiones de Payandé y Prado, departamento del Tolima, Colombia. Geología Colombiana, (21): 3–40.

Nakamura, N. 1974. Determination of REE, Ba, Fe, Mg, Na and K in carbonaceous and ordinary chondrites. Geochimica et Cosmochimica Acta, 38(5): 757–775. https://doi.org/10.1016/0016-7037(74)90149-5

Nelson, H.W. 1957. Contribution to the geology of the Central and Western Cordillera of Colombia in the sector between Ibagué and Cali. Leidse Geologische Meaedelingen, 22, 75 p. Leiden, the Netherlands.

Nelson, W.H. 1962. Contribución al conocimiento de la cordillera Central de Colombia sección entre Ibagué y Armenia. Boletín Geológico, 10(1–3): 161–202.

Noble, S.R., Aspden, J.A. & Jemielita, R. 1997. Northern Andean crustal evolution: New U–Pb geochronological constraints from Ecuador. Geological Society of America Bulletin, 109(7): 789–798. https://doi.org/10.1130/0016-7606(1997)109<0789:NACENU>2.3.CO;2

Núñez, A. 2001. Memoria explicativa: Mapa geológico del departamento del Tolima: Geología, recursos geológicos y amenazas geológicas. Scale 1:250 000. Ingeominas, 100 p. Bogotá.

Núñez, A. 2002. Batolito de Ibagué. Catálogo de unidades litoestratigráficas de Colombia. Ingeominas, 26 p. Bogotá.

Ordóñez–Carmona, O., Restrepo, J.J. & Pimentel, M.M. 2006. Geochronological and isotopical review of pre–Devonian crustal basement of the Colombian Andes. Journal of South American Earth Sciences, 21(4): 372–382. https://doi.org/10.1016/j.jsames.2006.07.005

Pearce, J. 1982. Trace element characteristics of lavas from destructive plate boundaries. In: Thorpe, R.S. (editor), Andesites: Orogenic andesites and related rocks. John Wiley and Sons, p. 525–548.

Pearce, J.A. 1996. A user's guide to basalt discrimination diagrams. In: Wyman, D.A. (editor), Trace element geochemistry of volcanic rocks: Applications for massive sulphide exploration. Geological Association of Canada, Short Course Notes 12, p. 79–113. Winnipeg, Canada.

Pearce, J.A. 2008. Geochemical fingerprinting of oceanic basalts with applications to ophiolite classification and the search for Archean oceanic crust. Lithos, 100(1–4): 14–48. https://doi.org/10.1016/j.lithos.2007.06.016

Pearce, J.A., Harris, N.B.W. & Tindle, A.G. 1984. Trace element discrimination diagrams for the tectonic interpretation of granitic rocks. Journal of Petrology, 25(4): 956–983. https://doi.org/10.1093/petrology/25.4.956

Peccerillo, A. & Taylor, S.R. 1976. Geochemistry of Eocene calc–alkaline volcanic rocks from the Kastamonu area, northern Turkey. Contributions to Mineralogy and Petrology, 58(1): 63–81. https://doi.org/10.1007/BF00384745

Pindell, J. & Dewey, J.F. 1982. Permo–Triassic reconstruction of western Pangea and the evolution of the Gulf of Mexico and south Caribbean region. Tectonics, 1(2): 179–211. https://doi.org/10.1029/TC001i002p00179

Restrepo, J.J. & Toussaint, J.F. 1988. Terranes and continental accretion in the Colombian Andes. Episodes, 11(3): 189–193. https://doi.org/10.18814/epiiugs/1988/v11i3/006

Restrepo, J.J. & Toussaint, J.F. 1989. Terrenos alóctonos en los Andes colombianos: Explicación de algunas paradojas geológicas. V Congreso Colombiano de Geología. Memoirs, I, p. 92–107. Bucaramanga.

Restrepo, J.J., Ordóñez–Carmona, O., Martens, U. & Correa, A.M. 2009. Terrenos, complejos y provincias en la cordillera Central colombiana. Ingeniería, Investigación y Desarrollo, 9(2): 49–56.

Restrepo, J.J., Ordóñez–Carmona, O., Armstrong, R. & Pimentel, M.M. 2011. Triassic metamorphism in the northern part of the Tahamí Terrane of the Central Cordillera of Colombia. Journal of South American Earth Sciences, 32(4): 497–507. https://doi.org/10.1016/j.jsames.2011.04.009

Restrepo, J.J., Ibañez–Mejia, M. & García–Casco, A. 2012. U–Pb zircon ages of the Medellín Amphibolites (Central Cordillera of Colombia) reveal mid–Cretaceous tectonic juxtaposition of Triassic and mid–Cretaceous metamorphic complexes. VIII South American Symposium on Isotope Geology. USB memory device, 33 slides. Medellín.

Restrepo–Pace, P. 1995. Late Precambrian to early Mesozoic tectonic evolution of the Colombian Andes based on new geocronological, geochemical and isotopic data. Doctoral thesis, University of Arizona, 195 p. Arizona.

Restrepo–Pace, P.A. & Cediel, F. 2010. Northern South America basement tectonics and implications for paleocontinental reconstructions of the Americas. Journal of South American Earth Sciences, 29(4): 764–771. https://doi.org/10.1016/j.jsames.2010.06.002

Restrepo–Pace, P.A., Ruiz, J., Gehrels, G. & Cosca, M. 1997. Geochronology and Nd isotopic data of Grenville–age rocks in the Colombian Andes: New constraints for late Proterozoic–early Paleozoic paleocontinental reconstructions of the Americas. Earth and Planetary Science Letters, 150(3–4): 427–441. https://doi.org/10.1016/S0012-821X(97)00091-5

Ríos, C., García, C. & Takusa, A. 2003. Tectono–metamorphic evolution of the Silgará Formation metamorphic rocks in the southwestern Santander Massif, Colombian Andes. Journal of South American Earth Sciences, 16(2): 133–154. https://doi.org/10.1016/S0895-9811(03)00025-7

Rodríguez, G. 1995a. Petrografía y microtexturas del Grupo Garzón y el Granito de anatexis de El Recreo, Macizo de Garzón, cordillera Oriental–Colombia. Revista Ingeominas, (5): 17–36.

Rodríguez, G. 1995b. Petrografía del Macizo de La Plata, departamento del Huila. Revista Ingeominas, (5): 5–16.

Rodríguez, G. & Fuquen, J.A. 1989. Geología y prospección geoquímica de la plancha 302 Aipe (Huila). Ingeominas, internal report 2103, 152 p. Ibagué.

Rodríguez, G. & Núñez, A. 1999. Geología del departamento del Tolima. Scale 1:300 000. Ingeominas. Bogotá.

Rodríguez, G., Ferreira, P., Velandia, F. & Núñez, A. 1998. Geología de la plancha 366 Garzón. Scale 1:100 000. Ingeominas. Bogotá.

Rodríguez, G., Zapata, G., Velásquez, M.E., Cossio, U. & Londoño, A.C. 2003. Memoria explicativa: Geología de las planchas 367

Gigante, 368 San Vicente del Caguán, 389 Timaná, 390 Puerto Rico, 391 Lusitania (parte noroccidental) y 414 El Doncello. Scale 1:100 000. Ingeominas, 166 p. Bogotá.

Rodríguez, G., González, H. & Zapata, G. 2005. Memoria explicativa: Geología de la plancha 147 Medellín oriental. Scale: 1:100 000. Ingeominas, 300 p. Medellín.

Rodríguez, G., Arango, M.I., Zapata, G. & Bermúdez, J.G. 2015a. Características petrográficas, geoquímicas y edad U–Pb de los plutones jurásicos del Valle Superior del Magdalena. XV Congreso Colombiano de Geología. Poster. Bucaramanga.

Rodríguez, G., Arango, M.I., Bermúdez, J.G. & Zapata, G. 2015b. Cuarzomonzonita de Los Naranjos. Catálogo de unidades litoestratigráficas de Colombia. Servicio Geológico Colombiano, 28 p. Medellín.

Rodríguez, G., Arango, M.I., Zapata, G. & Bermúdez, J.G. 2015c. Cuarzomonzodiorita de El Astillero. Catálogo de unidades litoestratigráficas de Colombia. Servicio Geológico Colombiano, 27 p. Medellín.

Rodríguez, G., Zapata, G., Arango, M.I. & Bermúdez, J.G. 2015d. Monzogranito de Algeciras. Catálogo de unidades litoestratigraficas de Colombia. Servicio Geológico Colombiano, 36 p. Medellín.

Rodríguez, G., Arango, M.I., Bermúdez, J.G. & Zapata, G. 2015e. Granito de Garzón. Catálogo de unidades litoestratigráficas de Colombia. Servicio Geológico Colombiano, 23 p. Medellín.

Rodríguez, G., González, H., Zapata, G., Cossio, U. & Correa–Martínez. A.M. 2016a. Geología de la plancha 147 Medellín Oriental. Scale 1:50 000. Servicio Geológico Colombiano, 464 p. Bogotá.

Rodríguez, G., Arango, M.I., Zapata, G. & Bermúdez, J.G. 2016b. Formación Saldaña. Catálogo de las unidades litoestratigráficas de Colombia. Servicio Geológico Colombiano, 90 p. Medellín.

Rodríguez, G., Zapata, G., Arango, M.I. & Bermúdez, J.G. 2017a. Caracterización petrográfica, geoquímica y geocronología de rocas granitoides pérmicas al occidente de La Plata y Pacarní, Huila, Valle Superior del Magdalena, Colombia. Boletín de Geología, 39(1): 41–68. https://doi.org/10.18273/revbol.v39n1-2017002

Rodríguez, G., Zapata, G., Correa–Martínez, A.M. & Arango, M.I. 2017b. Caracterización petrográfica, química y geocronológica del magmatismo Triásico–Jurásico del Macizo de Santander, Colombia. XVI Congreso Colombiano de Geología y III Simposio de Exploradores. Memoirs, p. 1430–1433. Santa Marta.

Rodríguez, G., Correa, A.M., Zapata, G. & Arango, M.I. 2017c. Monzogranito de La Corcova. Catálogo de unidades litoestratigráficas de Colombia. Servicio Geológico Colombiano, 105 p. Medellín.

Rodríguez, G., Arango, M.I., Zapata, G. & Correa–Martínez, A.M. 2017d. Tonalita de San Martín. Catálogo de las unidades litoestratigráficas de Colombia. Servicio Geológico Colombiano, 55 p. Medellín.

Rodríguez, G., Arango, M.I., Zapata, G. & Bermúdez, J.G. 2018a. Petrotectonic characteristics, geochemistry, and U–Pb geochronology of Jurassic plutons in the Upper Magdalena Valley–Colombia: Implications on the evolution of magmatic arcs in the NW Andes. Journal of South American Earth Sciences, 81: 10–30. https://doi.org/10.1016/j.jsames.2017.10.012

Rodríguez, G., Arango, M.I., Correa, A.M. & Zapata, G. 2018b. Riolita de San Joaquín. Catálogo de unidades litoestratigráficas de Colombia. Servicio Geológico Colombiano, 46 p. Medellín.

Rodríguez, G., Zapata, G., Arango, M.I. & Correa, A.M. 2018c. Monzogranito de Santa Bárbara. Catálogo de unidades litoestratigráficas de Colombia. Servicio Geológico Colombiano, 95 p. Medellín.

Rodríguez–García, G., Correa–Martínez, A.M., Zapata–Villada, J.P. & Obando–Erazo, G. 2019. Fragments of a Permian arc on the western margin of the Neoproterozoic basement of Colombia. In: Gómez, J. & Mateus–Zabala, D. (editors), The Geology of Colombia, Volume 1 Proterozoic – Paleozoic. Servicio Geológico Colombiano, Publicaciones Geológicas Especiales 35, p. 205–239. Bogotá. https://doi.org/10.32685/pub.esp.35.2019.10

Ross, M.I. & Scotese, C.R. 1988. A hierarchical tectonic model of the Gulf of Mexico and Caribbean region. Tectonophysics, 155(1–4): 139–168. https://doi.org/10.1016/0040-1951(88)90263-6

Royero, J.M. & Clavijo, J. 2001. Memoria explicativa: Mapa geológico generalizado, departamento de Santander. Scale 1:400 000. Ingeominas, 91 p. Bogotá.

Shand, S.J. 1943. Eruptive rocks. Their genesis, composition, classification and their relation to ore deposits, with a chapter on meteorites. Wiley & Sons, 488 p. New York.

Siivola, J. & Schmid, R. 2007. List of mineral abbreviations. In: Fettes, D. & Desmons, J. (editors), Metamorphic Rocks: A Classification and Glossary of Terms. Recommendations of the International Union of Geological Sciences Subcommission on the Systematics of Metamorphic Rocks. Cambridge University Press, p. 93–110. Cambridge, UK

Slama, J., Kosler, J., Condon, D.J., Crowley, J.L., Gerdes, A., Hanchar, J.M., Horstwood, M.S.A., Morris, G.A., Nasdala, L., Norberg, N., Schaltegger, U., Schoene, B., Tubrett, M. & Whitehouse, M.J. 2008. Plešovice zircon–A new natural reference material for U–Pb and Hf isotopic microanalysis. Chemical Geology, 249(1–2): 1–35. https://doi.org/10.1016/j.chemgeo.2007.11.005

Solari, L., Gómez–Tuena, A., Bernal, J.P., Pérez–Arvizu, O. & Tanner, M. 2010. U–Pb zircon geochronology with an integrated LA–ICP–MS microanalytical workstation: Achievements in precision and accuracy. Geostandards and Geoanalytical Research, 34(1): 5–18. https://doi.org/10.1111/j.1751-908X.2009.00027.x

Spikings, R., Cochrane, R., Villagómez, D., van der Lelij, R., Vallejo, C., Winkler, W. & Beate, B. 2015. The geological history of northwestern South America: From Pangaea to the early collision of the Caribbean Large Igneous Province (290–75 Ma). Gondwana Research, 27(1): 95–139. https://doi.org/10.1016/j.gr.2014.06.004

Stacey, J.S. & Kramers, J.D. 1975. Approximation of terrestrial lead isotope evolution by a two–stage model. Earth and Planetary Science Letters, 26(2): 207–221. https://doi.org/10.1016/0012-821X(75)90088-6

Stibane, F. & Forero, A. 1969. Los afloramientos del Paleozoico en la Jagua (Huila) y río Nevado (Santander del sur). Geología Colombiana, (6): 31–66.

Streckeisen, A. 1974. Classification and nomenclature of plutonic rocks recommendations of the IUGS subcommission on the systematics of igneous rocks. Geologische Rundschau., 63(2): 773–786. https://doi.org/10.1007/BF01820841

Streckeisen, A. 1979. Classification and nomenclature of volcanic rocks, lamprophyres, carbonatites, and melilitic rocks: Recommendations and suggestions of the IUGS subcommission on the systematics of igneous rocks. Geology, 7(7): 331–335. https://doi.org/10.1130/0091-7613(1979)7<331:-CANOVR>2.0.CO;2

Sun, S.S. & McDonough, W.F. 1989. Chemical and isotopic systematics of oceanic basalts: Implications for mantle composition and processes. In: Saunders, A.D. & Norry, M.J. (editors), Magmatism in the ocean basins. Geological Society of London, Special Publications 42, p. 313–345. https://doi.org/10.1144/GSL.SP.1989.042.01.19

Toussaint, J.F. 1995. Evolución geológica de Colombia; 2 Triásico–Jurásico. Universidad Nacional de Colombia, 94 p. Medellín.

Ulloa, C. & Rodríguez, G.I. 1982. Intrusiones ácidas ordovícicas y post–devónicas en la Floresta (Boyacá). IV Congreso Colombiano de Geología. Memoirs, p. 23. Cali.

van der Lelij, R. 2013. Reconstructing northwestern Gondwana with implications for the evolution of the Iapetus and Rheic oceans: A geochronological, thermochronological and geochemical study. Doctoral thesis, University of Genève, 248 p. Genève. https://doi.org/10.13097/archive-ouverte/unige:31653

van der Lelij, R., Spikings, R.A. & Mora, A. 2016. Thermochronology and tectonics of the Mérida Andes and the Santander Massif, NW South America. Lithos, 248–251: 220–239. https://doi.org/10.1016/j.lithos.2016.01.006

Vargas, R. & Arias, A. 1981a. Geología de la plancha 86 Ábrego. Scale 1:100 000. Ingeominas. Bogotá.

Vargas, R. & Arias, A. 1981b. Geología de la plancha 97 Cáchira. Scale 1:100 000. Ingeominas. Bogotá.

Vargas, R., Arias, A., Jaramillo, L., & Tellez, N. 1984. Geología de la Plancha 136 Málaga. Scale 1:100 000. Ingeominas. Bogotá.

Velandia, F., Morales, C.J., Caicedo, J.C. & Núñez, A. 2000. Geología de la plancha 345 Campoalegre. Scale 1:100 000. Ingeominas. Bogotá.

Velandia, F., Ferreira, P., Rodríguez, G. & Núñez, A. 2001a. Memoria explicativa: Levantamiento geológico de la plancha 366 Garzón. Ingeominas, 81 p. Bogotá.

Velandia, F., Nuñez, A. & Marquínez, G. 2001b. Memoria explicativa: Mapa geológico del departamento del Huila. Scale 1:300 000. Ingeominas, 151 p. Bogotá.

Velandia, F., Acosta, J., Terraza, R. & Villegas, H. 2005. The current tectonic motion of the northern Andes along the Algeciras Fault System in SW Colombia. Tectonophysics, 399(1–4): 313–329. https://doi.org/10.1016/j.tecto.2004.12.028

Vesga, C.J. & Barrero, D. 1978. Edades K/Ar en rocas ígneas y metamórficas de la cordillera Central de Colombia y su implicación geológica. II Congreso Colombiano de Geología. Abstracts, p. 19. Bogotá.

Villagómez, D., Spikings, R., Magna, T., Kammer, A., Winkler, W. & Beltrán, A. 2011. Geochronology, geochemistry and tectonic evolution of the Western and Central cordilleras of Colombia. Lithos, 125(3–4): 875–896. https://doi.org/10.1016/j.lithos.2011.05.003

Villagómez, D., Martens, U. & Pindell, J. 2015. Are Jurassic and some older blocks in the northern Andes in–situ or far–travelled? Potential correlations and new geochronological data from Colombia and Ecuador. Conference paper. Tectónica jurásica en la parte noroccidental de Sur América y bloques adyacentes. Universidad EAFIT, 1 p. Medellín.

Villarroel, C. & Mojica, J. 1988. El Paleozoico superior (Carbonífero–Pérmico) sedimentario de Colombia: Afloramientos conocidos y características generales. Geología Colombiana, (16): 81–87.

Vinasco, C.J., Cordani, U.G., González, H., Weber, M. & Peláez, C. 2006. Geochronological, isotopic, and geochemical data from Permo–Triassic granitic gneisses and granitoids of the Colombian central Andes. Journal of South American Earth Sciences, 21(4): 355–371. https://doi.org/10.1016/j.jsames.2006.07.007

Ward, D.E., Goldsmith, R., Cruz, J. & Restrepo, H. 1973. Geología de los cuadrángulos H–12 Bucaramanga y H–13 Pamplona, departamento de Santander. Boletín Geológico, 21(1–3): 132 p.

Ward, D.E., Goldsmith, R., Cruz, J., Jaramillo, L. & Vargas, R. 1977a. Geología de la plancha 110 Pamplona. Scale 1:100 000. Ingeominas. Bogotá.

Ward, D.E., Goldsmith, R., Cruz, J., Jaramillo, L. & Vargas, R. 1977b. Mapa geológico del cuadrángulo Pamplona H–13. Scale 1:100 000. Ingeominas. Bogotá.

Ward, D.E., Goldsmith, R., Cruz, J., Téllez, N. & Jaramillo, L. 1977c. Mapa geológico San Gil y Málaga (parte de los cuadrángulos I–12 y I–13), Colombia. Scale 1:100 000. Ingeominas. Bogotá.

Ward, D.E., Goldsmith, R., Jimeno, A., Cruz, J., Restrepo, H. & Gómez, E. 1977d. Geología de la plancha 109 Rionegro. Scale 1:100 000. Ingeominas. Bogotá.

Ward, D.E., Goldsmith, R., Jimeno, A., Cruz, J., Restrepo, H. & Gómez, E. 1977e. Geología de la plancha 120 Bucaramanga. Scale 1:100 000. Ingeominas. Bogotá.

Ward, D.E., Goldsmith, R., Cruz, J., Jaramillo, L. & Vargas, R. 1977f. Geología de la plancha 121 Cerrito. Scale 1:100 000. Ingeominas. Bogotá.

Whalen, J.B., Currie, K.L. & Chappell, B.W. 1987. A–type granites: Geochemical characteristics, discrimination and petrogenesis. Contributions to Mineralogy and Petrology, 95(4): 407–419. https://doi.org/10.1007/BF00402202

Wiedenbeck, M., Allé, P., Corfu, F., Griffin, W.L., Meier, M., Oberli, F., von Quadt, A., Roddick, J.C. & Spiegel, W. 1995. Three natural zircon standards for U–Th–Pb, Lu–Hf, trace element and REE analyses. Geostandards Newsletter, 19(1): 1–23. https://doi.org/10.1111/j.1751-908X.1995.tb00147.x

Zapata, G., Rodríguez, G., Arango, M.I. & Bermúdez, J.G. 2015. Cuarzomonzodiorita de Páez. Catálogo de unidades litoestratigráficas de Colombia. Servicio Geológico Colombiano, 51 p. Medellín.

Zapata, S., Cardona, A., Jaramillo, C., Valencia, V. & Vervoort, J. 2016a. U–Pb LA–ICP–MS geochronology and geochemistry of Jurassic volcanic and plutonic rocks from the Putumayo region (southern Colombia): Tectonic setting and regional correlations. Boletín de Geología, 38(2): 1–38. https://doi.org/10.18273/revbol.v38n2-2016001

Zapata, G., Correa, A.M., Rodríguez, G. & Arango, M.I. 2016b. Granito de Pescadero. Catálogo de unidades litoestratigráficas de Colombia. Servicio Geológico Colombiano, 54 p. Medellín.

Zapata, G., Rodríguez, G. & Arango, M.I. 2017a. Petrografía, geoquímica y geocronología de rocas metamórficas aflorantes en San Francisco Putumayo y la vía Palermo–San Luis asociadas a los complejos La Cocha–Río Téllez y Aleluya. Boletín de Ciencias de la Tierra, (41): 48–65.

Zapata, G., Correa–Martínez, A.M., Rodríguez, G. & Arango, M.I. 2017b. Monzogranito de Santa Rosita. Catálogo de unidades litoestratigráficas de Colombia. Servicio Geológico Colombiano, 57 p. Medellín.

Zapata, G., Arango, M.I., Rodríguez, G. & Correa–Martínez, A.M. 2018. Riolitas El Uvo. Catálogo de unidades litoestratigráficas de Colombia. Servicio Geológico Colombiano, 39 p. Medellín.

Zuluaga, C.A., Amaya, S., Urueña, C. & Bernet, M. 2017. Migmatization and low–pressure overprinting metamorphism as record of two pre–Cretaceous tectonic episodes in the Santander Massif of the Andean basement in northern Colombia (NW South America). Lithos, 274–275: 123–146. https://doi.org/10.1016/j.lithos.2016.12.036

Explanation of Acronyms, Abbreviations, and Symbols:

ACG	Arc calc–alkaline granitoids
CL	Cathodoluminescence
E–MORB	Enriched mid–ocean ridge basalt
HFSE	High field strength element
HREE	Heavy rare earth element
KCG	High–K calc–alkaline granitoids
ICP–MS	Inductively coupled plasma mass spectrometry
LA–ICP–MS	Laser ablation inductively coupled plasma mass spectrometry
LAI	Laboratorio de Estudios Isotópicos
LCL	Lithological Characterization Laboratory
LILE	Large–ion lithophile element
LOI	Loss on ignition
LREE	Light rare earth element
MORB	Mid–ocean ridge basalt
N–MORB	Normal mid–ocean ridge basalt
NBIB	Northern block of Ibagué Batholith
OIB	Ocean island basalt
REE	Rare earth element
SGC	Servicio Geológico Colombiano
SM	Santander Massif
SNSM	Sierra Nevada de Santa Marta
UNAM	Universidad Autónoma de México
UMV	Upper Magdalena Valley
XRF	X–ray fluorescence

Authors' Biographical Notes

Gabriel RODRÍGUEZ–GARCÍA graduated in 1987 with a degree in geological engineering from the Universidad Nacional de Colombia, Sede Medellín. Subsequently, he completed specialization studies at the École Nationale Supérieure des Mines de Paris in 1995, specializing in technical evaluation–economics of mining projects. He has worked for 30 years at the Servicio Geológico Colombiano. He was the head of cartography of the regional headquarters of Ibagué, and acts as coordinator of projects and regional cartography and of work groups for the exploration and evaluation of deposits. He currently coordinates the Medellín headquarters and the Grupo de Estudios Geológicos Especiales of the Servicio Geológico Colombiano. He has previously been a professor of Colombian Geology, Field Geology I, and Physical Geology at Universidad EAFIT and the director of geology of Grupo Argos. He has authored over 100 publications, including geological maps, memoirs, and scientific articles in geology.

Ana María CORREA–MARTÍNEZ graduated in geological engineering from the Universidad Nacional de Colombia, Sede Medellín and has a PhD in geology from the Universidade de Brasília (Brasil), where she studied the petrogenesis of the Aburrá Ophiolite in the Colombian Central Cordillera. Between 2008 and 2013, she worked as a gold exploration geologist and chief of mineral exploration projects. She was lecturer at the Universidad Nacional de Colombia (Medellín) in the Departamento de Recursos Minerales. Since 2014, she has worked in the Servicio Geológico Colombiano on geochronology of metamorphic units from the northwestern slope of the Central Cordillera and on the project "Jurassic Magmatism in the Colombian Andes".

Gilberto ZAPATA–GARCÍA graduated with a degree in mining and geological engineering from the Russian State Geological Prospecting University (Российский государственный геологоразведочный университет) (MGRI–RSGPU) in 1977 and specialized in urban–regional planning at the Universidad Nacional de Colombia, Sede Medellín in 2000. He worked in geological mapping at a scale of 1:100.000, exploration, and petrography at Servicio Geológico Colombiano, from 1978 to 2017. Since 2014, he has been a member of the Proyecto Estudios Geológicos Especiales, participating in studies on Jurassic magmatism in Colombia.

María Isabel ARANGO–MEJÍA is a geologist who graduated from the Universidad de Caldas in 2008 and specialized in Geographic Information Systems (GIS) at the Universidad de San Buenaventura in 2016. She has worked on seismic projects, geological mapping, and geological research in Colombia. She is currently working on environmental projects.

Gloria OBANDO–ERAZO has a BS in geology, Universidad Nacional de Colombia Sede Bogotá, an MS in environmental geology with an emphasis in geophysics, processing and interpretation of aerial gamma ray spectrometry and aerial magnetometry (Universidade de Brasília, 2001), and is a PhD candidate in aerial geophysics (Universidade de Brasilia, 2006). She has worked since 1995 on multiple projects in Colombia using potential fields at the Servicio Geológico Colombiano. Since 2014, she has been working in the Grupo de Estudios Geológicos Especiales of the Servicio Geológico Colombiano on the project "Jurassic Magmatism in the Colombian Andes".

Juan Pablo ZAPATA–VILLADA is a geological engineer and MS in mineral resources of Universidad Nacional de Colombia Sede Medellín. He worked for the Cordilleran project of México (Tectonic Analysis) and has expertise in GIS, U–Pb analysis, and heavy minerals. He works for the Servicio Geológico Colombiano. His job includes GIS and the geochronology, and geochemistry of the Western Cordillera and Jurassic magmatism in Colombia. He has participated as a speaker at the Colombian Geological Congress, winning the Ricardo Lleras Codazzi in the XIV edition.

José Gilberto BERMÚDEZ graduated in 1989 with a degree in geology from the Universidad Pedagógica y Tecnológica de Sogamoso (UPTC), Boyacá, Colombia. He worked as a groundwater, geophysics and geology consultant from 1989 to 2009, was the general manager of Hidrocol Ltda and Gesprocom Ltda, worked as an exploration geologist for Coexminas and currently works as a basic geosciences specialist for the Servicio Geológico Colombiano. He has published more than 15 studies in the field of regional geology.